

https://dspace.org/

# Morphogenesis of hierarchal CaCO3: a novel "soft" colloidal template for the fabrication of carbon materials

**Makgae, Ofentse Alfred**

**2016-09-19**
http://hdl.handle.net/10539/21075

Downloaded from a DSpace repository. https://dspace.org/

# Morphogenesis of hierarchal $CaCO_3$: A novel "soft" colloidal template for the fabrication of carbon materials

**By**

**Ofentse Alfred Makgae**

**Student Number: 1156656**

A dissertation submitted to the Faculty of Science, University of the Witwatersrand, Johannesburg, in fulfilment of the requirements for the degree of Master of Science in Chemistry.

Supervisors: Prof. Shane H. Durbach

Dr Paul J. Franklyn

University of the Witwatersrand, Johannesburg. May 2016

# DECLARATION

I declare that this dissertation is my own, unaided work. It is being submitted for the degree of Master of Science at the University of the Witwatersrand, Johannesburg. It has not been submitted before for any degree or examination at any other University.




_____

Ofentse Alfred Makgae

_____day of May 2016 in Johannesburg.

# ABSTRACT

In this research project, the morphogenesis and polymorphism of calcium carbonate ($CaCO_3$) and its subsequent use as a template in the fabrication of hollow carbon spheres (HCS) is reported. A series of ratios (i.e. 5:0, 5:1, 5:2, 5:3, 5:4, 5:5, and 0:5) of binary solvent mixtures consisting of polar aprotic (dimethylformamide and dimethyl sulfoxide) and polar protic (methanol, ethanol, isopropanol, and 2-butanol) solvents, with 10% PEG200 as a crystal modifier, were used to influence the morphogenesis and polymorphism of precipitated $CaCO_3$ (PCC). The PCC products were characterised using scanning electron microscopy (SEM), powder X-ray diffraction (PXRD), and laser Raman spectroscopy. An increase in the ratio of the polar protic solvent (methanol, ethanol, isopropanol, and 2-butanol) relative to the polar aprotic solvent (DMF & DMSO) within the binary solvent mixture favored the formation of vaterite particles of different morphologies, while an increase in the ratio of polar aprotic solvent (DMF & DMSO) within the binary solvent mixture favored the precipitation of rhombohedral calcite crystals. Time-resolved *ex situ* PXRD and SEM measurements revealed that the nucleation and phase transformation of the $CaCO_3$ under polar protic and aprotic solvents followed the dissolution-reprecipitation mechanism. The major phase transformation occurred within 3 hours after mixing the precursor solutions.

The effect of poly (4-styrenesulfonic acid) (PSSA) as an additive in the crystallisation of $CaCO_3$ at different temperatures (i.e. 30, 40, 75, and 100 °C) and different crystallisation times (3, 6, 12, and 24 hrs) was investigated. The as-synthesised $CaCO_3$ products were subjected to: SEM, laser Raman spectroscopy, PXRD, thermogravimetric analysis (TGA), and transmission electron microscopy (TEM). The crystallisation of $CaCO_3$ in the presence of PSSA resulted in the self-assembly of vaterite particles into spherical bulk crystals. Varying the crystallisation temperature led to different particle attachment (CPA) pathways, which in turn resulted in bulk crystal morphologies that varied. Changes in the crystallisation temperature were found to not have changed the polymorphism of the precipitated $CaCO_3$ due to the kinetic stabilisation effects of PSSA, instead hollow vaterite spheres formed at 75 and 100 °C. The possibility to synthesise HCS using $CaCO_3$ as a template under chemical vapour deposition (CVD) at different temperatures (i.e. 600, 700 and 800 °C) was, for the first time, demonstrated. The evolution of $CO_2(g)$ from the decomposition of the template during CVD resulted in the formation of a rough surface topography on the carbon shell of the HCS. This surface roughness

increased with the increase in the reaction temperature due to the increased rate of $CaCO_3$ decomposition. The structural integrity of the spherical template was not affected by the $CO_2(g)$ evolution during carbonisation at all the reaction temperatures. The as-synthesised HCS at 600, 700, and 800 °C gave specific BET surface areas of: 193, 55, and 51 $m^2/g$, respectively.

## DEDICATION

To my granny,

# Mary Makgae

"Now unto Him who is able to do exceedingly abundantly above all that we ask or think…" Ephesians 3:20

# ACKNOWLEDGEMENTS

I would like to thank my Family for the patience and support throughout my studies.

My supervisors: Dr Durbach and Dr Franklyn for allowing me to learn from their wisdom and all the support and guidance throughout my study.

Wits Microscopy and Microanalysis for the help with acquiring my microscopy data, the PXRD Unit led Prof D Billing, and Dr Erasmus for all the laser Raman data.

A BIG thank you goes to the CATOMMAT group! I found best friendships, family, and colleagues.

To Professor Neil Coville, many THANKS and God continue to bless you!

The support of the DST-NRF Centre of Excellence in Strong Materials (CoE-SM) towards this research is hereby acknowledged. Opinions expressed and conclusions arrived at, are those of the author and are not necessarily to be attributed to the CoE-SM.

I am grateful to the Council for Geoscience for all the funding throughout out my studies.

Lastly, to my patient better half, Dr Clara Maila, and to the Almighty God for all that I have seen and yet to see.

# PRESENTATIONS

**Ofentse Makgae**, Shane Durbach, and Paul Franklyn. *Biomimetic crystallisation of $CaCO_3$: Inspiring Nature.* (**Best poster presentation**), Annual CoE-SM/AMSEN Presentations, April 2015

**Ofentse Makgae**, Gciniwe Mathejwa, Rudolph Erasmus, Paul Franklyn, and Shane Durbach. *Morphogenic and polymorphic transition between calcite and hollow vaterite spheres in binary polar aprotic-protic solvent mixtures: The effect of the solvent ratio.* (**Poster presentation**). Indaba 8, August 2015.

**Ofentse Makgae**, Rajesh Molose, Rudolph Erasmus, Paul Franklyn, and Shane Durbach. *Crystal Tectonics: Temperature induced self-assembly of poly (4-styrenesulfonic acid)-stabilized vaterite nanocrystals into hierarchical spheres.* (**Best oral presentation**). SACI Young Chemist symposium, November 2015.

**Ofentse Makgae**, Rajesh Molose, Rudolph Erasmus, Paul Franklyn, and Shane Durbach. *Crystal Tectonics: Temperature induced self-assembly of poly (4-styrenesulfonic acid)-stabilized vaterite nanocrystals into hierarchical spheres.* (**Poster presentation**). Microscopy Society of South Africa, December 2015.

**Ofentse Makgae**, Tumelo Phaahlamohlaka, Rudolph Erasmus, Paul Franklyn, and Shane Durbach. *Structured inorganic "softer" colloidal templates for the fabrication of hollow carbon spheres.* **(Oral presentation).** 3rd International Nanocarbon Workshop, January 2016.

**Ofentse Makgae**, Tumelo Phaahlamohlaka, Rudolph Erasmus, Paul Franklyn, and Shane Durbach. *Structured Calcium Carbonate ($CaCO_3$) as a novel "softer" template for the fabrication of hollow carbon spheres: A paradigm shift.* **(Best oral presentation in Science and Cross-Faculty categories)**. 7th Cross-Faculty graduate symposium, March 2016.

# TABLE OF CONTENTS

## Table of Contents

DECLARATION ..... i

ABSTRACT ..... ii

DEDICATION ..... iv

ACKNOWLEDGEMENTS ..... v

PRESENTATIONS ..... vi

LIST OF FIGURES ..... x

LIST OF TABLES ..... xv

Chapter 1: Research question and hypothesis ..... 1

1.1 Introduction ..... 1

1.1.1 Templated synthesis of micro- and nanomaterials ..... 1

1.1.2 Morphogenesis of calcium carbonate: A deviation from silica ..... 2

1.2 Objectives of the study ..... 4

1.3 Hypotheses and questions ..... 5

1.4 Outline of dissertation ..... 6

1.5 References ..... 7

Chapter 2: Literature review ..... 12

2.1 Synthesis of hollow nano and micromaterials by templating ..... 12

2.1.1 Various classes of templates, their properties, advantages and disadvantages ..... 12

2.1.2 The templated synthesis of hollow nano and microcarbon materials ..... 15

2.2 Morphogenesis and polymorphism of $CaCO_3$ ..... 18

2.2.1 Factors influencing the nucleation and growth of $CaCO_3$ ..... 18

2.2.2 Studies on the calcium carbonate crystal growth mechanism ..... 24

2.2.3 Crystal tectonics: Beyond the classical crystal growth model ..... 25

2.2.4 Proposed advantages of crystal tectonics to materials science ..... 27
2.3 Conclusions ..... 28
2.4 References ..... 29
Chapter 3: Experimental and characterisation procedures for the synthesis of calcium carbonate and hollow carbon microspheres ..... 39
3.1 Method for synthesising $CaCO_3$ ..... 39
3.1.1 Chemicals ..... 39
3.1.2 General synthesis of $CaCO_3$ ..... 39
3.2 Experimental procedure for hollow carbon spheres synthesis ..... 39
3.2.1 Gases ..... 39
3.2.2 Chemical Vapour Deposition (CVD) reactor set-up ..... 40
3.4 Characterisation techniques ..... 40
3.4.1 Transmission electron microscopy (TEM) ..... 41
3.4.2 Powder X-ray diffraction ..... 41
3.4.3 Laser Raman spectroscopy ..... 42
3.4.4 Scanning electron microscopy ..... 43
3.4.5 Brunauer-Emmet and Teller surface area measurement ..... 43
3.4.6 Thermogravimetric analyses ..... 44
3.5 References ..... 45
Chapter 4: Morphogenesis and polymorphism of calcium carbonate in binary polar aprotic-protic solvent mixtures ..... 46
4.1 Introduction ..... 46
4.2 Experimental ..... 47
4.2.1 Materials ..... 47
4.2.2 Crystallisation of Calcium Carbonate ..... 47
4.2.3 Characterisation ..... 48

4.3 Results and Discussion ..... 48
4.4 Conclusions ..... 69
4.5 References ..... 69
Chapter 5: Crystal Tectonics - Temperature induced self-assembly of PSSA-stabilized vaterite nanocrystals into hierarchical spheres ..... 74
5.1 Introduction ..... 74
5.2 Experimental ..... 75
5.2.1 Materials ..... 75
5.2.2 Self-assembly crystallisation reactions ..... 75
5.2.3 Characterisation ..... 76
5.3 Results and Discussion ..... 76
5.4 Conclusions ..... 89
5.5 References ..... 89
Chapter 6: Morphogenesis of vaterite spheres: A novel “softer” colloidal template for the fabrication of hollow carbon spheres ..... 94
6.1 Introduction ..... 94
6.2 Experimental ..... 95
6.2.1 Materials ..... 95
6.2.2 Synthesis of calcium carbonate ..... 95
6.2.3 Synthesis of hollow carbon spheres ..... 96
6.2.4 Characterisation ..... 96
6.3 Results and Discussion ..... 96
6.4 Conclusions ..... 108
6.5 References ..... 109
Chapter 7: General conclusions and recommendations ..... 113
7.1 Conclusions ..... 113

7.2 Recommendations ..... 115

APPENDIX 1 ..... 116

# LIST OF FIGURES

Figure 2. 1. Classification of templates: (a) Types of templates, (b) Synthetic strategies[2]. . 13

Figure 2. 2. Synthetic strategy for the hydrothermal carbonisation (HTC) of hollow carbon spheres using PS latex as a soft colloidal template and biomass as a carbon source[13]. ..... 14

Figure 2. 3. General schematic for the templated synthesis of HCS[1]. ..... 16

Figure 2. 4. Templating strategies, based on the nature of the template, for the synthesis of HCS[1]. ..... 16

Figure 2. 5. The effect of temperature on the polymorphism of $CaCO_3$ in water.[36] ..... 19

Figure 2. 6. PXRD patterns of $CaCO_3$ deposits formed with various $Mg^{2+}$ concentrations. As the $Mg^{2+}$ concentration was increased the (104) diffraction peak weakened and shifted to higher 2θ angle.[49] ..... 21

Figure 2. 7. The effect of different polymeric additives and their concentration on the polymorphism of $CaCO_3$. (a) Calcite selectivity. (b) Aragonite selectivity (had no effect: acetate, alanine, arginine, chondroitinsulfate, citrate, dextrose, galactose, glutamate, glycine, glycogen, glycoprotein, glycylglycine, lactate, malate, pyruvate, and succinate). (c) Vaterite selectivity (had no effect: acetate, alanine, arginine, chondroitinsulfate, citrate, galactose, lactate, malate, pyruvate, succinate, and taurine)[67]. ..... 23

Figure 2. 8. Effects of pH on the polymorphism of $CaCO_3$ at 24 °C. Key: (V) – vaterite; (A) – aragonite; (C) – calcite[77] ..... 24

Figure 2. 9. Schematic representation of classical and non-classical models of crystallisation. (a) Classical crystallisation pathway, (b) oriented attachment of primary nanoparticles forming an iso-oriented crystal upon fusing, (c) mesocrystal formation via crystal tectonics of primary nanoparticles covered with organic molecules[88]. ..... 26

Figure 2. 10. Schematic of the synthesis of : (1) Mesoporous bimetallic PdPt spheres, (2) Mesoporous trimetallic Au@PdPt spheres, and (3) Mesoporous trimetallic PdPtCu spheres[99]. ..... 28

Figure 3. 1. Horizontal CVD set up. ....40
Figure 3. 2. FEI Tecnai T12 transmission electron microscope. ....41
Figure 3. 3. Bruker D2 PHASER desktop powder X-ray diffractometer. ....42
Figure 3. 4. Horiba Jobin-Yvon LabRAM HR Raman spectrometer. ....42
Figure 3. 5. FEI Nova Nanolab 600 FIB/SEM microscope. ....43
Figure 3. 6. Micromeritics Tristar Surface area and Porosity analyser. ....44
Figure 3. 7. Perkin Elmer STA 4000 Simultaneous Thermal Analyser. ....44

Figure 4. 1. PXRD patterns of the PCC products synthesized in alcohols of different molecular weight in the presence of 10% PEG (200 Mw) as a crystal modifier. ....48
Figure 4. 2. Laser Raman spectra of the two polymorphs of calcium carbonate and their optical microscope images from which the spectra were acquired. (a) Calcite, (b) Image of calcite, (c) Vaterite, and (d) Image of vaterite. ....50
Figure 4. 3. SEM micrographs of the PCC products formed in: (a) Methanol, (b) Ethanol, (c) Isopropanol, and (d) 2-butanol. Inserts show the presence of calcite (confirmed from optical microscopy images in Figure 4.2 above) crystals in the samples. ....51
Figure 4. 4. SEM micrographs of: (a) “Flower” shaped vaterite particle formed from the fusion of the individual vaterite ellipsoids; (b) Broken hollow vaterite ellipsoid. ....52
Figure 4. 5. PXRD patterns showing the polymorphism of the PCC as a function of the binary solvent ratio. (a) Ratios of DMF to methanol, (b) Ratios of DMF to ethanol, (c) Ratios of DMF to isopropanol, and (d) Ratios of DMF to 2-butanol. ....53
Figure 4. 6. PXRD patterns showing the polymorphism of the PCC as a function of the binary solvent ratio. (a) Ratios of DMSO to methanol, (b) Ratios of DMSO to ethanol, (c) Ratios of DMSO to isopropanol, and (d) Ratios of DMSO to 2-butanol. ....54
Figure 4. 7. Standard calibration curve of the ratio of vaterite to calcite peak areas versus (mass) percentage of vaterite. ....55
Figure 4. 8. Time-resolved ex-situ PXRD patterns showing the kinetics, mechanism of nucleation and phase transformation of the PCC under polar aprotic solvent and polar protic solvent: (a) DMSO, (b) Isopropanol. ....58
Figure 4. 9. Time-resolved SEM micrographs showing the kinetics, mechanism of nucleation and phase transformation of the PCC under a polar aprotic solvent and a polar protic solvent:

(a)-(e) Isopropanol; at 5, 15, 30 min, 1, and 3 hrs, respectively. (f)-(j) DMSO; at 5, 15, 30 min, 1, and 3 hrs, respectively. .....59
Figure 4. 10. SEM micrographs showing the effect of the solvent ratio of DMF and methanol on the morphology of the PCC. (a) Pure DMF, (b) 5:1 of DMF to methanol, (c) 5:2 of DMF to methanol, (d) 5:3 of DMF to methanol, (e) 5:4 of DMF to methanol, and (f) 5:5 of DMF to methanol. Crystallites of calcite were present in (a)-(e), while vaterite and calcite (PXRD proved calcite was also present) were present in (f). .....61
Figure 4. 11. SEM micrographs showing the effect of the solvent ratio of DMSO and methanol on the morphology of the PCC. (a) Pure DMSO, (b) 5:1 of DMSO to methanol, (c) 5:2 of DMSO to methanol, (d) 5:3 of DMSO to methanol, (e) 5:4 of DMSO to methanol, and (f) 5:5 of DMSO to methanol. Crystallites of calcite were present in (a)-(c), while mixtures of vaterite and calcite were present in (e)-(f). .....62
Figure 4. 12. SEM micrographs showing the effect of the solvent ratio of DMF and ethanol on the morphology of the PCC. (a) Pure DMF, (b) 5:1 of DMF to ethanol, (c) 5:2 of DMF to ethanol, (d) 5:3 of DMF to ethanol, (e) 5:4 of DMF to ethanol, and (f) 5:5 of DMF to ethanol. Crystallites of calcite are present in (a)-(e), while crystallites of vaterite were present in (f). 63
Figure 4. 13. SEM micrographs showing the effect of the solvent ratio between DMSO and ethanol on the morphology of the PCC. (a) Pure DMSO, (b) 5:1 of DMSO to ethanol, (c) 5:2 of DMSO to ethanol, (d) 5:3 of DMSO to ethanol, (e) 5:4 of DMSO to ethanol, and (f) 5:5 of DMSO to ethanol. Crystallites of calcite were present in (a)-(c), while crystallites of vaterite were present in (e)-(f). .....64
Figure 4. 14. SEM micrographs showing the effect of the solvent ratio of DMF and isopropanol on the morphology of the PCC. (a) Pure DMF, (b) 5:1 of DMF to isopropanol, (c) 5:2 of DMF to isopropanol, (d) 5:3 of DMF to isopropanol, (e) 5:4 of DMF to isopropanol, and (f) 5:5 of DMF to isopropanol. Crystallites of calcite were present in (a)-(d), and mixtures of calcite and vaterite were present in (e)-(f). .....65
Figure 4. 15. SEM micrographs showing the effect of the solvent ratio of DMSO and isopropanol on the morphology of the PCC. (a) Pure DMSO, (b) 5:1 of DMSO to isopropanol, (c) 5:2 of DMSO to isopropanol, (d) 5:3 of DMSO to isopropanol, (e) 5:4 of DMSO to isopropanol, and (f) 5:5 of DMSO to isopropanol. Crystallites of calcite were present in (a)-(c), and mixtures of calcite and vaterite were present in (d)-(f). .....66
Figure 4. 16. SEM micrographs showing the effects of solvent ratio of DMF and 2-butanol on the morphology of the PCC. (a) Pure DMF, (b) 5:1 of DMF to 2-butanol, (c) 5:2 of DMF to 2-butanol, (d) 5:3 of DMF to 2-butanol, (e) 5:4 of DMF to 2-butanol, and (f) 5:5 of DMF to

2-butanol. Crystallites of calcite were present in (a)-(b), while mixtures of vaterite and calcite were present in (c)-(f). .....67
Figure 4. 17. SEM micrographs showing the effect of the solvent ratio of DMSO and 2-butanol on the morphology of the PCC. (a) Pure DMSO, (b) 5:1 of DMSO to 2-butanol, (c) 5:2 of DMSO to 2-butanol, (d) 5:3 of DMSO to 2-butanol, (e) 5:4 of DMSO to 2-butanol, and (f) 5:5 of DMSO to 2-butanol. Crystallites of calcite were present in (a)-(b), while mixtures of vaterite and calcite were present in (c)-(f). .....68

Figure 5. 1. PXRD diffractograms showing the ability of PSSA to stabilize the vaterite polymorph across different reaction temperatures and times, i.e. at: (a) 3 hrs, (b) 6 hrs, (c) 12 hrs, and (d) 24 hrs. Indexed according to ICSD 015879. .....77
Figure 5. 2. Schematic of the effect of temperature on the self-assembly of vaterite crystals: systematic morphogenesis. .....78
Figure 5. 3. SEM micrographs showing the effect of reaction temperature on the morphology of the bulk self-assembled vaterite crystals precipitated at 3 hrs into the crystallisation process at: (a) 30 ˚C, (b) 40 ˚C, (c) 75 ˚C, (d) 100 ˚C. .....79
Figure 5. 4. Magnification series of the self-assembly of vaterite nanocrystals showing: (a) The oriented attachment of nanocrystalline particles from a thin section at the edge a bulk sphere (TEM micrograph), (b) The directed self-assembly of hexagonal vaterite particles into a vaterite sphere (SEM micrograph), and (c) A vaterite sphere formed from self-assembled hexagonal vaterite particles (SEM micrograph). .....80
Figure 5. 5. SEM micrographs showing the effect of temperature on the morphology of the bulk self-assembled vaterite crystals precipitated at 6 hrs into the crystallisation process at: (a) 30 ˚C, (b) 40 ˚C, (c) 75 ˚C, (d) 100 ˚C. .....82
Figure 5. 6. SEM-FIB micrographs of the dissected solid core vaterite bulk crystals. (a) 90 ˚ incident angle, (b) 51 ˚ incident angle. .....82
Figure 5. 7. Laser Raman spectra showing the pure vaterite polymorph and the effect of reaction temperature on the surface roughness of the vaterite spheres at different reaction times, i.e. at: (a) 3 hrs, (b) 6 hrs, (c) 12 hrs, and (d) 24 hrs. .....84
Figure 5. 8. The first derivatives of the TGA thermograms for the bulk self-assembled vaterite crystals formed at: (a) 3 hrs, (b) 6 hrs, (c) 12 hrs and (d) 24 hrs. .....85

Figure 5. 9. SEM micrographs showing the effect of temperature on the morphology of bulk self-assembled vaterite crystals precipitated 12 hrs into the crystallisation process at: (a) 30 ˚C, (b) 40 ˚C, (c) 75 ˚C and (d) 100 ˚C. ..... 86
Figure 5. 10. SEM micrographs showing the effect of temperature on the morphology of self-assembled vaterite crystals precipitated after 24 hrs at: (a) 30 ˚C, (b) 40 ˚C, (c) 75 ˚C and (d) 100 ˚C. ..... 88

Figure 6. 1. A PXRD pattern of the white-coloured precipitate, which was found to be the vaterite polymorph of calcium carbonate. ..... 97
Figure 6. 2. A laser Raman spectrum of the white-coloured precipitate, which was found to be the vaterite polymorph of calcium carbonate. ..... 98
Figure 6. 3. SEM micrographs of the precipitated $CaCO_3$ spheres: (a)-(b) SEM magnification series showing the morphology of the spheres, (c) Particle size distribution of the $CaCO_3$ spheres ..... 99
Figure 6. 4. SEM micrographs showing the effect of reaction temperature on the surface roughness of the spherical $CaCO_3$ particles after being exposed to acetylene at: 600 °C (a) & (d), 700 °C (b) & (e), and 800 °C (c) & (f). Arrows show the rough topography on the spheres ..... 100
Figure 6. 5. Laser Raman spectra of spherical $CaCO_3$ particles which had been exposed to acetylene at reaction temperatures of: (a) 600 °C, (b) 700 °C, and (c) 800 °C. ..... 101
Figure 6. 6. TEM micrographs of the carbon coated vaterite spheres which had been synthesised at: (a) 600 °C, (b) 700 °C, and (c) 800 °C, after exposure to acetic acid for 24 hrs. Arrows show the presence of residue inside the spheres. ..... 102
Figure 6. 7. Magnified TEM micrographs of the HCS synthesised at: (a) 600 °C, (b) 700 °C, and (c) 800 °C. ..... 103
Figure 6. 8. TEM micrographs of HCSs synthesised at 800 °C. (a) Lower magnification displaying the larger portion of the HCS. (b) High magnification TEM micrograph of the surface of the same HCS synthesised at 800 °C. ..... 105
Figure 6. 9. TGA thermograms of the $CaCO_3$ template, and the HCSs synthesised at reaction temperatures between 600 °C and 800 °C. ..... 106

Figure S. 1. TGA patterns showing the presence of the PSSA within the vaterite spheres by the decomposition peak around 450 ˚C at, (a) 3 hrs, (b) 6 hrs, (c) 12 hrs, (d) 24 hrs reaction times. ..... 116
Figure S. 2. SEM micrographs showing the hollow nature of the bulk vaterite spheres crystallised at: (a) & (b) 75 °C, and (c) & (d) 100 °C. ..... 117
Figure S. 3. The amount (wt. %) of the occluded PSSA at different reaction temperatures for different reaction times. ..... 118

# LIST OF TABLES

Table 4. 1. Polymorph distributions in the PCC, as a function of solvent ratio. ..... 56

Table 6. 1. The ratio of the D and G peak intensities ($I_D/I_G$) of HCS which were synthesised under different reaction temperatures. ..... 104
Table 6. 2. BET surface area, pore volumes and average size (diameter) of the $CaCO_3$ template and the HCS synthesised at different reaction temperatures and etched with acetic acid for 24 hrs. ..... 107

# Chapter 1: Research question and hypothesis

## 1.1 Introduction

### 1.1.1 Templated synthesis of micro- and nanomaterials

Carbon micro- and nanomaterials have received increased interest since their discovery due to their remarkable physical and chemical properties such as: low density, good mechanical robustness, high surface area, high electron density and surface permeability[1]. These materials have found immense application in various scientific fields such as medical research in the area of drug delivery[2], nanotubes for waste water treatment[3], nanospheres as catalyst supports for iron oxide-based Fischer-Tropsch synthesis[4], exfoliated reduced graphene oxide and nanographene-structured hollow carbon spheres in lithium ion batteries[5], nitrogen doped carbon nanospheres in gas storage[6], hollow carbon spheres as supercapacitors[7] and in solar cells as well as in fuel cells[8].

The precise, and controlled, growth of highly ordered and porous functional carbon materials through the use of structured templates is essential for obtaining materials with the dimensions and properties of interest. Hence these aspects have received attention over the last two decades[9]. Employing a tailored template as a synthesis mould offers a high degree of control over the shape, polymorphic composition and structural dimensions. This can be as fine as controlling the pore volume and size of the desired materials[10]. The fabrication of structured micro and nano-sized carbon materials from a template involves at least four aspects.

1) The selection of an appropriate material that can withstand a wide variety of conditions (i.e. chemical/physical or both) in order to be deemed suitable as a template.
2) The application of experimental methodologies to enable the synthesis of the chosen material, in desired dimensions of required morphologies for use as templates.
3) The development of appropriate techniques to reliably coat a target material (e.g. carbon) onto the chosen template.
4) Where necessary, the establishment of a dependable procedure for the subsequent removal of the template.

Templates may be classed according to their chemical and physical nature; the ease of removal of the template from the desired synthesised material and the synthetic route used to produce

the template[10]. There are several classes of templates. One class, the non-colloidal templates, are commonly one-dimensional (1D) nanowires (e.g. nanotubes or nanofibers) onto which a precursor material or the material of interest is coated. For example, the synthesis of $ZrO_2$ nanotubes using carbon nanotubes as a template, via the sol-gel method[11]. Another class are soft colloidal templates that comprise: micro or macro-emulsions and micelles or vesicles (with/without other polymers) which are utilised in solution synthesis. However, these are not thermodynamically stable and tend to give a range of morphological sizes from 10 nm to tens of microns[12].

Another class of templates that has received immense attention is the class of hard colloidal physical templates, such as silica colloidal particles which are synthesised by the Stöber method [13]. Here tetraethyl orthosilicate is hydrolysed in an aqueous ethanol solution that is catalysed by an ammonia solution at room temperature. The resultant as-synthesised spheres are in the size range of 100 - 500 nm [14].

Although the Stöber method has been successful in the synthesis of hollow carbon spheres, it is not ideal for two reasons, namely: 1) the harsh chemicals (e.g. HF) that are required to remove the silica template and 2) the time consuming steps to do so.

Several attempts have been made to use other sacrificial hard colloidal chemical templates such as polystyrene beads. These can be made simply by emulsion polymerisation or by purchasing commercial polystyrene beads [15]. One advantage of this type of sacrificial hard colloidal chemical template is that after coating with the desired carbon layer, the polymer can be burned off during carbonisation at high temperatures and chemically transformed into the resultant material, which eliminates the chemical template removal step [15]. One disadvantage of this approach is that the resultant material formed this way may not have the strength characteristics required, which may limit its eventual use[16].

Hence alternative environmentally friendly and "softer" colloidal templates are needed. In this study a semi-hard colloidal template i.e. shaped calcium carbonate, was investigated as one such possible alternative.

### 1.1.2 Morphogenesis of calcium carbonate: A deviation from silica

*Crystal growth of calcium carbonate*

Crystallisation behaviour of calcium carbonate in solution is one of the most widely studied processes in the area of crystal growth and engineering. Calcium carbonate is abundant as a

biomineral in nature and it has industrial relevance (e.g. used a filler for paint and paper[17] and its crystallisation causing lime scaling in water pipes[18], [19]). The vast abundance of crystallised $CaCO_3$ in natural water has led to the extensive study in understanding its formation and transformation mechanism in that medium since the 1960-80s[20], [21].

Anhydrous calcium carbonate exists as three different polymorphs: the metastable vaterite and aragonite phases, and the stable calcite phase[22]. These polymorphs can exist under different reaction conditions during the precipitation of calcium carbonate in water, where the effect of temperature on polymorph formation is the most studied variable[21]. For instance, it has been reported that calcite and vaterite co-exist at temperatures between 10-30 °C, while all three polymorphs co-exist at intermediate temperatures of 40-50 °C[23]. Lastly studies have shown that aragonite and calcite co-exist at temperatures of 60 °C and above[23].

*Factors influencing crystal growth of calcium carbonate*

Crystal structures of the three polymorphs of $CaCO_3$ have been reported as:

- rhombohedral - calcite
- hexagonal - vaterite, and
- orthorhombic - aragonite[24].

The incorporation of additives, the synthesis temperature, pH, and the synthesis solvent during crystal growth results in the inhibition or preferred growth of specific crystal facets. This is achieved through the surface lattice energies of specific crystal planes, thereby favouring specific crystal morphologies[25].

The presence of cations in natural water has been the underpinning of studying the crystallisation and polymorphism behaviour of calcium carbonate in the presence of cations such as: magnesium, iron and other alkali earth metals[26], [27]. It has been observed that incorporating small amounts of magnesium ions during the crystallisation of calcium carbonate helps to stabilise the amorphous calcium carbonate. Further it favours the polymorph transformation of the aragonite phase by inhibiting calcite crystal growth[28]–[30].

There have been increasing efforts in studying solvent induced morphogenesis and polymorphism of calcium carbonate[31]–[34]. It has been shown that the difference in the polarity of the solvents can be used to influence the crystal growth of calcium carbonate. For instance, alcoholic solutions are known to favour the formation of vaterite crystals while inhibiting crystal growth of calcite and aragonite[19], [35], [36]. Polar aprotic solvents are also

known to inhibit the vaterite and aragonite polymorphs and favour the precipitation of the calcite phase[37]–[39].

Amphipathic block co-polymers have also been widely studied for their use in the controlled synthesis of calcium carbonate hierarchal structures [40]. These types of co-polymers consist of hydrophilic and hydrophobic functional groups, which not only influence the crystal lattice parameters of the solid calcium carbonate, as demonstrated by the anisotropic lattice distortions found in mollusc-made aragonite[41], but through their ionic nature interact with the calcium ions prior to crystallisation[42]. This allows them to assume a pseudo-template nature [43]–[46].

Amphipathic block co-polymers have proven successful at influencing the morphology of calcium carbonate. However, they often lack structural control and lead to hetero-structured calcium carbonate particles due to the dual hydrophobic-hydrophilic nature of the co-polymers [47], [48].

Precipitation of calcium carbonate in solution is favoured by pH between 9-12 and the yield increases with an increase in pH [49]. This chemical behaviour has been used in water treatment research to control the scale formation of calcium carbonate in water plants [50]. It has been shown that during specific reaction conditions polymorphism of calcium carbonate can be controlled by adjusting the pH of the reaction medium e.g. at elevated temperatures, a pH above 12 favours aragonite formation [49].

## 1.2 Objectives of the study

The aims of this research project were to:

1) Investigate the effects of: reaction time, solvent type, solvent ratio, pH, temperature, calcium counter ion, polymer type and loading on the morphology and size of precipitated calcium carbonate. This was to provide a clear understanding of the factors affecting the crystal growth of calcium carbonate under different conditions.
2) Fully characterise the synthesised calcium carbonate micro- and nanostructures using a wide range of techniques including: powder and variable temperature X-ray diffraction, thermal analysis (TGA/DSC), electron microscopy (SEM, TEM and SEM/TEM based

EDS), BET surface area and pore size analysis, selected area electron diffraction and *in situ* laser Raman as well as continuous laser Raman spectroscopy. All these analyses were performed in an attempt to understand the phase transformations that occur during the synthesis and post-synthesis conditions of the micro- and nanostructures of calcium carbonate.

3) Explore the possibility of using the calcium carbonate precipitates (particularly those that were spherically shaped) as templates for shaped carbon deposition.
4) Determine the conditions that would be required to remove the micro or nanostructured calcium carbonate templates (especially those that were spherically shaped) from within the shaped carbon materials after deposition.

## 1.3 Hypotheses and questions

In spite of the undeniable evident success of the Stöber method in the fabrication of highly porous carbon spheres (HPCS), the removal of this template often takes hours and involves the use of harsh chemicals such as hydrofluoric acid and concentrated alkali solutions. Therefore, this study sought to circumvent such conditions by providing a novel semi-hard colloidal template method by addressing the following research questions:

1. Can different morphologies of calcium carbonate be synthesised from the proposed reaction conditions?
2. Can the size and shape of these calcium carbonate precipitates be manipulated by varying specific reaction conditions?
3. Can carbon be deposited (by either chemical vapour deposition (CVD) or the hydrothermal method) onto the surface of the as-synthesised calcium carbonate precipitates (particularly those that were spherically shaped)?
4. What role would the decomposition of calcium carbonate into calcium oxide and carbon dioxide at higher temperatures (ca. 800 °C) play, if carbon deposition on these spherically shaped templates is successful? If the calcium carbonate materials are to be used as a template for carbon coating under CVD two things may hypothetically occur during the carbon deposition:
    i. The carbon dioxide gas coming out of the spherically shaped calcium carbonate precipitate may cause it to disintegrate and lose its morphology or;

ii. The exiting gas may create larger pore structures on the carbon shell, which would be very much preferential for yolk-shell catalyst formation (i.e. this would provide high surface area, less induction periods, high diffusion rates and may even lead to higher catalytic activity).

5. Will the success of this synthetic template route open a whole new avenue within the template synthesis of HPCS which can be applied in a wide range of different research areas?

## 1.4 Outline of dissertation

Chapter 1: Gives the main motive of this research and the associated research questions and hypotheses.

Chapter 2: Gives a detailed review on the synthesis of hollow carbon materials by the templating method, the chemistry of $CaCO_3$ and its potential to be used as a template.

Chapter 3: Provides experimental and characterisation procedures for the synthesis of $CaCO_3$ and hollow carbon spheres.

Chapter 4: Reports on the manipulation of the morphology and polymorphic distribution of $CaCO_3$ using binary polar aprotic-protic solvent mixtures.

Chapter 5: Reports on the use of temperature to influence the self-assembly of the poly (4-styrene sulfonic acid)-stabilised vaterite crystals.

Chapter 6: Reports on the use of vaterite spheres as templates for the fabrication of hollow carbon spheres.

Chapter 7: Provides conclusions of the study and recommendations.

## 1.5 References


[1] Z. Yang, Y. Zhang, J. Kong, S. Y. Wong, X. Li, and J. Wang, "Hollow Carbon Nanoparticles of Tunable Size and Wall Thickness by Hydrothermal Treatment of α-Cyclodextrin Templated by F127 Block Copolymers," *Chem. Mater.*, vol. 25, no. 5, pp. 704–710, 2013.

[2] L. Lacerda, A. Bianco, M. Prato, and K. Kostarelos, "Carbon nanotubes as nanomedicines: from toxicology to pharmacology," *Adv. Drug Deliv. Rev.*, vol. 58, no. 14, pp. 1460–70, 2006.

[3] Y. H. Li, Y. M. Zhao, W. B. Hu, I. Ahmad, Y. Q. Zhu, X. J. Peng, and Z. K. Luan, "Carbon nanotubes - the promising adsorbent in wastewater treatment," *J. Phys. Conf. Ser.*, vol. 61, pp. 698–702, 2007.

[4] G. Yu, B. Sun, Y. Pei, S. Xie, S. Yan, M. Qiao, K. Fan, X. Zhang, and B. Zong, "Fe x O y @C Spheres as an Excellent Catalyst for Fischer−Tropsch Synthesis," *J. Am. Chem. Soc.*, vol. 132, no. 3, pp. 935–937, 2010.

[5] S. Yang, X. Feng, L. Zhi, Q. Cao, J. Maier, and K. Müllen, "Nanographene-constructed hollow carbon spheres and their favorable electroactivity with respect to lithium storage," *Adv. Mater.*, vol. 22, no. 7, pp. 838–42, 2010.

[6] S. Feng, W. Li, Q. Shi, Y. Li, J. Chen, Y. Ling, A. M. Asiri, and D. Zhao, "Synthesis of nitrogen-doped hollow carbon nanospheres for $CO_2$ capture," *Chem. Commun. (Camb).*, vol. 50, no. 3, pp. 329–31, 2014.

[7] X. Chen, K. Kierzek, K. Wenelska, K. Cendrowski, J. Gong, X. Wen, T. Tang, P. K. Chu, and E. Mijowska, "Electrochemical characteristics of discrete, uniform, and monodispersed hollow mesoporous carbon spheres in double-layered supercapacitors," *Chem. Asian J.*, vol. 8, no. 11, pp. 2627–33, 2013.

[8] R. Kou, Y. Shao, D. Wang, M. H. Engelhard, J. H. Kwak, J. Wang, V. V. Viswanathan, C. Wang, Y. Lin, Y. Wang, I. A. Aksay, and J. Liu, "Enhanced activity and stability of Pt catalysts on functionalised graphene sheets for electrocatalytic oxygen reduction," *Electrochem. commun.*, vol. 11, no. 5, pp. 954–957, 2009.

[9] X. Fang, S. Liu, J. Zang, C. Xu, M. Zheng, Q. Dong, D. Sun, and N. Zheng, "Precisely controlled resorcinol-formaldehyde resin coating for fabricating core-shell, hollow,

and yolk-shell carbon nanostructures," *Nanoscale*, vol. 5, no. 15, pp. 6908–16, 2013.

[10] Y. Liu, J. Goebl, and Y. Yin, "Templated synthesis of nanostructured materials.," *Chem. Soc. Rev.*, vol. 42, no. 7, pp. 2610–53, 2013.

[11] C. N. R. Rao, B. C. Satishkumar, and A. Govindaraj, "Zirconia nanotubes," *Chem. Commun.*, vol. 2, no. 16, pp. 1581–1582, 1997.

[12] H. Wennerström, O. Söderman, U. Olsson, and B. Lindman, "Macroemulsions versus microemulsions," *Colloids Surfaces A Physicochem. Eng. Asp.*, vol. 123–124, pp. 13–26, 1997.

[13] W. Stöber, A. Fink, and E. Bohn, "Controlled growth of monodisperse silica spheres in the micron size range," *J. Colloid Interface Sci.*, vol. 26, no. 1, pp. 62–69, 1968.

[14] Y. Han, X. Dong, C. Zhang, and S. Liu, "Hierarchical porous carbon hollow-spheres as a high performance electrical double-layer capacitor material," *J. Power Sources*, vol. 211, pp. 92–96, 2012.

[15] J. Fu, Q. Xu, J. Chen, Z. Chen, X. Huang, and X. Tang, "Controlled fabrication of uniform hollow core porous shell carbon spheres by the pyrolysis of core/shell polystyrene/cross-linked polyphosphazene composites," *Chem. Commun. (Camb).*, vol. 46, no. 35, pp. 6563–5, 2010.

[16] Y. Ma and L. Qi, "Solution-phase synthesis of inorganic hollow structures by templating strategies," *J. Colloid Interface Sci.*, vol. 335, no. 1, pp. 1–10, 2009.

[17] H. Balard and E. Papirer, "Characterisation and modification of fillers for paints and coatings," *Prog. Org. Coatings*, vol. 22, no. 1–4, pp. 1–17, 1993.

[18] J. Y. Gal, J. C. Bollinger, H. Tolosa, and N. Gache, "Calcium carbonate solubility: a reappraisal of scale formation and inhibition," *Talanta*, vol. 43, no. 9, pp. 1497–509, 1996.

[19] S. R. Dickinson and K. M. McGrath, "Switching between kinetic and thermodynamic control: calcium carbonate growth in the presence of a simple alcohol," *J. Mater. Chem.*, vol. 13, no. 4, pp. 928–933, 2003.

[20] T. Ogino, T. Suzuki, and K. Sawada, "The formation and transformation mechanism of calcium carbonate in water," *Geochim. Cosmochim. Acta*, vol. 51, no. 10, pp. 2757–2767, 1987.

[21] Y. Kitano, "A Study of the Polymorphic Formation of Calcium Carbonate in Thermal

Springs with an Emphasis on the Effect of Temperature," *Bull. Chem. Soc. Jpn.*, vol. 35, no. 12, pp. 1980–1985, 1962.

[22] Q. Shen, H. Wei, L. Wang, Y. Zhou, Y. Zhao, Z. Zhang, D. Wang, G. Xu, and D. Xu, "Crystallisation and Aggregation Behaviors of Calcium Carbonate in the Presence of Poly(vinylpyrrolidone) and Sodium Dodecyl Sulfate," *J. Phys. Chem. B*, vol. 109, no. 39, pp. 18342–18347, 2005.

[23] J. Chen and L. Xiang, "Controllable synthesis of calcium carbonate polymorphs at different temperatures," *Powder Technol.*, vol. 189, no. 1, pp. 64–69, 2009.

[24] N. H. De Leeuw and S. C. Parker, "Surface Structure and Morphology of Calcium Carbonate Polymorphs Calcite , Aragonite , and Vaterite : An Atomistic Approach," *J. Phys. Chem. B*, vol. 5647, no. 97, pp. 2914–2922, 1998.

[25] F. Bruneval, D. Donadio, and M. Parrinello, "Molecular Dynamics Study of the Solvation of Calcium Carbonate in Water," *J. Phys. Chem. B*, vol. 111, no. 42, pp. 12219–12227, 2007.

[26] N. H. de Leeuw, "Molecular Dynamics Simulations of the Growth Inhibiting Effect of $Fe^{2+}$ , $Mg^{2+}$ , $Cd^{2+}$ , and $Sr^{2+}$ on Calcite Crystal Growth," *J. Phys. Chem. B*, vol. 106, no. 20, pp. 5241–5249, 2002.

[27] Y. J. Han, L. M. Wysocki, M. S. Thanawala, T. Siegrist, and J. Aizenberg, "Template-Dependent Morphogenesis of Oriented Calcite Crystals in the Presence of Magnesium Ions," *Angew. Chemie*, vol. 117, no. 16, pp. 2438–2442, 2005.

[28] Y. Liu, J. Jiang, M. Gao, B. Yu, L. Mao, and S. Yu, "Phase Transformation of Magnesium Amorphous Calcium Carbonate (Mg-ACC) in a Binary Solution of Ethanol and Water," *Cryst. Growth Des.*, vol. 13, no. 1, pp. 59–65, 2013.

[29] M. M. M. G. P. G. Mantilaka, D. G. G. P. Karunaratne, R. M. G. Rajapakse, and H. M. T. G. Pitawala, "Precipitated calcium carbonate/poly(methyl methacrylate) nanocomposite using dolomite: Synthesis, characterisation and properties," *Powder Technol.*, vol. 235, pp. 628–632, 2013.

[30] G. Falini, M. Gazzanob, and A. Ripamonti, "Magnesium calcite crystallisation from water-alcohol mixtures," *Chem. Commun. (Camb).*, pp. 1037–1038, 1996.

[31] A. Szcześ, "Influence of the surfactant nature on the calcium carbonate synthesis in water-in-oil emulsion," *J. Cryst. Growth*, vol. 311, no. 4, pp. 1129–1135, Feb. 2009.

[32] H. S. Lee, T. H. Ha, and K. Kim, “Fabrication of unusually stable amorphous calcium carbonate in an ethanol medium,” *Mater. Chem. Phys.*, vol. 93, no. 2–3, pp. 376–382, 2005.

[33] F. Manoli and E. Dalas, “Spontaneous precipitation of calcium carbonate in the presence of ethanol, isopropanol and diethylene glycol,” *J. Cryst. Growth*, vol. 218, no. 2–4, pp. 359–364, 2000.

[34] X. H. Guo, S. H. Yu, and G. B. Cai, “Crystallisation in a Mixture of Solvents by Using a Crystal Modifier: Morphology Control in the Synthesis of Highly Monodisperse $CaCO_3$ Microspheres,” *Angew. Chemie*, vol. 118, no. 24, pp. 4081–4085, Jun. 2006.

[35] R. Qi and Y. Zhu, “Microwave-Assisted Synthesis of Calcium Carbonate ( Vaterite ) of Various Morphologies in Water - Ethylene Glycol Mixed Solvents,” *J. Phys. Chem. B*, vol. 110, pp. 8302–8306, 2006.

[36] K. S. Seo, C. Han, J. H. Wee, J. K. Park, and J. W. Ahn, “Synthesis of calcium carbonate in a pure ethanol and aqueous ethanol solution as the solvent,” *J. Cryst. Growth*, vol. 276, no. 3–4, pp. 680–687, 2005.

[37] Z. Nan, X. Chen, Q. Yang, X. Wang, Z. Shi, and W. Hou, “Structure transition from aragonite to vaterite and calcite by the assistance of SDBS.,” *J. Colloid Interface Sci.*, vol. 325, no. 2, pp. 331–6, 2008.

[38] M. Lei, P. G. Li, Z. B. Sun, and W. H. Tang, “Effects of organic additives on the morphology of calcium carbonate particles in the presence of CTAB,” *Mater. Lett.*, vol. 60, no. 9–10, pp. 1261–1264, 2006.

[39] X. Guo, A. Xu, and S. Yu, “Crystallisation of Calcium Carbonate Mineral with Hierarchical Structures in DMF Solution under Control of Poly(ethylene glycol)- b -poly( l -glutamic acid): Effects of Crystallisation Temperature and Polymer Concentration,” *Cryst. Growth Des.*, vol. 8, no. 4, pp. 1233–1242, 2008.

[40] L. He, Y. Zhang, L. Ren, Y. Chen, H. Wei, and D. Wang, “Double-Hydrophilic Polymer Brushes: Synthesis and Application for Crystallisation Modification of Calcium Carbonate,” *Macromol. Chem. Phys.*, vol. 207, no. 7, pp. 684–693, 2006.

[41] B. Pokroy, A. N. Fitch, P. L. Lee, J. P. Quintana, E. N. Caspi, and E. Zolotoyabko, “Anisotropic lattice distortions in the mollusk-made aragonite: a widespread phenomenon,” *J. Struct. Biol.*, vol. 153, no. 2, pp. 145–50, 2006.

[42] H. Tong, W. Ma, L. Wang, P. Wan, J. Hu, and L. Cao, “Control over the crystal phase, shape, size and aggregation of calcium carbonate via a L-aspartic acid inducing process,” *Biomaterials*, vol. 25, no. 17, pp. 3923–9, 2004.

[43] H. Wei, Q. Shen, Y. Zhao, Y. Zhou, D. Wang, and D. Xu, “Effect of anionic surfactant–polymer complexes on the crystallisation of calcium carbonate,” *J. Cryst. Growth*, vol. 264, no. 1–3, pp. 424–429, 2004.

[44] E. Altay, T. Shahwan, and M. Tanoğlu, “Morphosynthesis of CaCO3 at different reaction temperatures and the effects of PDDA, CTAB, and EDTA on the particle morphology and polymorph stability,” *Powder Technol.*, vol. 178, no. 3, pp. 194–202, 2007.

[45] H. Wei, Q. Shen, Y. Zhao, Y. Zhou, D. Wang, and D. Xu, “On the crystallisation of calcium carbonate modulated by anionic surfactants,” *J. Cryst. Growth*, vol. 279, no. 3–4, pp. 439–446, 2005.

[46] H. Imai, N. Tochimoto, Y. Nishino, Y. Takezawa, and Y. Oaki, “Oriented Nanocrystal Mosaic in Monodispersed CaCO 3 Microspheres with Functional Organic Molecules,” *Cryst. Growth Des.*, vol. 12, no. 2, pp. 876–882, 2012.

[47] S. S. Wang, A. Picker, H. Cölfen, and A. W. W. Xu, “Heterostructured Calcium Carbonate Microspheres with Calcite Equatorial Loops and Vaterite Spherical Cores,” *Angew. Chemie Int. Ed.*, vol. 52, no. 24, pp. 6317–6321, 2013.

[48] G. Yan, L. Wang, and J. Huang, “The crystallisation behavior of calcium carbonate in ethanol/water solution containing mixed nonionic/anionic surfactants,” *Powder Technol.*, vol. 192, no. 1, pp. 58–64, 2009.

[49] C. Y. Tai and F. B. Chen, “Polymorphism of CaCO3, precipitated in a constant-composition environment,” *AIChE J.*, vol. 44, no. 8, pp. 1790–1798, 1998.

[50] S. A. Parsons, B. L. Wang, S. J. Judd, and T. Stephenson, “Magnetic treatment of calcium carbonate scale—effect of pH control,” *Water Res.*, vol. 31, no. 2, pp. 339–342, 1997.

# Chapter 2: Literature review

## 2.1 Synthesis of hollow nano and micromaterials by templating

### 2.1.1 Various classes of templates, their properties, advantages and disadvantages

In recent years, the precise control of the dimensions (size, shape, channel replication, pores, and spatial arrangement) of nano- and micro-structured materials has become increasingly important to materials science in order to improve the physicochemical properties of the desired materials[1]–[4]. A high degree of control of the size, shape and pore sizes has been achieved by employing pre-existing (or pre-synthesised) materials with desired features as templates in the synthesis of materials with unique morphologies and properties[1], [5]. These types of templated syntheses of nano- and micro-structured materials have typically been carried out through the following steps: (1) selection and/or preparation of an appropriate template, (2) synthesis of the target material using the template, and (3) removal of the template (if necessary)[4]. Generally speaking, a template is any material which possesses the specific dimensions of interest. Templates are typically classed based on their physicochemical properties, and their templating methods (Figure 2.1)[2]. With that being said, there are a vast range of materials which can be selected as templates. These can be naturally occurring materials such as inorganic minerals, or they can be synthetic materials.

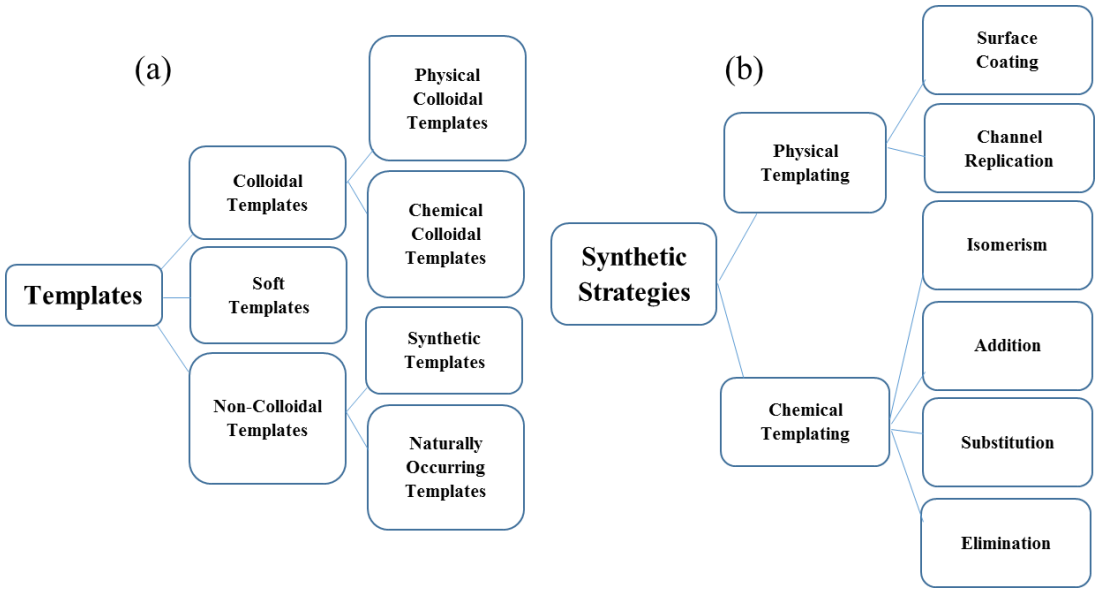



Figure 2. 1. Classification of templates: (a) Types of templates, (b) Synthetic strategies[2].

There are generally two main types of templates: colloidal, and non-colloidal [2], [6]. Colloidal templates may be further branched into hard colloidal physical templates, hard colloidal chemical templates, and soft colloidal templates. Hard colloidal physical templates are one of the most effective templates in the synthesis of hollow structured materials with well-defined pore structures[7], [8]. These are typically solid colloidal particles such as silica particles, synthesised by the Stöber method[9] (or the modification of this method). This method is generally based on the ammonia-catalysed hydrolysis of tetraethyl orthosilicate (TEOS) in an aqueous ethanol solution. The resultant as-synthesised silica particles have a spherical morphology with diameters ranging from 100 nm to a few microns[7], [9], [10]. This method is typically modified by the formation of an additional mesoporous layer of silica on top of the silica spheres by using a porogen in order to obtain a template with well-defined pore structures[5], [11].

Synthetic strategies for the synthesis of the desired target material (using hard colloidal physical templates), are usually carried out by physical templating (Figure 2.1) via surface coating and channel replication. Here the final material bares the pore dimensions of the template after its removal by chemical etching (depending on the chemical nature of the template)[12]. Attempts have been made to synthesize structured target materials by soft colloidal templates which can be easily removed without the need of chemical etching

methods[13], [14]. Soft colloidal templates are typically polymers, macro or microemulsions, micelles, and molecular assemblies[2]. For example, polyvinyl alcohol has been used as a soft colloidal template in the large scale hydrothermal synthesis of hollow carbon spheres (HCS) with high specific surface areas of 1036 $m^2/g$ using a phenolic resin as a carbon source[14]. The idea is that the polymer template collapses/decomposes under high calcination temperatures hence eliminating the template removal step. Similarly, polystyrene (PS) latex beads have been used to synthesize HCS using the hydrothermal method (Figure 2.2)[13]. (PS) latex beads can either be purchased or simply be made by the polymerisation of styrene monomers in a water emulsion catalysed by free radicals[13]. They typically have diameters of about 100 nm to a few microns.

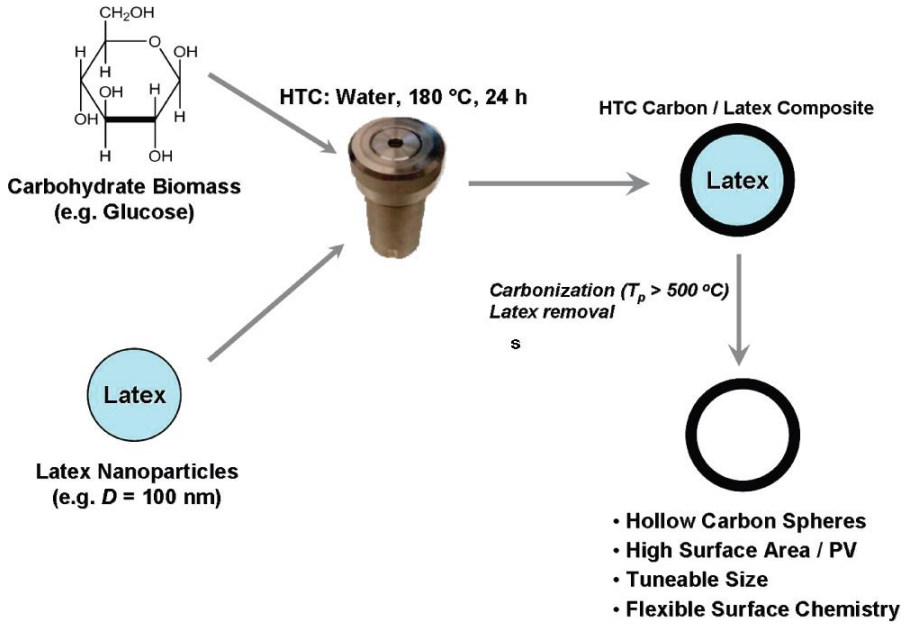



Figure 2. 2. Synthetic strategy for the hydrothermal carbonisation (HTC) of hollow carbon spheres using PS latex as a soft colloidal template and biomass as a carbon source[13].

Recent advances have been made to develop hollow structured materials with well-defined pores without the need of a preformed template[3]. Hard colloidal chemical templates do not only act as a mould during the synthesis of the target material, they are also chemically transformed into the resultant target material[3], [6]. These are typically self-templating reactions occurring via Ostwald ripening or the Kirkendall effect[6]. The advantages of this method are that it does not require the preparation of a template, and the template removal stage

is eliminated[3]. For example, mesoporous hollow silica spheres have been prepared by the self-templating method without the need of a preformed solid template[6], [15].

Another class of templates which has been increasingly explored in the synthesis of structured nano and micro-materials is non-colloidal[2]. Non-colloidal templates are synthetic materials commonly derived from non-colloidal syntheses such as: 1D nanowires and nanotubes synthesised by catalytic chemical vapour deposition (CVD) or electrospinning, and porous materials like zeolites, or they can be naturally occurring materials with intricate morphologies like diatoms, onto which target materials can be deposited[2]. For example, the synthesis of $ZrO_2$ nanotubes have been synthesised using carbon nanotubes as a template, via the sol-gel method[16]. Zeolite-templated carbon materials prepared by gas phase CVD have been prepared and used for hydrogen storage due to the intricate zeolite pores embedded on the resultant target material[17]. Hierarchically structured micro-carbon materials have been synthesised using naturally occurring diatoms as templates[18]. Although non-colloidal templates give target materials with well-defined structural dimensions, little can be done in manipulating the morphology of the template.

### 2.1.2 The templated synthesis of hollow nano and microcarbon materials

#### 2.1.2.1 Different types of synthetic strategies to obtain hollow carbon materials

Functional carbon nano and micromaterials are one of the most extensively applied materials in various scientific fields and technological applications, including areas such as: drug delivery [19], waste-water treatment[20], catalyst supports[21], energy storage[22]–[24], and gas storage[25]. In particular HCS, ranging in size from nanometers[14] to micrometers[10], have received increasing interest over the past few years owing to their promising physico-chemical properties such as: low density, chemical inertness, high surface area, high electron density and surface permeability[1].

The precise controlled synthesis of well-ordered and porous advanced functional HCS has been achieved through the use of pre-synthesised structured templates[5], as shown schematically in Figure 2.3.

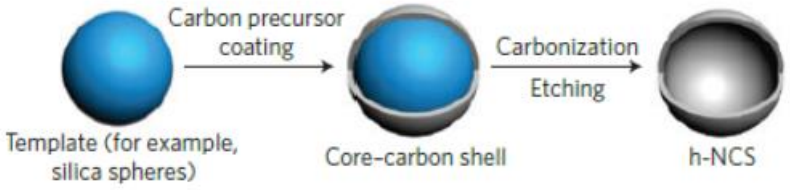



Figure 2. 3. General schematic for the templated synthesis of HCS[1].

This can be performed under gas-phase chemical vapour deposition (CVD) wherein a carbon source (i.e. acetylene gas or bubbled toluene) is decomposed at high temperatures and consequently deposit on the template, followed by the removal of the template[10]. Alternatively HCS can be synthesised by the hydrothermal method in a high pressure autoclave reactor, wherein a biomass monomer (such as glucose) is catalytically polymerised in solution in the presence of a template, and subsequently calcined at high temperature to carbonize the polymeric coating[13], [26]. CVD is typically advantageous in that the HCS are highly graphitic, however hydrothermally prepared HCS typically have higher specific surface areas due to their high porosity, as opposed to CVD synthesised HCS[10].

There are two main strategies used in the templated synthesis of HCS: (1) Hard templating, and (2) Soft templating, (as shown in Figure 2.4)[1].

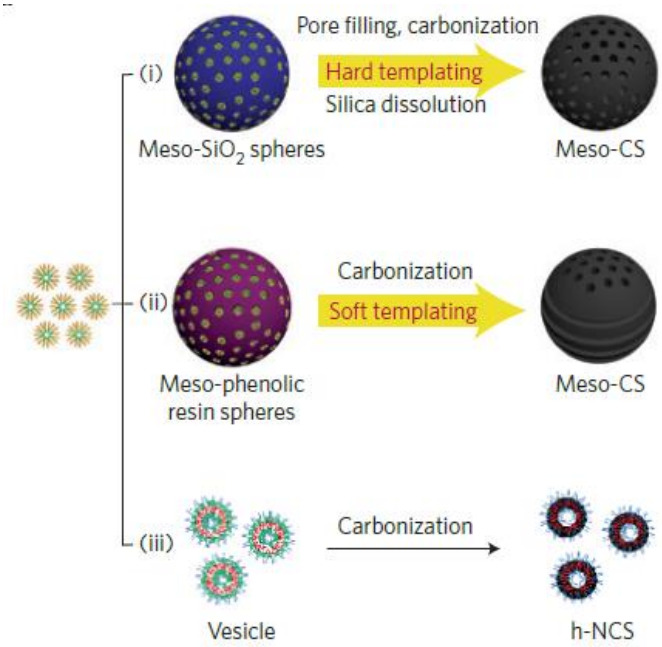



Figure 2. 4. Templating strategies, based on the nature of the template, for the synthesis of HCS[1].

Again these colloidal templates were categorised according to their (chemical) nature, just as described earlier in the review. For instance, hard templating methods are typically based on mesoporous silica spheres synthesised by the modified Stöber method[10], [11]. In this method an extra mesoporous layer of silica is grown on the surface on the Stöber spheres using a porogen, such as cetyltrimethylammonium bromide (CTAB), in order to increase the porosity of the template so that channel replication may be achieved during carbon coating.

For example, Mokaya's group performed a study where they compared mesoporous micro-HCS, which were synthesised using a silica template by the conventional CVD method under a temperature range of 950–1100 °C, and HCS that were synthesised by the hydrothermal method and subsequently annealed at 900 °C[10]. Here they observed, through powder X-ray (PXRD) analyses, that the crystallinity of the HCS synthesised by CVD increased with increased reaction temperature. However the specific Brunauer, Emmett and Teller (BET) surface area of the as-synthesised HCS (from CVD) decreased with increased reaction temperature. HCS from hydrothermal synthesis generally had higher BET surface area and pore volume due to the use of a porogen during the liquid-phase polymerisation of the carbon precursor in the high-pressure autoclave hydrothermal reactor. These observations were attributed to the decrease in the pore volumes of the highly crystalline CVD HCS were consistent with the results obtained by Coville's group when HCS synthesised by CVD and hydrothermal synthesis were compared[11].

Soft templating methods for hollow carbon materials are generally based on the use of sacrificial templates or self-templating techniques which either eliminate the requirement of a template (self-template) or the step pertaining to its chemical removal[13], [14], [26], [27]. This method makes use of polymer beads (such as polystyrene), self-assembled micelles or vesicles as sacrificial templates in the synthesis of HCS (Figure 2.4). Syntheses are typically carried out by the hydrothermal method, followed by calcination of the material in a furnace to crystallise the polymeric coated carbon and burn off the template in the process. For example, White *et al*. demonstrated the ability to synthesize HCS carbon spheres (with diameters ranging between 100 and 130 nm) by hydrothermal methods using PS latex beads and glucose as a carbon source, followed by removal of the template by carbonisation[13]. These HCS had specific BET surface areas of about 400 $m^2/g$. Similarly, Fu *et al*. have also reported on the

hydrothermal synthesis of HCS where a sacrificial PS template was used and poly-cyclotriphosphazene-co-4,4-sulfonyldiphenol was employed as the carbon source [27].

Although soft templating methods are quite advantageous in the way that they frequently do not require the removal of a template or a template itself, the HCS that result often lack the structural integrity and uniformity of hierarchically structured materials that are synthesised by hard templating. These HCS also suffer from low specific BET surface areas compared to their hard templated HCS counterparts. However, an attempt has been made to obtain high surface area HCS by the soft templating method using polyvinyl alcohol micelles as templates and a phenolic resin as the carbon precursor[14]. Using this method, HCS with average diameters of 1.1 mm, average shell thickness of about 0.2 mm, and high surface areas of 1036 $m^2/g$ were successfully synthesised.

#### 2.1.2.2 Beyond the Stöber method paradigm

The Stöber method has been quite successful in the synthesis of well-ordered, monodisperse and porous HCS, as has been discussed in this review. However, the limitations brought by the need for employment of harsh chemicals like hydrofluoric acid (HF) in the template removal step, calls for more environmentally benign colloidal templating methods to be invoked in order to improve on the already successful hard templating technique.

Calcium carbonate ($CaCO_3$) is one of the most abundant biominerals on earth[28], which precipitates under basic conditions and dissolves under mildly acidic conditions. Synthetically, $CaCO_3$ can be shaped into a variety of morphologies using additives such as organic molecules or inorganic ions[29], [30]. This makes it an ideal template candidate for the synthesis of HCS. However, the thermal decomposition of $CaCO_3$ at high temperatures (typically 700–800 °C)[31] into $CO_2(g)$ and $CaO(s)$ could potentially be a limitation if this material is to be used as a template in the high temperature CVD synthesis of HCS. Nonetheless it is a material of interest.

## 2.2 Morphogenesis and polymorphism of $CaCO_3$

### 2.2.1 Factors influencing the nucleation and growth of $CaCO_3$

Solution-based precipitation of $CaCO_3$ has been extensively studied in the area of crystal growth and design by biomineralisation[28]. Biomineralisation is a process by which inorganic

minerals such as mollusc shells and coccolith structures, are crystallised by natural organisms [32]–[34]. Biomimetic crystallisation is the *in vitro* formation of biominerals by using organic additives such as the ones present in the formation of natural shells[35]. This has led to studies in the understanding the formation and transformation mechanism of calcium carbonate in water since the 1960-80s [36], [37].

Anhydrous calcium carbonate exists in three different polymorphs: vaterite, aragonite, and calcite, in their order of increasing thermodynamic stability[38]. Crystal structures of the three polymorphs of $CaCO_3$ with their bulk and surface lattice energies have been reported as:

1) rhombohedral crystal structure – calcite,
2) hexagonal crystal structure – vaterite, and
3) orthorhombic crystal structure – aragonite[39].

Different polymorphs can exist or co-exist under different crystallisation conditions. Understanding the nucleation and crystal growth mechanism of $CaCO_3$ offers a powerful tool which can be used to manipulate the morphological and polymorphic transformation. For instance, it has been reported that calcite and vaterite co-exist at temperatures between 10-30 °C, while all three polymorphs co-exist at intermediate temperatures of 40-50 °C[40]. Lastly studies have shown that aragonite and calcite co-exist at temperatures of 60 °C and above[40]. The abundance of these polymorphs of calcium carbonate, as a function of temperature in water (in the absence of additives), is shown in Figure 2.5.

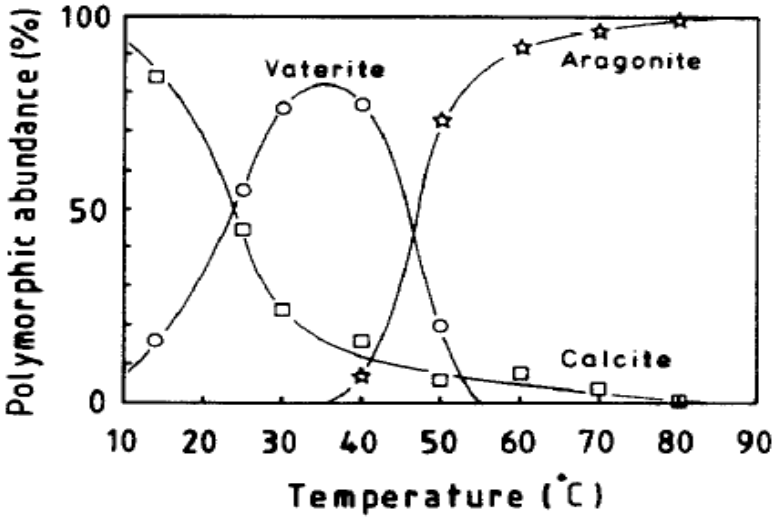



Figure 2. 5. The effect of temperature on the polymorphism of $CaCO_3$ in water.[36]

This may seem like a straight-forward way of manipulating polymorphism of $CaCO_3$. However biominerals in nature form under complex conditions with extremely highly crystallochemical specificity, resulting in highly ordered and complex crystal morphologies which are often difficult to produce synthetically[33], [34]. Various factors influence the crystallisation of $CaCO_3$ including the: incorporation of additives, synthesis temperature, pH, synthesis solvent during nucleation and process of crystal growth. Collectively these factors result in the inhibition or preferred growth of certain crystal facets by affecting the surface lattice energies of selected crystal planes, thereby favouring specific thermodynamically stable crystal morphologies[41].

Surface energy changes associated with these molecular interactions have been used in computational methods, such as Monte Carlo and molecular dynamics simulations, to study the most favoured or highest probable interactions between specific crystal facets and additive molecules or solvents in order to understand how the fundamental crystal structure's lattice parameters are modified to result in a specific crystal shape[42], [43]. This information has been used to predict the morphologies of crystals under specific growth conditions[41], [44]. For instance Leeuw and Parker have demonstrated an ability to predict, by atomic simulations, the favoured surface structures and morphologies for different $CaCO_3$ polymorphs[39]. In their study, they investigated the effect of molecular adsorption of water on the low-index surfaces of calcite, aragonite, and vaterite. Here they were able to show that for calcite the (104) surface was the most stable and that hydration had a stabilising effect on that surface[39]. Overall, using their simulations they found that the morphologies of the hydrated crystals (calcite, vaterite, and aragonite) were in good agreement with those of the synthetic morphologies, and their calculated bulk lattice energies reflected their thermodynamic stability[39].

The crystallisation of biogenic calcite in natural water is largely influenced by the presence of divalent cations. This has been the driving force to understand the effects of these divalent metals ions in the morphogenesis and polymorphism of $CaCO_3$[42], [45]. It has been suggested that crystallising $CaCO_3$ in the presence of magnesium ions ($Mg^{2+}$) could stabilise the amorphous calcium carbonate[46]–[48]. Nishino *et al*. demonstrated, through PXRD, that there was a significant shift to higher 2θ angles and a broadening of the (104) calcite diffraction peak (Figure 2.6) with an increase in the $Mg^{2+}/Ca^{2+}$ratio[49]. An increase in the $Mg^{2+}/Ca^{2+}$ratio during the nucleation and crystal growth of calcite has been suggested to be accompanied by anisotropic lattice distortions (elongation) along the c-axis[45].

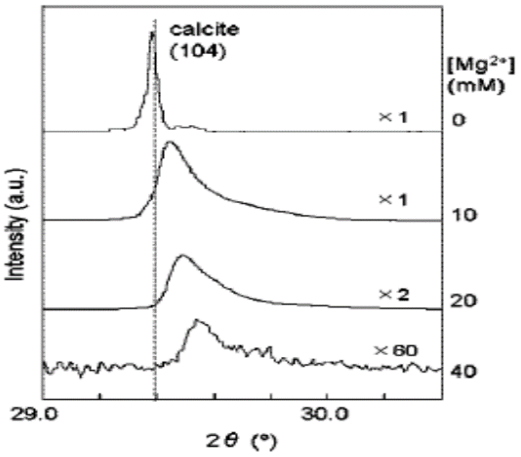



Figure 2. 6. PXRD patterns of $CaCO_3$ deposits formed with various $Mg^{2+}$ concentrations. As the $Mg^{2+}$ concentration was increased the (104) diffraction peak weakened and shifted to higher 2θ angle.[49]

Leeuw reported on molecular dynamics (MD) simulations of the growth inhibition effect of : iron ($Fe^{2+}$), magnesium ($Mg^{2+}$), cadmium ($Cd^{2+}$), and strontium ($Sr^{2+}$) on the crystal proliferation of calcite[42]. It was discovered from the MD simulation results that calcite augmentation was a slightly endothermic process in the absence of any impurity (on average +1.8 to +35 $kJ.mol^{-1}$), and the presence of impurity ions at the step edges impeded the crystal proliferation. The average enthalpies of the $CaCO_3$ growth process increased to +15 to +75 $kJ.mol^{-1}$, depending on the nature of the impurity ion. In her study, the MD simulations suggested that competing nucleation and growth of these impurity carbonates ($MCO_3$, where M= $Fe^{2+}$, $Mg^{2+}$, $Cd^{2+}$, and $Sr^{2+}$) at the calcite steps was initially a thermodynamically favourable process[42]. However, further incorporation of impurities became more endothermic with the increase in the concentration of these impurities, hence inhibiting further calcite growth[42]. These MD results were in good agreement with experimental results reported by Nishino *et al*. where an increase in $Mg^{2+}$ concentration resulted in the decrease in the crystallinity of the (104) diffraction peak of calcite, as previously seen in Figure 2.6[49].

Morphogenesis and polymorphism of $CaCO_3$ in pure or mixtures of solvents has perhaps been the most rapidly emerging method of biomimetic crystallisation of $CaCO_3$[50]–[56]. Reports have suggested that when alcoholic solvents have been used, these have resulted in the preferred formation of metastable polymorphs of $CaCO_3$ (mostly ACC and vaterite) by kinetic inhibition of the growth of the thermodynamically stable polymorph – calcite[51], [54], [57].

Kinetic studies by Manoli and Dalas showed that the rate of vaterite crystallisation, as a function of the relative solution supersaturation, in the presence of ethanol, diethylene glycol, and isopropanol was much higher in each of these alcohols than in the absence of any alcohol – supporting the kinetic inhibition argument[51].

Underpinned by the presence of biopolymers within the hierarchically structured shells of marine organisms[58], [59], polymeric organic molecules are by far the most explored forms of additives in the biomineralisation of $CaCO_3$[52], [60]–[73]. Of these, amphipathic block co-polymers, or the so-called double-hydrophilic block co-polymers, have been widely investigated[60], [72], [73]. These types of polymeric organic molecules (such as poly(ethylene glycol)-*block*-poly(methacrylic acid) (PEG-b-PMAA)) consist of hydrophilic and hydrophobic functional groups. These have been suggested to influence the crystal growth and polymorphism of $CaCO_3$ via molecular recognition, due to their ionic interaction with the calcium ions prior to crystallisation and selective surface binding of the organic functional motifs on specific growing crystal facets, thus resulting in systematic morphogenesis and polymorphism of the growing crystals by kinetic effects[60], [74].

Although these double-hydrophilic block co-polymers have proven to be successful at influencing the morphology of $CaCO_3$, they often lacked the crystallochemical specificity observed in natural marine biominerals due to their dual hydrophobic-hydrophilic nature, and thus have led to hetero-structured $CaCO_3$[70], [75]. Single or pure polymeric additives such as amino acids, have been used to influence the polymorphism and morphogenesis of $CaCO_3$[62], [67]. Kitano and Hood investigated the effect of different amino acids and their concentration on the polymorphism of $CaCO_3$[67]. In their study, it was observed that most of the amino acids that were not selective towards the crystallisation of calcite (as their concentration was increased) were in fact selective towards the vaterite polymorph (Figure 2.7). It was later shown by Density Functional Theory (DFT) and MD calculations by Okhrimenko *et al*. that the adsorption energies of alcohols on the calcite polymorph were higher than on the vaterite polymorph of $CaCO_3$, thus inhibiting further growth of calcite[76]. This again, reaffirms the kinetic inhibition model of polymorphic selection during the nucleation and growth of calcium carbonate in the presence of alcohols.

Another important factor in the controlled crystal growth of $CaCO_3$ in solution is the pH[60], [77]. Studies by Tai and Chen showed that $CaCO_3$ precipitated from solution at pH's ranging between 9-12[77]. In their study, they were able to demonstrate the polymorphic control of

$CaCO_3$ using varied pH conditions at different temperatures. Significantly, it was observed from their study that the effect of pH was most prominant at room temperature (i.e. 24 °C). The dependence of polymorphic distribution on pH when the solution temperature was maintained at 24 °C (without any additives) is shown in Figure 2.8[77].

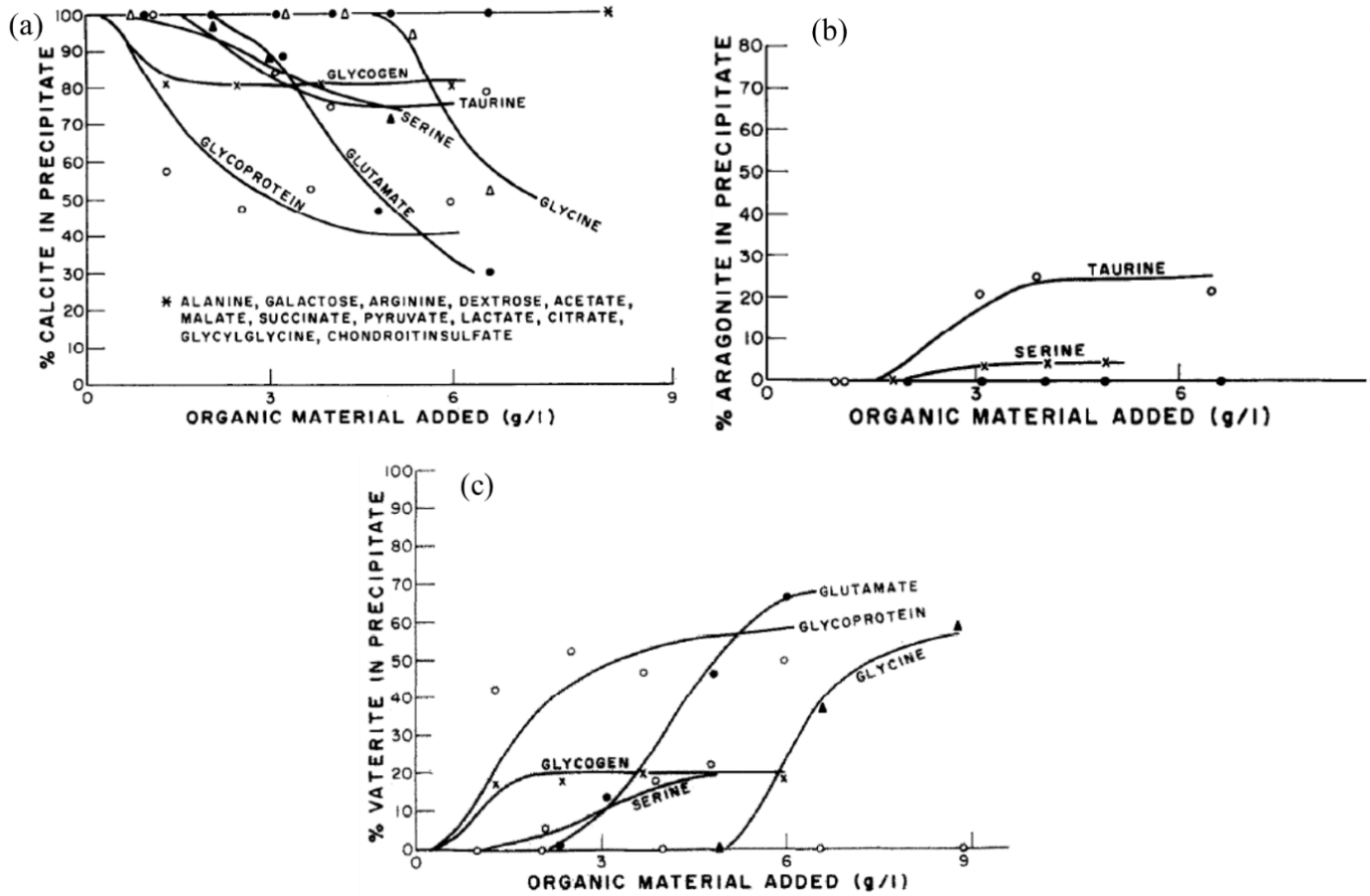



Figure 2. 7. The effect of different polymeric additives and their concentration on the polymorphism of $CaCO_3$. (a) Calcite selectivity. (b) Aragonite selectivity (had no effect: acetate, alanine, arginine, chondroitinsulfate, citrate, dextrose, galactose, glutamate, glycine, glycogen, glycoprotein, glycylglycine, lactate, malate, pyruvate, and succinate). (c) Vaterite selectivity (had no effect: acetate, alanine, arginine, chondroitinsulfate, citrate, galactose, lactate, malate, pyruvate, succinate, and taurine)[67].

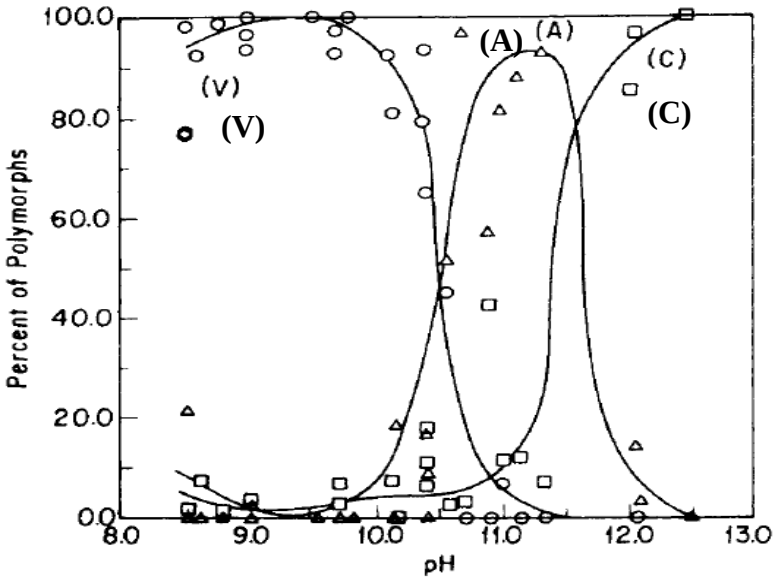



Figure 2. 8. Effects of pH on the polymorphism of $CaCO_3$ at 24 °C. Key: (V) – vaterite; (A) – aragonite; (C) – calcite[77].

However, the influence of pH may change in the presence of other additives, such as polymers. Cölfen and Qi have reported on the influence of pH on the morphology and polymorph of crystallised $CaCO_3$ in the presence of poly(ethylene glycol)-block-poly(methacrylic acid)[60]. Here it was interesting to note that the variation of pH drastically changed the morphology of the $CaCO_3$ i.e. decreasing the pH from 11 to 9 resulted in the formation of rod-like particles (c.a. 15 µm long), while a mixture of ellipsoidal particles and irregular aggregates were formed at pH 11[60]. Despite this, the PXRD results suggested that calcite remained the dominant polymorph throughout.

### 2.2.2 Studies on the calcium carbonate crystal growth mechanism

So far in this review, it can be seen that polymorphic and morphogenic control during crystal growth is really an ancillary system governed by the interplay between energetic and kinetic factors, and not a trivial system that can be manipulated by one factor; hence the same crystal can have many different shapes[28], [78], [79]. Therefore in general, energetically, the final shape/morphology of a crystal is that which minimizes the total surface free energy of the bulk crystal. Lower energy faces (and phases, in the case of crystals with different polymorphs) will always be favoured[78]. On the other hand, kinetically, the slowest growing face become more pronounced, and the fastest growing faces (and phases, in the case of crystals with different

polymorphs) either become small or disappear altogether[78]. Consequently, faces which are lower in energy tend to be the slowest in proliferation and preferentially expressed in the shape of the bulk crystal.

This has served as a rationalisation behind the Ostwald-Lussac law of phases[78], generally referred to as the Ostwald step rule, which states that: "A crystallisation system will go through a series of available metastable phases before finally forming the lowest free energy, stable phase"[79]. In the case of the crystallisation of $CaCO_3$, this will follow the sequence: amorphous $CaCO_3$ (ACC) followed by vaterite, aragonite, and finally calcite. This transition is believed to occur through dissolution of the precursor phase and precipitation of the more stable phase i.e. the so-called dissolution-reprecipitation mechanism[29], [79], [83]. However, this sequence can be altered by factors which can influence the kinetics and energetics of the crystallising system such as additives, as we have already discussed earlier in the review. Hence several researchers of the *in situ* nucleation and crystal growth processes have reported different pathways. For example, *in situ* PXRD studies by Rodriguez-Navarro *et al*. have suggested the formation of ACC and its transformation directly into calcite at room temperature[80]. By contrast *in situ* PXRD results by Rodriguez-Blanco *et al*. have suggested that the transformation of ACC into calcite occurs via vaterite formation at 7.5 °C[81], a mechanism which has also been reported by Nielsen *et al.* in their *in situ* TEM studies[82]. While differences in the suggested pathways do exist, most importantly, all of these researchers have agreed upon the dissolution-reprecipitation mechanism based on the general Ostwald step rule.

### 2.2.3 Crystal tectonics: Beyond the classical crystal growth model

The classical model of crystal growth postulates that crystallisation occurs by an ion-by-ion or single-molecule attachment to a critical nucleus where growth takes place via the amplification and enlargement of the unit-cell into a single bulk crystal without structural changes in the bulk, i.e. the bulk crystal resembles the symmetry of the unit-cell[83]. By contrast, if there is enough (kinetic) stabilisation of the preformed growing crystals by foreign additives (mostly organic molecules), the aggregation of these crystals into a bulk crystal of the most energetically favoured shape, may take place (Figure 2.9)[84]–[87].

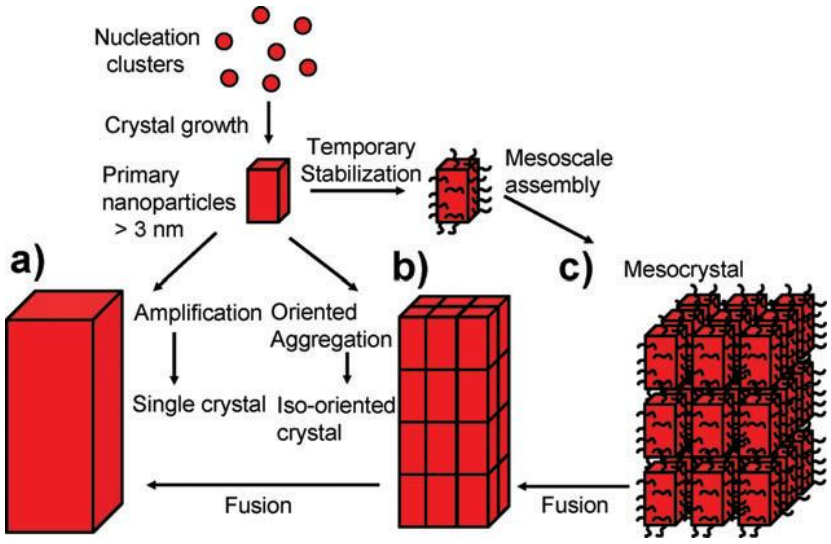



Figure 2. 9. Schematic representation of classical and non-classical models of crystallisation. (a) Classical crystallisation pathway, (b) oriented attachment of primary nanoparticles forming an iso-oriented crystal upon fusing, (c) mesocrystal formation via crystal tectonics of primary nanoparticles covered with organic molecules[88].

This has also been referred to as non-classical crystallisation. Hence, crystal tectonics is the directed or self-assembly of individual preformed crystals into complex, hierarchically structured bulk crystals[71], [84]. This term was first introduced by Stephen Mann, in an attempt to explain the formation of the intricate and complex morphologies of biominerals in nature, mostly those of $CaCO_3$[29], [84], [89]. These types of crystals were then referred to as mesocrystals by Helmut Cölfen[88], [90], [91], i.e. crystal clusters formed by the self-assembly of nanocrystals ranging between 1–1000 nm in size.

The complexity of the morphologies of biomineral mesocrystals found in nature, such as the coccolith structure[33], and their formation strategies could not be explained by the simple classical ion-by-ion meditated crystal growth, hence the non-classical crystal growth had to be invoked. This was due to the fact that the *in vivo* crystallochemical specificity and the sophisticated cellular processing of biominerals in biological organisms, which allows them to strictly control the energetic and kinetics of their biominerals, is still often difficult to fully understand and reproduce synthetically[28], [35]. In recent years, however, advances in the *in vitro* biomineralisation by directed self-assembly of nanostructures into complex hierarchal $CaCO_3$ structures[71], [92]–[94] has provided massive insights into new methods of growing

inorganic crystals, which could play a vital role in materials science, in particular the synthesis of advanced functional materials with superior properties.

### 2.2.4 Proposed advantages of crystal tectonics to materials science

Crystal tectonics of nanoparticles/nanocrystals into higher-ordered superstructures, which retain the size-dependant properties of their nano-sised building blocks, has been suggested to result in materials which have superior physicochemical properties compared to their single nanoparticle counterparts[86], [92], [95]. Open framework materials such as zeolites, have been tailored via crystal tectonics (self-assembly) with a high level of control of the structural dimensions required for a specific application[96]. Controlled synthesis of binary nanoparticle super-lattices has produced materials with better magnetic and conducting properties by using combinations of semiconducting, metallic and magnetic nanoparticle building blocks[97], [98].

Crystal tectonics is not only limited to the assembly of already preformed nanoparticles into hierarchical structures. *In situ* synthesis of nanoparticles and their controlled assembly into highly ordered structures has seen much interest in the current literature[99], [100]. Mesoporous metal oxides such as $TiO_2$, with high surface area and ordered pore structures have been synthesised by the hydrolysis of $TiCl_4$ in the presence of 1-butyl-3 methylimidazoliumtetrafluoroborate as an organic additive[100]. Jiang *et al*. have reported on the synthesis of multi-metallic mesoporous spherical platinum-based electrocatalysts by *in situ* organic surfactant-directed synthesis (as seen schematically in Figure 2.10)[99]. These catalysts were reported to perform better that the conventional single platinum nanoparticles in the methanol oxidation reaction[99].

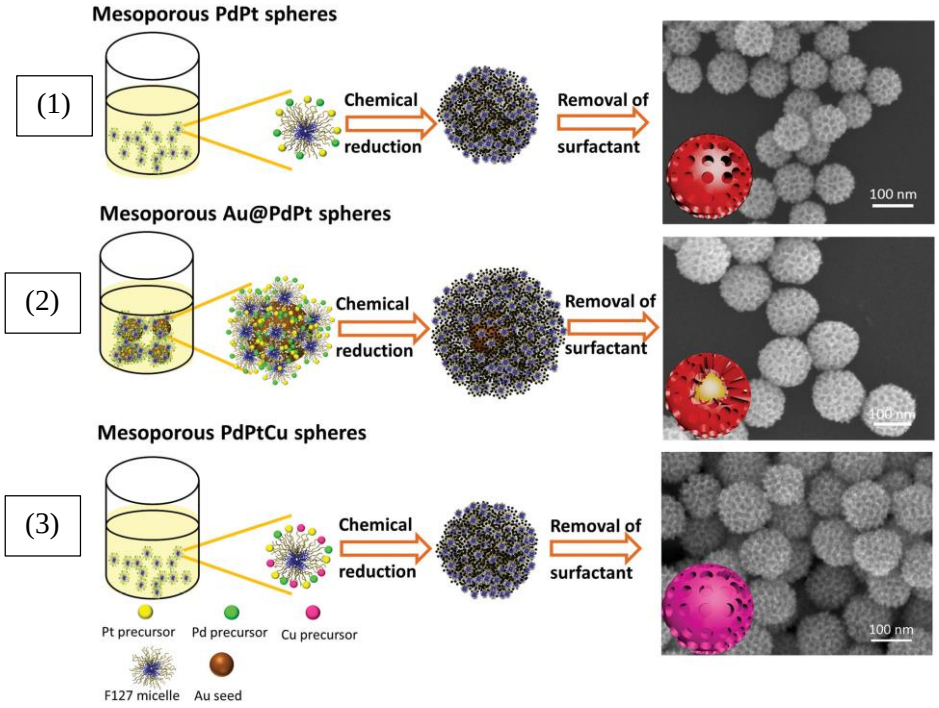



Figure 2. 10. Schematic of the synthesis of : (1) Mesoporous bimetallic PdPt spheres, (2) Mesoporous trimetallic Au@PdPt spheres, and (3) Mesoporous trimetallic PdPtCu spheres[99].

## 2.3 Conclusions

In this review, the different types of templates used in the templated synthesis of micro and nanostructured materials were discussed. A brief description of the synthesis of each type of template was given. The advantages and disadvantages of different types of templates and their synthetic strategies were explained. Brief examples of materials synthesised by different types of templates were given. A comprehensive review on the templated synthesis of micro and nanocarbon materials was also reported. The description of the hard and soft templating methods was provided. Soft templating methods are more advantageous in that they eliminate either the requirement of a template or the template removal step. However, hard templating techniques have been suggested to give the best hierarchically structured and monodisperse porous HCS. The limitations of this method were given, and thus an alternative template ($CaCO_3$) was suggested. Different methods for the morphogenesis and polymorphism of $CaCO_3$ were thoroughly discussed. Factors affecting the growth of $CaCO_3$ were given.

Different crystal growth mechanisms of $CaCO_3$ were also discussed. Lastly the benefits of crystal tectonics (self-assembly) to materials science were proposed.

## 2.4 References


[1] J. Liu, N. P. Wickramaratne, S. Z. Qiao, and M. Jaroniec, "Molecular-based design and emerging applications of nanoporous carbon spheres," *Nat. Mater.*, vol. 14, no. 8, pp. 763–774, 2015.

[2] Y. Liu, J. Goebl, and Y. Yin, "Templated synthesis of nanostructured materials.," *Chem. Soc. Rev.*, vol. 42, no. 7, pp. 2610–53, 2013.

[3] Q. Zhang, W. Wang, J. Goebl, and Y. Yin, "Self-templated synthesis of hollow nanostructures," *Nano Today*, vol. 4, no. 6, pp. 494–507, 2009.

[4] X. S. Zhao, F. Su, Q. Yan, W. Guo, X. Y. Bao, L. Lv, and Z. Zhou, "Templating methods for preparation of porous structures," *J. Mater. Chem.*, vol. 16, no. 7, p. 637, 2006.

[5] C. Liang, Z. Li, and S. Dai, "Mesoporous carbon materials: synthesis and modification," *Angew. Chem. Int. Ed. Engl.*, vol. 47, no. 20, pp. 3696–717, 2008.

[6] X. Fang, X. Zhao, W. Fang, C. Chen, and N. Zheng, "Self-templating synthesis of hollow mesoporous silica and their applications in catalysis and drug delivery," *Nanoscale*, vol. 5, no. 6, pp. 2205–18, 2013.

[7] Z. Qiao, B. Guo, A. J. Binder, J. Chen, G. M. Veith, and S. Dai, "Controlled Synthesis of Mesoporous Carbon Nanostructures via a 'Silica-Assisted' Strategy," *Nano Lett.*, vol. 13, no. 1, pp. 207–212, 2013.

[8] Y. Li and J. Shi, "Hollow-structured mesoporous materials: chemical synthesis, functionalization and applications," *Adv. Mater.*, vol. 26, no. 20, pp. 3176–205, 2014.

[9] W. Stöber, A. Fink, and E. Bohn, "Controlled growth of monodisperse silica spheres in the micron size range," *J. Colloid Interface Sci.*, vol. 26, no. 1, pp. 62–69, 1968.

[10] Y. Xia and R. Mokaya, "Synthesis of Ordered Mesoporous Carbon and Nitrogen-Doped Carbon Materials with Graphitic Pore Walls via a Simple Chemical Vapor

Deposition Method," *Adv. Mater.*, vol. 16, no. 17, pp. 1553–1558, 2004.

[11] T. N. Phaahlamohlaka, D. O. Kumi, M. W. Dlamini, L. L. Jewell, and N. J. Coville, "Ruthenium nanoparticles encapsulated inside porous hollow carbon spheres: A novel catalyst for Fischer–Tropsch synthesis," *Catal. Today*, 2016.

[12] F. Su, X. S. Zhao, Y. Wang, L. Wang, and J. Y. Lee, "Hollow carbon spheres with a controllable shell structure," *J. Mater. Chem.*, vol. 16, no. 45, p. 4413, 2006.

[13] R. J. White, K. Tauer, M. Antonietti, and M. Titirici, "Functional Hollow Carbon Nanospheres by Latex Templating," *J. Am. Chem. Soc.*, vol. 132, no. 49, pp. 17360–17363, 2010.

[14] G. Sun, K. Li, J. Wang, H. He, J. Wang, Y. Li, Y. Liu, and J. Gu, "A novel approach for fabrication of hollow carbon spheres with large size and high specific surface area," *Microporous Mesoporous Mater.*, vol. 139, no. 1–3, pp. 207–210, 2011.

[15] S. Shi, M. Wang, C. Chen, F. Lu, X. Zheng, J. Gao, and J. Xu, "Preparation of hydrophobic hollow silica nanospheres with porous shells and their application in pollutant removal," *RSC Adv.*, vol. 3, no. 4, p. 1158, 2013.

[16] C. N. R. Rao, B. C. Satishkumar, and A. Govindaraj, "Zirconia nanotubes," *Chem. Commun.*, vol. 2, no. 16, pp. 1581–1582, 1997.

[17] Z. Yang, Y. Xia, X. Sun, and R. Mokaya, "Preparation and Hydrogen Storage Properties of Zeolite-Templated Carbon Materials Nanocast via Chemical Vapor Deposition: Effect of the Zeolite Template and Nitrogen Doping," *J. Phys. Chem. B*, vol. 110, no. 37, pp. 18424–18431, 2006.

[18] X. Cai, G. Zhu, W. Zhang, H. Zhao, C. Wang, S. Qiu, and Y. Wei, "Diatom-Templated Synthesis of Ordered Meso/Macroporous Hierarchical Materials," *Eur. J. Inorg. Chem.*, vol. 2006, no. 18, pp. 3641–3645, 2006.

[19] L. Lacerda, A. Bianco, M. Prato, and K. Kostarelos, "Carbon nanotubes as nanomedicines: from toxicology to pharmacology," *Adv. Drug Deliv. Rev.*, vol. 58, no. 14, pp. 1460–70, 2006.

[20] Y. H. Li, Y. M. Zhao, W. B. Hu, I. Ahmad, Y. Q. Zhu, X. J. Peng, and Z. K. Luan, "Carbon nanotubes - the promising adsorbent in wastewater treatment," *J. Phys. Conf. Ser.*, vol. 61, pp. 698–702, 2007.

[21] G. Yu, B. Sun, Y. Pei, S. Xie, S. Yan, M. Qiao, K. Fan, X. Zhang, and B. Zong, “Fe x O y @C Spheres as an Excellent Catalyst for Fischer−Tropsch Synthesis,” *J. Am. Chem. Soc.*, vol. 132, no. 3, pp. 935–937, 2010.

[22] S. Yang, X. Feng, L. Zhi, Q. Cao, J. Maier, and K. Müllen, “Nanographene-constructed hollow carbon spheres and their favorable electroactivity with respect to lithium storage,” *Adv. Mater.*, vol. 22, no. 7, pp. 838–42, 2010.

[23] X. Chen, K. Kierzek, K. Wenelska, K. Cendrowski, J. Gong, X. Wen, T. Tang, P. K. Chu, and E. Mijowska, “Electrochemical characteristics of discrete, uniform, and monodispersed hollow mesoporous carbon spheres in double-layered supercapacitors.,” *Chem. Asian J.*, vol. 8, no. 11, pp. 2627–33, 2013.

[24] R. Kou, Y. Shao, D. Wang, M. H. Engelhard, J. H. Kwak, J. Wang, V. V. Viswanathan, C. Wang, Y. Lin, Y. Wang, I. A. Aksay, and J. Liu, “Enhanced activity and stability of Pt catalysts on functionalized graphene sheets for electrocatalytic oxygen reduction,” *Electrochem. commun.*, vol. 11, no. 5, pp. 954–957, 2009.

[25] S. Feng, W. Li, Q. Shi, Y. Li, J. Chen, Y. Ling, A. M. Asiri, and D. Zhao, “Synthesis of nitrogen-doped hollow carbon nanospheres for $CO_2$ capture,” *Chem. Commun. (Camb).*, vol. 50, no. 3, pp. 329–31, 2014.

[26] Z. Yang, Y. Zhang, J. Kong, S. Y. Wong, X. Li, and J. Wang, “Hollow Carbon Nanoparticles of Tunable Size and Wall Thickness by Hydrothermal Treatment of α-Cyclodextrin Templated by F127 Block Copolymers,” *Chem. Mater.*, vol. 25, no. 5, pp. 704–710, 2013.

[27] J. Fu, Q. Xu, J. Chen, Z. Chen, X. Huang, and X. Tang, “Controlled fabrication of uniform hollow core porous shell carbon spheres by the pyrolysis of core/shell polystyrene/cross-linked polyphosphazene composites,” *Chem. Commun. (Camb).*, vol. 46, no. 35, pp. 6563–5, 2010.

[28] S. Mann, *Biomineralization, Principles and Concepts in Bioinorganic Materials Chemistry*. New York: oxford university press, 2001.

[29] H. Cölfen and S. Mann, “Higher-order organization by mesoscale self-assembly and transformation of hybrid nanostructures,” *Angew. Chemie - Int. Ed.*, vol. 42, no. 21, pp. 2350–2365, 2003.

[30] S. Ouhenia, D. Chateigner, M. A. Belkhir, E. Guilmeau, and C. Krauss, “Synthesis of calcium carbonate polymorphs in the presence of polyacrylic acid,” *J. Cryst. Growth*, vol. 310, no. 11, pp. 2832–2841, 2008.

[31] G. Narsimhan, “Thermal decomposition of calcium carbonate,” *Chem. Eng. Sci.*, vol. 16, no. 1–2, pp. 7–20, 1961.

[32] B. Pokroy, A. N. Fitch, P. L. Lee, J. P. Quintana, E. N. Caspi, and E. Zolotoyabko, “Anisotropic lattice distortions in the mollusk-made aragonite: a widespread phenomenon,” *J. Struct. Biol.*, vol. 153, no. 2, pp. 145–50, 2006.

[33] J. Young, S. Davis, P. Bown, and S. Mann, “Coccolith ultrastructure and biomineralisation,” *J. Struct. Biol.*, vol. 126, no. 3, pp. 195–215, 1999.

[34] M. Marsh, “Regulation of $CaCO_3$ formation in coccolithophores,” *Comp. Biochem. Physiol. Part B Biochem. Mol. Biol.*, vol. 136, no. 4, pp. 743–754, 2003.

[35] S. Mann, “Biomineralization and biomimetic materials chemistry,” *J. Mater. Chem.*, vol. 5, no. 7, p. 935, 1995.

[36] T. Ogino, T. Suzuki, and K. Sawada, “The formation and transformation mechanism of calcium carbonate in water,” *Geochim. Cosmochim. Acta*, vol. 51, no. 10, pp. 2757–2767, 1987.

[37] Y. Kitano, “A Study of the Polymorphic Formation of Calcium Carbonate in Thermal Springs with an Emphasis on the Effect of Temperature,” *Bull. Chem. Soc. Jpn.*, vol. 35, no. 12, pp. 1980–1985, 1962.

[38] Q. Shen, H. Wei, L. Wang, Y. Zhou, Y. Zhao, Z. Zhang, D. Wang, G. Xu, and D. Xu, “Crystallization and Aggregation Behaviors of Calcium Carbonate in the Presence of Poly(vinylpyrrolidone) and Sodium Dodecyl Sulfate,” *J. Phys. Chem. B*, vol. 109, no. 39, pp. 18342–18347, 2005.

[39] N. H. De Leeuw and S. C. Parker, “Surface Structure and Morphology of Calcium Carbonate Polymorphs Calcite , Aragonite , and Vaterite : An Atomistic Approach,” *J. Phys. Chem. B*, vol. 5647, no. 97, pp. 2914–2922, 1998.

[40] J. Chen and L. Xiang, “Controllable synthesis of calcium carbonate polymorphs at different temperatures,” *Powder Technol.*, vol. 189, no. 1, pp. 64–69, 2009.

[41] F. Bruneval, D. Donadio, and M. Parrinello, “Molecular Dynamics Study of the Solvation of Calcium Carbonate in Water,” *J. Phys. Chem. B*, vol. 111, no. 42, pp. 12219–12227, 2007.

[42] N. H. de Leeuw, “Molecular Dynamics Simulations of the Growth Inhibiting Effect of $Fe^{2+}$ , $Mg^{2+}$ , $Cd^{2+}$ , and $Sr^{2+}$ on Calcite Crystal Growth,” *J. Phys. Chem. B*, vol. 106, no. 20, pp. 5241–5249, 2002.

[43] H. Xu, S. Zhou, X. Jin, and Y. Liu, “Monte Carlo simulation of the induction time and particle size distribution in the nucleation of calcium carbonate,” *Powder Technol.*, vol. 253, pp. 242–246, 2014.

[44] G. A. Tribello, F. Bruneval, C. Liew, and M. Parrinello, “A Molecular Dynamics Study of the Early Stages of Calcium Carbonate Growth,” *J. Phys. Chem. B*, vol. 113, pp. 11680–11687, 2009.

[45] Y. J. Han, L. M. Wysocki, M. S. Thanawala, T. Siegrist, and J. Aizenberg, “Template-Dependent Morphogenesis of Oriented Calcite Crystals in the Presence of Magnesium Ions,” *Angew. Chemie*, vol. 117, no. 16, pp. 2438–2442, 2005.

[46] Y. Liu, J. Jiang, M. Gao, B. Yu, L. Mao, and S. Yu, “Phase Transformation of Magnesium Amorphous Calcium Carbonate (Mg-ACC) in a Binary Solution of Ethanol and Water,” *Cryst. Growth Des.*, vol. 13, no. 1, pp. 59–65, 2013.

[47] M. M. M. G. P. G. Mantilaka, D. G. G. P. Karunaratne, R. M. G. Rajapakse, and H. M. T. G. a. Pitawala, “Precipitated calcium carbonate/poly(methyl methacrylate) nanocomposite using dolomite: Synthesis, characterization and properties,” *Powder Technol.*, vol. 235, pp. 628–632, 2013.

[48] G. Falini, M. Gazzanob, and A. Ripamonti, “Magnesium calcite crystallization from water-alcohol mixtures,” *Chem. Commun. (Camb).*, pp. 1037–1038, 1996.

[49] Y. Nishino, Y. Oaki, and H. Imai, “Magnesium-mediated nanocrystalline mosaics of calcite,” *Cryst. Growth Des.*, vol. 9, no. 1, pp. 223–226, 2009.

[50] H. S. Lee, T. H. Ha, and K. Kim, “Fabrication of unusually stable amorphous calcium carbonate in an ethanol medium,” *Mater. Chem. Phys.*, vol. 93, no. 2–3, pp. 376–382, 2005.

[51] F. Manoli and E. Dalas, “Spontaneous precipitation of calcium carbonate in the

presence of ethanol, isopropanol and diethylene glycol," *J. Cryst. Growth*, vol. 218, no. 2–4, pp. 359–364, 2000.

[52] X. H. Guo, S. H. Yu, and G. B. Cai, "Crystallization in a Mixture of Solvents by Using a Crystal Modifier: Morphology Control in the Synthesis of Highly Monodisperse $CaCO_3$ Microspheres," *Angew. Chemie*, vol. 118, no. 24, pp. 4081–4085, 2006.

[53] S. F. Chen, H. Cölfen, M. Antonietti, and S. H. Yu, "Ethanol assisted synthesis of pure and stable amorphous calcium carbonate nanoparticles," *Chem. Commun. (Camb).*, vol. 49, no. 83, pp. 9564–6, 2013.

[54] K. S. Seo, C. Han, J. H. Wee, J. K. Park, and J. W. Ahn, "Synthesis of calcium carbonate in a pure ethanol and aqueous ethanol solution as the solvent," *J. Cryst. Growth*, vol. 276, no. 3–4, pp. 680–687, 2005.

[55] S. F. Chen, S. H. Yu, J. Hang, F. Li, and Y. Liu, "Polymorph discrimination of $CaCO_3$ mineral in an ethanol/water solution: Formation of complex vaterite superstructures and aragonite rods," *Chem. Mater.*, vol. 18, no. 1, pp. 115–122, 2006.

[56] S. R. Dickinson and K. M. McGrath, "Switching between kinetic and thermodynamic control: calcium carbonate growth in the presence of a simple alcohol," *J. Mater. Chem.*, vol. 13, no. 4, pp. 928–933, 2003.

[57] R. Qi and Y. Zhu, "Microwave-Assisted Synthesis of Calcium Carbonate ( Vaterite ) of Various Morphologies in Water - Ethylene Glycol Mixed Solvents," *J. Phys. Chem. B*, vol. 110, pp. 8302–8306, 2006.

[58] B. Pokroy, A. N. Fitch, and E. Zolotoyabko, "The microstructure of biogenic calcite: A view by high-resolution synchrotron powder diffraction," *Adv. Mater.*, vol. 18, no. 18, pp. 2363–2368, 2006.

[59] S. Blank, M. Arnoldi, S. Khoshnavaz, L. Treccani, M. Kuntz, K. Mann, G. Grathwohl, and M. Fritz, "The nacre protein perlucin nucleates growth of calcium carbonate crystals," *J. Microsc.*, vol. 212, no. 3, pp. 280–291, 2003.

[60] H. Cölfen and L. Qi, "A systematic examination of the morphogenesis of calcium carbonate in the presence of a double-hydrophilic block copolymer," *Chemistry*, vol. 7, no. 1, pp. 106–116, 2001.

[61] A. Sugawara, T. Nishimura, Y. Yamamoto, H. Inoue, H. Nagasawa, and T. Kato,

"Self-Organization of Oriented Calcium Carbonate/Polymer Composites: Effects of a Matrix Peptide Isolated from the Exoskeleton of a Crayfish," *Angew. Chemie Int. Ed.*, vol. 45, no. 18, pp. 2876–2879, 2006.

[62] F. Manoli, J. Kanakis, P. Malkaj, and E. Dalas, "The effect of aminoacids on the crystal growth of calcium carbonate," *J. Cryst. Growth*, vol. 236, no. 1–3, pp. 363–370, 2002.

[63] S. F. Chen, S. H. Yu, T. X. Wang, J. Jiang, H. Cölfen, B. Hu, and B. Yu, "Polymer-Directed Formation of Unusual $CaCO_3$ Pancakes with Controlled Surface Structures," *Adv. Mater.*, vol. 17, no. 12, pp. 1461–1465, 2005.

[64] A. W. Xu, M. Antonietti, S. H. Yu, and H. Cölfen, "Polymer-Mediated Mineralization and Self-Similar Mesoscale-Organized Calcium Carbonate with Unusual Superstructures," *Adv. Mater.*, vol. 20, no. 7, pp. 1333–1338, 2008.

[65] H. Wei, Q. Shen, Y. Zhao, Y. Zhou, D. Wang, and D. Xu, "Effect of anionic surfactant–polymer complexes on the crystallization of calcium carbonate," *J. Cryst. Growth*, vol. 264, no. 1–3, pp. 424–429, 2004.

[66] K. Naka, Y. Tanaka, and Y. Chujo, "Effect of Anionic Starburst Dendrimers on the Crystallization of CaCO 3 in Aqueous Solution: Size Control of Spherical Vaterite Particles," *Langmuir*, vol. 18, no. 9, pp. 3655–3658, 2002.

[67] Y. Kitano and D. W. Hood, "The influence of organic material on the polymorphic crystallization of calcium carbonate," *Geochim. Cosmochim. Acta*, vol. 29, no. 1, pp. 29–41, 1965.

[68] P. Raiteri, R. Demichelis, J. D. Gale, M. Kellermeier, D. Gebauer, D. Quigley, L. B. Wright, and T. R. Walsh, "Exploring the influence of organic species on pre- and post-nucleation calcium carbonate," *Faraday Discuss.*, vol. 159, 2012.

[69] Y. Oaki, R. Adachi, and H. Imai, "Self-organization of hollow-cone carbonate crystals through molecular control with an acid organic polymer," *Polym. J.*, vol. 44, no. 6, pp. 612–619, 2012.

[70] S. S. Wang, A. Picker, H. Cölfen, and A. W. W. Xu, "Heterostructured Calcium Carbonate Microspheres with Calcite Equatorial Loops and Vaterite Spherical Cores," *Angew. Chemie Int. Ed.*, vol. 52, no. 24, pp. 6317–6321, 2013.

[71] R. Q. Song, H. Cölfen, A. W. Xu, J. Hartmann, and M. Antonietti, “Polyelectrolyte-directed nanoparticle aggregation: Systematic morphogenesis of calcium carbonate by nonclassical crystallization,” *ACS Nano*, vol. 3, no. 7, pp. 1966–1978, 2009.

[72] P. Kašparová, M. Antonietti, and H. Cölfen, “Double hydrophilic block copolymers with switchable secondary structure as additives for crystallization control,” *Colloids Surfaces A Physicochem. Eng. Asp.*, vol. 250, no. 1–3, pp. 153–162, 2004.

[73] L. He, Y. Zhang, L. Ren, Y. Chen, H. Wei, and D. Wang, “Double-Hydrophilic Polymer Brushes: Synthesis and Application for Crystallization Modification of Calcium Carbonate,” *Macromol. Chem. Phys.*, vol. 207, no. 7, pp. 684–693, Apr. 2006.

[74] S. Mann, “Molecular recognition in biomineralization,” *Nature*, vol. 332, no. 6160, pp. 119–124, Mar. 1988.

[75] G. Yan, L. Wang, and J. Huang, “The crystallization behavior of calcium carbonate in ethanol/water solution containing mixed nonionic/anionic surfactants,” *Powder Technol.*, vol. 192, no. 1, pp. 58–64, May 2009.

[76] D. V. Okhrimenko, J. Nissenbaum, M. P. Andersson, M. H. M. Olsson, and S. L. S. Stipp, “Energies of the adsorption of functional groups to calcium carbonate polymorphs: The importance of -OH and -COOH groups,” *Langmuir*, vol. 29, no. 35, pp. 11062–11073, 2013.

[77] C. Y. Tai and F. B. Chen, “Polymorphism of $CaCO_3$, precipitated in a constant-composition environment,” *AIChE J.*, vol. 44, no. 8, pp. 1790–1798, 1998.

[78] J. J. DeYoreo and P. G. Vekilov, “Principles of Crystal Nucleation and Growth,” *Rev. Mineral. Geochemistry*, vol. 54, no. 1, pp. 57–93, 2003.

[79] A. Navrotsky, “Energetic clues to pathways to biomineralization: precursors, clusters, and nanoparticles,” *Proc. Natl. Acad. Sci. U. S. A.*, vol. 101, no. 33, pp. 12096–12101, 2004.

[80] C. Rodriguez-Navarro, K. Kudłacz, Ö. Cizer, and E. Ruiz-Agudo, “Formation of amorphous calcium carbonate and its transformation into mesostructured calcite,” *CrystEngComm*, vol. 17, no. 1, pp. 58–72, 2015.

[81] J. D. Rodriguez-Blanco, S. Shaw, and L. G. Benning, “The kinetics and mechanisms

of amorphous calcium carbonate (ACC) crystallization to calcite, viavaterite.," *Nanoscale*, vol. 3, no. 1, pp. 265–271, 2011.

[82] M. H. Nielsen, S. Aloni, and J. J. De Yoreo, "*In situ* TEM imaging of $CaCO_3$ nucleation reveals coexistence of direct and indirect pathways," *Science*, vol. 218, no. 2004, pp. 213–218, 2013.

[83] W. K. Burton, N. Cabrera, and F. C. Frank, "The Growth of Crystals and the Equilibrium Structure of their Surfaces," *Philos. Trans. R. Soc. A Math. Phys. Eng. Sci.*, vol. 243, no. 866, pp. 299–358, 1951.

[84] S. Mann, S. Davis, S. R. Hall, M. Li, K. H. Rhodes, W. Shenton, S. Vaucher, and B. Zhang, "Crystal tectonics: Chemical construction and self-organization," *J. Chem. Soc. Dalt. Trans.*, no. 21, pp. 3753–3763, 2000.

[85] S. Babu Mukkamala and A. K. Powell, "Biomimetic assembly of calcite microtrumpets: crystal tectonics in action," *Chem. Commun. (Camb).*, no. 8, pp. 918–919, 2004.

[86] J. J. De Yoreo, P. U. P. A. Gilbert, N. A. J. M. Sommerdijk, R. L. Penn, S. Whitelam, D. Joester, H. Zhang, J. D. Rimer, A. Navrotsky, J. F. Banfield, A. F. Wallace, F. M. Michel, F. C. Meldrum, H. Colfen, and P. M. Dove, "Crystallization by particle attachment in synthetic, biogenic, and geologic environments," *Science*, vol. 349, no. 6247, pp. aaa6760–aaa6760, 2015. DOI: 10.1126/science.aaa6760

[87] A. P. Alivisatos, "BIOMINERALIZATION: Enhanced: Naturally Aligned Nanocrystals," *Science*, vol. 289, no. 5480, pp. 736–737, 2000.

[88] M. Niederberger and H. Colfen, "Oriented attachment and mesocrystals: Non-classical crystallization mechanisms based on nanoparticle assembly," *Phys. Chem. Chem. Phys.*, vol. 8, no. 28, p. 3271, 2006.

[89] S. Mann and G. A. Ozin, "Synthesis of inorganic materials with complex form," *Nature*, vol. 382, no. 6589, pp. 313–318, 1996.

[90] H. Cölfen and M. Antonietti, "Mesocrystals: Inorganic Superstructures Made by Highly Parallel Crystallization and Controlled Alignment," *Angew. Chemie Int. Ed.*, vol. 44, no. 35, pp. 5576–5591, 2005.

[91] R. Q. Song and H. Cölfen, "Mesocrystals-Ordered Nanoparticle Superstructures," *Adv.*

*Mater.*, vol. 22, no. 12, pp. 1301–1330, 2010.

[92] S. Mann, "Self-assembly and transformation of hybrid nano-objects and nanostructures under equilibrium and non-equilibrium conditions," *Nat. Mater.*, vol. 8, no. 10, pp. 781–792, 2009.

[93] T. Wang, H. Cölfen, and M. Antonietti, "Nonclassical crystallization: Mesocrystals and morphology change of $CaCO_3$ crystals in the presence of a polyelectrolyte additive," *J. Am. Chem. Soc.*, vol. 127, no. 10, pp. 3246–3247, 2005.

[94] Y. Y. Kim, A. S. Schenk, J. Ihli, A. N. Kulak, N. B. J. Hetherington, C. C. Tang, W. W. Schmahl, E. Griesshaber, G. Hyett, and F. C. Meldrum, "A critical analysis of calcium carbonate mesocrystals," *Nat. Commun.*, vol. 5, pp. 1–14, 2014.

[95] S. A. D. W. Shenton, "Directed Self-Assembly of Nanoparticles into Macroscopic Materials Using Antibody ± Antigen Recognition **," *Adv. Mater.*, pp. 1997–2000, 1999.

[96] M. Kumar, H. Luo, Y. Román-Leshkov, and J. D. Rimer, "SSZ-13 Crystallization by Particle Attachment and Deterministic Pathways to Crystal Size Control," *J. Am. Chem. Soc.*, vol. 137, no. 40, pp. 13007–13017, 2015.

[97] E. V Shevchenko, D. V Talapin, N. a Kotov, S. O'Brien, and C. B. Murray, "Structural diversity in binary nanoparticle superlattices," *Nature*, vol. 439, no. 7072, pp. 55–59, 2006.

[98] A. Dong, J. Chen, P. M. Vora, J. M. Kikkawa, and C. B. Murray, "Binary nanocrystal superlattice membranes self-assembled at the liquid-air interface," *Nature*, vol. 466, no. 7305, pp. 474–477, 2010.

[99] B. Jiang, C. Li, M. Imura, J. Tang, and Y. Yamauchi, "Multimetallic Mesoporous Spheres Through Surfactant-Directed Synthesis," *Adv. Sci.*, vol. 2, no. 8, p. n/a–n/a, Aug. 2015. DOI: 10.1002/advs.201500112

[100] Y. Zhou and M. Antonietti, "Synthesis of Very Small $TiO_2$ Nanocrystals in a Room-Temperature Ionic Liquid and Their Self-Assembly toward Mesoporous Spherical Aggregates," *J. Am. Chem. Soc.*, vol. 125, no. 49, pp. 14960–14961, 2003.

# Chapter 3: Experimental and characterisation procedures for the synthesis of calcium carbonate and hollow carbon microspheres

## 3.1 Method for synthesising $CaCO_3$

### 3.1.1 Chemicals

All chemicals were of analytical grade. Calcium chloride, ammonium carbonate, polyethylene glycol (Mw 200), poly (4-styrenesulfonic acid) (PSSA) $M_w$ ~75 000, 18 wt. % in $H_2O$, methanol (CP), ethanol (CP), isopropanol (AR) were purchased from Sigma-Aldrich. 2-Butanol (98 %) and sodium hydroxide pellets were purchased from Merck (Pty) Ltd South Africa. The ammonia solution of 25 %, hydrochloric acid (HCl) of 32 %, dimethyl sulfoxide (CP) (DMSO), and dimethylformamide (CP) (DMF) were all purchased from ACE associated chemical enterprises. All chemicals were used without any further purification.

### 3.1.2 General synthesis of $CaCO_3$

It has been reported that the pH, polymer type, polymer concentration, initial precursor salt concentration and reaction temperature all have a significant influence in the calcium carbonate polymorph and morphology that is produced [1], [2]. These variables were changed during synthesis to see how they affected the morphology and polymorph of the as-synthesised calcium carbonate ($CaCO_3$) particles. For the sake of convenience, specific reaction conditions are discussed in the relevant results chapters.

## 3.2 Experimental procedure for hollow carbon spheres synthesis

### 3.2.1 Gases

Both acetylene Technical (99.9%) and argon Baseline 5.0 (99.9%) gases used in the Chemical Vapour Deposition (CVD) were purchased from AFROX (African Oxygen) Ltd. The flow rates of the gases were kept at 100 ml/min for the duration of the CVD reaction.

### 3.2.2 Chemical Vapour Deposition (CVD) reactor set-up

The synthesis of carbon coated $CaCO_3$ microspheres was carried out by atmospheric pressure CVD (Figure 3.1). A mass of 2 g of $CaCO_3$ microspheres were placed inside a quartz boat in the centre of a quartz tube and then inside a horizontal temperature-controlled tube furnace. The furnace temperature was ramped to a desired reaction temperature (e.g. 600 ˚C, 700 ˚C or 800 ˚C) at a heating rate of 10 ˚C/min, while flowing argon gas at a constant flow rate of 100 ml/min. After the furnace was heated to the desired temperature, the argon gas flow was stopped and a constant 100 ml/min flow of acetylene (the carbon source) was introduced into the reaction chamber for 90 minutes. After the reaction, the products were allowed to cool to room temperature under the constant 100 ml/min flow of argon. The resultant products were then treated with pure acetic acid for 24 hrs in an attempt to remove the calcium carbonate microspherical template in an attempt to produce hollow carbon microspheres.

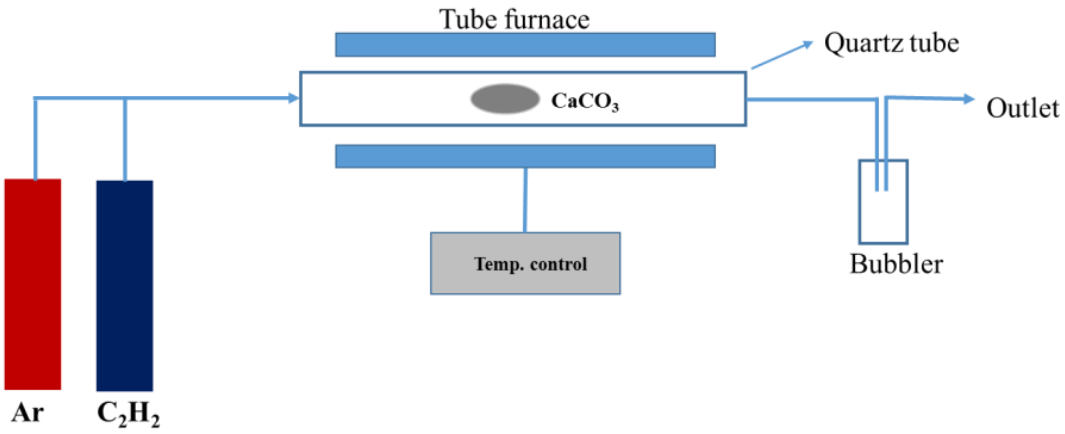



Figure 3. 1. Horizontal CVD set up.

## 3.4 Characterisation techniques

The following techniques were used to probe the physical and chemical properties (i.e. thermal stability, morphology and topography, surface area, etc.) of the synthesised materials in order to understand the synthetic process and hence select the best conditions to enable the most useful products.

### 3.4.1 Transmission electron microscopy (TEM)

TEM micrographs were obtained using an FEI Tecnai T12 Transmission Electron Microscope (Oregon, USA) operated at 120 kV fitted with a TVIPS-TEM-Cam F416 retractable transmission electron microscope camera (GmbH, Germany). Samples were suspended in methanol or deionised water and ultra-sonicated for 30 minutes, and then a drop was added on to a copper grid using a pipette and dried prior to imaging.

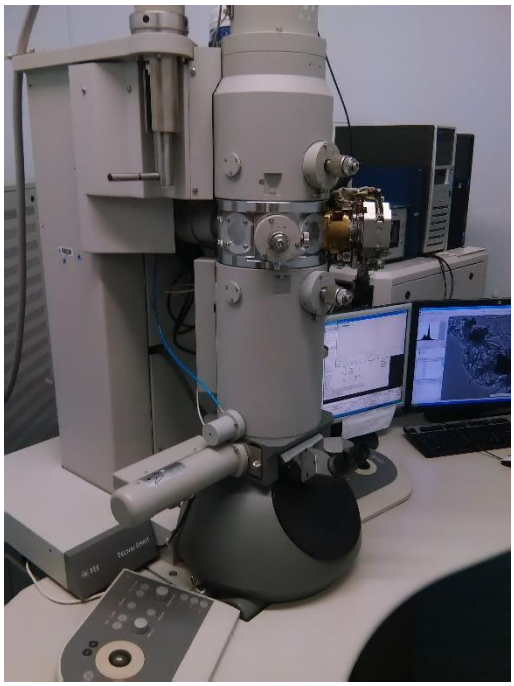


Figure 3. 2. FEI Tecnai T12 transmission electron microscope.

### 3.4.2 Powder X-ray diffraction

Powder X-ray diffraction (PXRD) patterns were obtained using a Bruker D2 PHASER desktop diffractometer equipped with a LYNXEYE PSD detector (set to measure a 5° 2θ angular range), 2.5° primary and secondary beam Soller slits, and Co X-ray micro-source (Kα with λ = 1.78897 Å) operated at 30 kV and 10 mA. The goniometer radius of the diffractometer was 70.7 mm. The instrument was also fitted with a secondary beam Fe filter to attenuate Kβ radiation and a 3 mm air-scatter slit. Diffraction data were collected in the 2θ range 10-90° in 0.0260° steps and at a count time of 0.5 sec/step.




Figure 3. 3. Bruker D2 PHASER desktop powder X-ray diffractometer.

### 3.4.3 Laser Raman spectroscopy

Laser Raman spectra were acquired using a Horiba Jobin-Yvon LabRAM HR Raman spectrometer with an Olympus BX41 optical microscope attachment. The excitation wavelength of 514.5 nm from an argon ion laser was directed onto the sample particles using a 100x objective (NA=0.90). The backscattered light was dispersed via a 600 lines $mm^{-1}$ grating onto a liquid nitrogen cooled CCD detector and the data was captured using LabSpec 5 software. The incident laser power was about 0.5 mW at the sample.

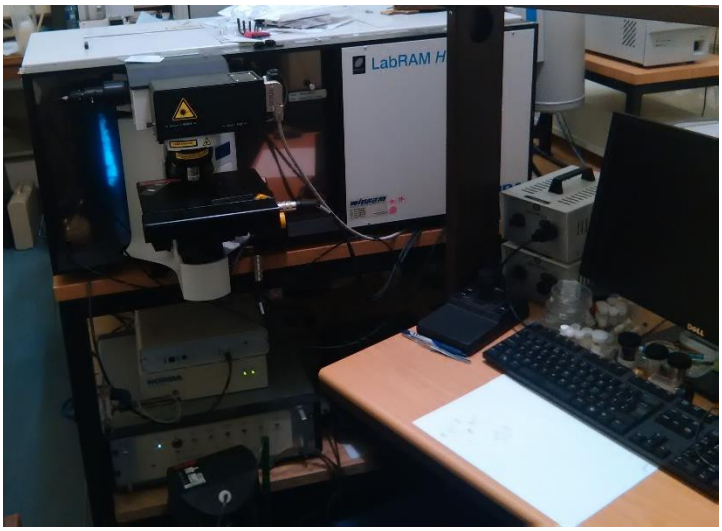



Figure 3. 4. Horiba Jobin-Yvon LabRAM HR Raman spectrometer.

### 3.4.4 Scanning electron microscopy

Scanning electron microscopy (SEM) micrographs were obtained using the FEI Nova Nanolab 600 FIB/SEM microscope, equipped with an E-T detector, at an accelerating voltage of 30 kV. For SEM analysis, samples were mounted on double sided carbon tape (SPI Supplies, West Chester, PA, USA) which was mounted on 35 mm aluminium stubs (SPI Supplies, West Chester, PA, USA). The mounted samples were then sputter coated with a 5 nm carbon layer prepared by an Emitech 950x Carbon Vacuum Evaporator (Quorum Technologies; Ashford, Kent, UK), and with a 5 nm gold-palladium layer prepared by an Emitech 550x Sputter Coater (Quorum Technologies; Ashford, Kent, UK) using a gold-palladium target from Electron Microscopy Sciences (EMS; Hatfield, PA, USA) prior to imaging.

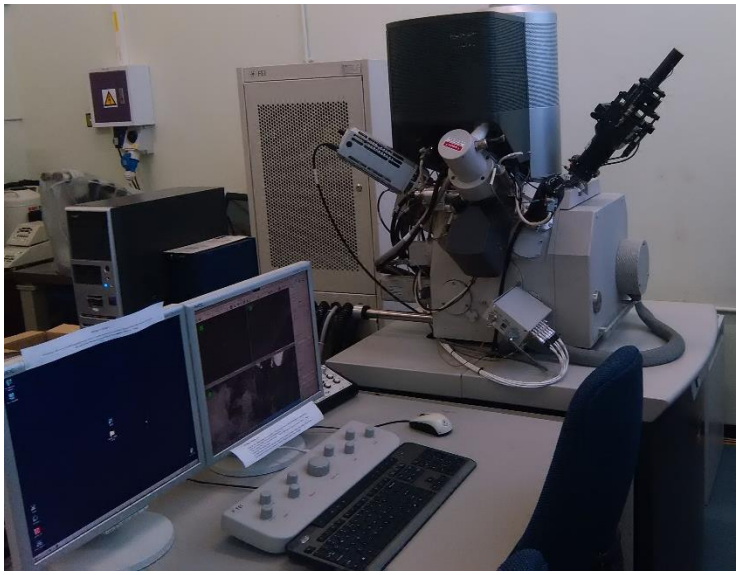


Figure 3. 5. FEI Nova Nanolab 600 FIB/SEM microscope.

### 3.4.5 Brunauer-Emmet and Teller surface area measurement

A Micromeritics Tristar Surface area and Porosity analyser was used, to determine the surface areas and porosities of the materials. Sample with mass of 0.2 g was degassed in nitrogen at 150 °C for 4 hrs prior to analysis using a Micromeritics flow Prep 060, sample degas system.




Figure 3. 6. Micromeritics Tristar Surface area and Porosity analyser.

### 3.4.6 Thermogravimetric analyses

A Perkin Elmer STA 4000 Simultaneous Thermal Analyser was used for thermal analysis of all samples in air Technical (99.9%) and nitrogen Baseline 5.0 (99.9%), at a constant heating rate of 10 ˚C/min in the temperature range of 30 - 900 ˚C. An approximate sample mass of 10 mg was used for the analysis with 20 mL/min flow rate of air.



Figure 3. 7. Perkin Elmer STA 4000 Simultaneous Thermal Analyser.

## 3.5 References

[1] Y. Kitano and D. W. Hood, “The influence of organic material on the polymorphic crystallisation of calcium carbonate,” *Geochim. Cosmochim. Acta*, vol. 29, no. 1, pp. 29–41, 1965.

[2] A. J. Xie, C. Y. Zhang, Y. H. Shen, L. G. Qiu, P. P. Xiao, and Z. Y. Hu, “Morphologies of calcium carbonate crystallites grown from aqueous solutions containing polyethylene glycol,” *Cryst. Res. Technol.*, vol. 41, no. 10, pp. 967–971, 2006.

# Chapter 4: Morphogenesis and polymorphism of calcium carbonate in binary polar aprotic-protic solvent mixtures

## 4.1 Introduction

Crystallisation behaviour of $CaCO_3$ has been one of the most widely studied biomineralisation processes[1]–[18]. This is due to the vast abundance of $CaCO_3$ as a biomineral in nature, its peculiar biomineralisation behavior in biological systems such as nacre shells,[19], [20] and coccolith spheres,[21], [22] its industrial relevance (e.g. as a filler for paint and paper),[23] and its crystallisation in water which results in lime scaling in water pipes[24], [25]. The precise control of the biomineralisation of $CaCO_3$ by living organisms has inspired numerous *in vitro* biomimetic crystallisations of intricate structures of $CaCO_3$ for various potential applications: additives in composites, catalyst supports or biomedical implants[26]–[28]. Understanding the conditions affecting the morphogenesis and polymorphism of $CaCO_3$ could provide important insights into its crystal growth mechanisms under various reaction conditions.

Anhydrous $CaCO_3$ exists in three different polymorphs (in order of increasing stability): vaterite, aragonite, and calcite[29]. These polymorphs can exist or co-exist under different conditions during the precipitation of $CaCO_3$ in natural water, where the effect of temperature on polymorphism has been the most studied.[30] For instance, it has been reported that calcite and vaterite co-exist at temperatures between 10-30 °C. All three polymorphs co-exist at intermediate temperatures between 40-50 °C. Aragonite and calcite co-exist at temperatures above 60 °C[31].

Reports on the use of mixtures of ethanol and water,[32] as well as dimethylformamide (DMF) and water,[33] to influence the polymorphism of $CaCO_3$ have been documented. There have been insufficient research reports on the effect that mixtures of polar aprotic and polar protic solvents have on controlling the morphology and polymorphism of precipitated $CaCO_3$ (PCC). Herein a detailed study is reported on the effect of using of a series of binary mixture ratios, comprising of polar aprotic (dimethylformamide (DMF) and dimethyl sulfoxide (DMSO)) and polar protic (methanol, ethanol, isopropanol, and 2-butanol) solvents which contained 10 % polyethylene glycol (PEG) 200 Mw as a crystal modifier, on the morphogenesis and

polymorphism of $CaCO_3$. Time-resolved *ex situ* PXRD and SEM studies allowed an analysis of the mechanism of nucleation and crystal growth.

## 4.2 Experimental

### 4.2.1 Materials

All chemicals were of analytical grade. Calcium chloride, ammonium carbonate, polyethylene glycol (Mw 200), methanol (CP), ethanol (CP), isopropanol (AR) were purchased from Sigma-Aldrich. 2-Butanol (98 %) and sodium hydroxide pellets were purchased from Merck (Pty) Ltd South Africa. The ammonia solution of 25 %, hydrochloric acid (HCl) of 32 %, dimethyl sulfoxide (CP) (DMSO), and dimethylformamide (CP) (DMF) were all purchased from ACE associated chemical enterprises. All chemicals were used without any further purification.

4.2.2 Crystallisation of Calcium Carbonate

Crystallisation reactions were carried out in a 250 mL round bottom flask kept at 30 °C in an oil bath. In a typical reaction, 10% of a polyethylene glycol (Mw 200) solution was prepared in a polar aprotic and polar protic solvent, in mixture ratios of: 5:0, 5:1, 5:2, 5:3, 5:4, 5:5, and 0:5. The pH of the resulting mixtures was adjusted to 9.6 with aqueous NaOH. The polar protic solvents used were: methanol, ethanol, isopropanol, and 2-butanol. The polar aprotic solvents used were: DMSO and DMF. To each of these mixtures, 50 mL of a 5 mmol $CaCl_2$ aqueous solution (adjusted to pH 8.5, using an aqueous $NH_3$ solution) was added dropwise under gentle stirring at 30 °C. The reaction mixtures were allowed to stir for an hour and then 50 mL of a 5 mmol $(NH_4)_2CO_3$ aqueous solution (adjusted to pH 10 with an aqueous HCl solution) was added dropwise under gentle stirring. These reaction solutions were kept at 30 °C for 24 hrs under gentle stirring. The crystallised $CaCO_3$ precipitates were collected by centrifuge and then washed several times with deionized water. Finally they were washed with ethanol and left to dry overnight at room temperature.

Time-resolved experiments were performed in the same way as above in polar protic (isopropanol) and polar aprotic (DMSO) pure solvents. Aliquots were drawn from the bulk reaction mixture at time intervals of: 5, 10, 15, 30, 60, 180 min, and lastly 24 hrs. These were centrifuged and then washed several times with deionized water. Finally they were washed

with ethanol and left to dry overnight at room temperature, and characterised by PXRD and SEM.

### 4.2.3 Characterisation

The as-synthesized products were characterised by PXRD, SEM, and laser Raman spectroscopy as described in Chapter 3, sections from 3.4.2 to 3.4.4.

## 4.3 Results and Discussion

Initially each of the polar protic solvents (i.e. methanol, ethanol, isopropanol, or 2-butanol) was examined, under the previously mentioned conditions, to establish the types of PCC polymorphs that were formed. PXRD analyses (Figure 4.1) revealed that in all cases, mixtures of vaterite (v) and calcite (c) were present, with vaterite (v) as the predominant polymorph. Peaks denoted "C" were indexed according to the crystallographic data published by Markgraf *et al.*[34] (**ICSD 040107**)), and peaks denoted "V" were indexed according to the crystallographic data published by Kamhi[35] (**ICSD 015879**).

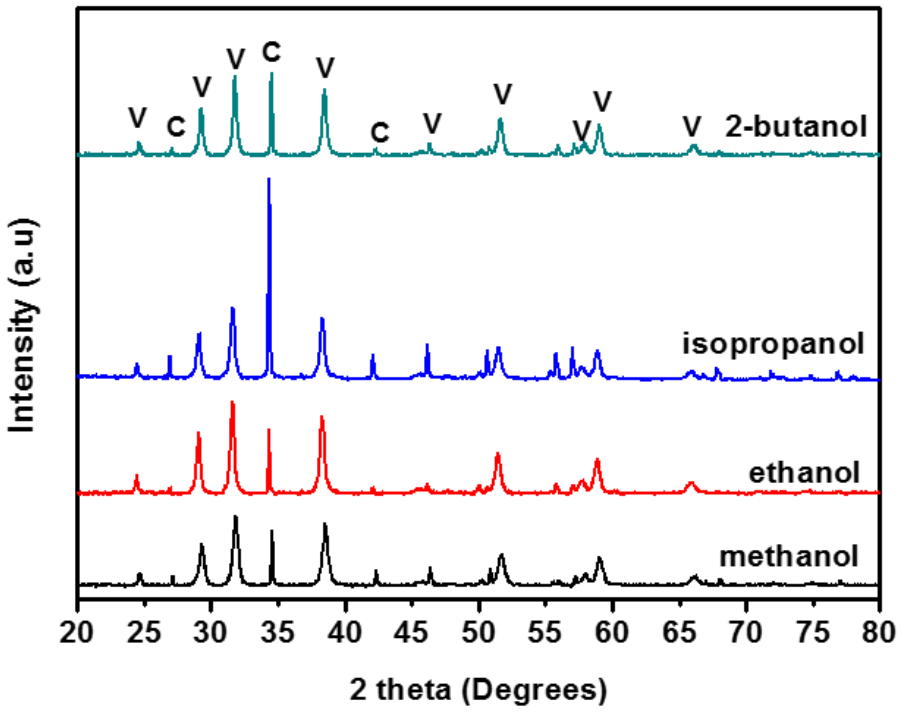



Figure 4. 1. PXRD patterns of the PCC products synthesized in alcohols of different molecular weight in the presence of 10% PEG (200 Mw) as a crystal modifier.

Figures 4.2 (a)-(d) below, show the laser Raman spectra of the calcite (a) and vaterite (c) polymorphs of the PCC and their optical images ((b) & (c), respectively) from which the spectra were acquired. Raman shifts of calcium carbonate polymorphs showed two main regions: the lattice modes which were in the region below 400 $cm^{-1}$ comprised of Raman shifts from the translational and rotational motions of the complete unit cell, and the internal modes which were in the region above 400 $cm^{-1}$ comprising of motions from the main molecular carbonate groups[36]–[38]. Calcite's internal modes (Figure 4.2 (a)) exhibited a characteristic intense sharp peak at 1085 $cm^{-1}$ due to the symmetric stretching of the carbonate ions, and a weak Raman shift around 711 $cm^{-1}$ due to the in-plane bending of the carbonate ions[36]–[38]. Lattice modes in calcite (Figure 4.2 (a)) showed two distinct Raman shifts around 156 and 285 $cm^{-1}$ due to the motions comprising of the complete unit cell[36]–[38].

The Raman shifts of vaterite (Figure 4.2 (c)) gave characteristic split peaks in both the lattice modes and internal modes. The internal modes comprised of the most intense peak, which was a doublet, with Raman shifts at 1075 and 1090 $cm^{-1}$ due to the symmetric stretching of the carbonate ions,[37] and a weak $CO_3^{2-}$ in-plane bending shift[37] which was also a doublet at 740 and 750 $cm^{-1}$. Lattice modes of vaterite gave broad split peaks, with the most intense ones being a doublet around 106 and 120 $cm^{-1}$, and another doublet around 269 and 301 $cm^{-1}$[36], [37].

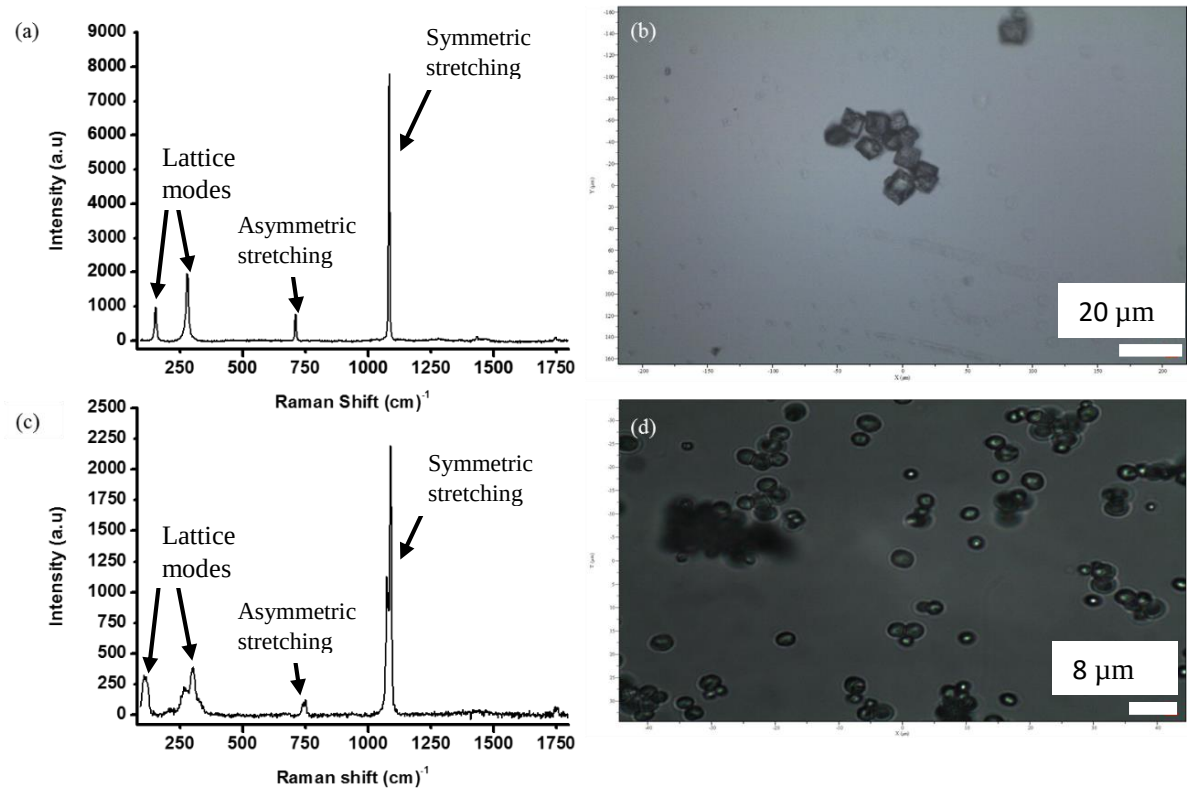



Figure 4. 2. Laser Raman spectra of the two polymorphs of calcium carbonate and their optical microscope images from which the spectra were acquired. (a) Calcite, (b) Image of calcite, (c) Vaterite, and (d) Image of vaterite.

Calcium carbonate is composed of isolated $CO_3^{2-}$ species which have a disordered point symmetry from their original "free carbonate ion" point symmetry due to the interaction of the $CO_3^{2-}$ ions with the mineral lattice[37]. Laser Raman active vibrational modes of calcium carbonate are dependent on the main carbonate groups, however the level of disordering of the $CO_3^{2-}$ ions' point symmetry was different in all the polymorphs of calcium carbonate due to the difference in their crystal structures[36]. Hence differences in the lattice modes and internal modes between calcite (Figure 4.2 (a)) and vaterite (Figure 4.2 (c)) were observed.

SEM micrographs of the PCC products that were synthesized from alcohols of different molecular weight, in the presence of 10% PEG (200 Mw), are shown in Figure 4.3. Based upon these analyses it was observed that methanol produced spherical particles that were predominantly composed of vaterite (Figure 4.3 (a)). However, as the molecular weight of each alcohol used increased i.e. from methanol to ethanol, a morphological change of these spheres into ellipsoid-type particles occurred (Figure 4.3 (b)). These ellipsoid-type of particles were

believed to have ultimately fused together into “flower-like” shaped vaterite particles (also shown in Figure 4.4 (a)) when they were crystallised in isopropanol (Figure 4.3 (c)), or 2-butanol as the main solvent (Figure 4.3 (d)).

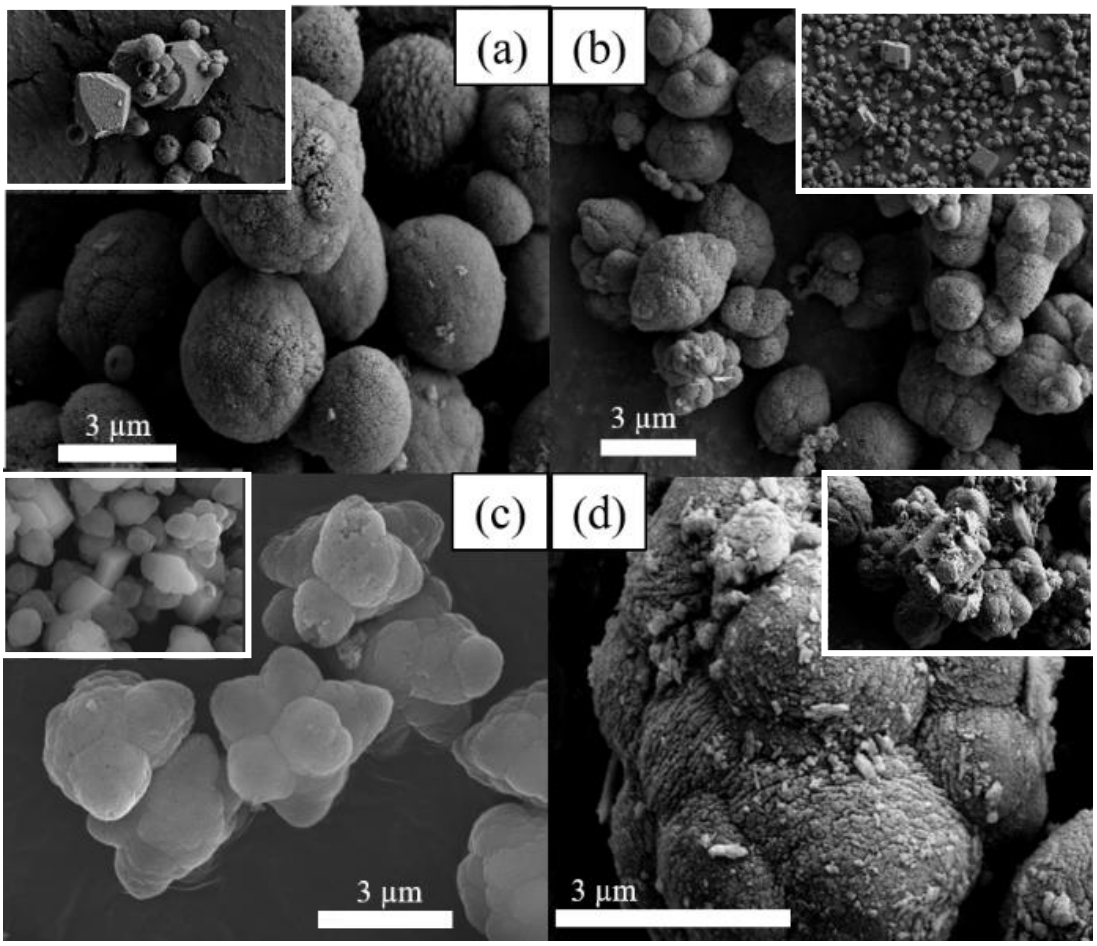



Figure 4. 3. SEM micrographs of the PCC products formed in: (a) Methanol, (b) Ethanol, (c) Isopropanol, and (d) 2-butanol. Inserts show the presence of calcite (confirmed from optical microscopy images in Figure 4.2 above) crystals in the samples.

It was also interesting to note that the crystal form (vaterite polymorph) was retained throughout all the different morphologies of the PCC crystallised in all the different alcohols. This observation implied that these alcohols had sufficient surface binding energies required to kinetically stabilise the meta-stable vaterite polymorph, while different enough to have induced different morphologies during crystal growth. The vaterite morphologies that were

observed differed significantly from the inherent hexagonal ($P6_3/mmc$) symmetry,[39], [35] of the vaterite unit cell.

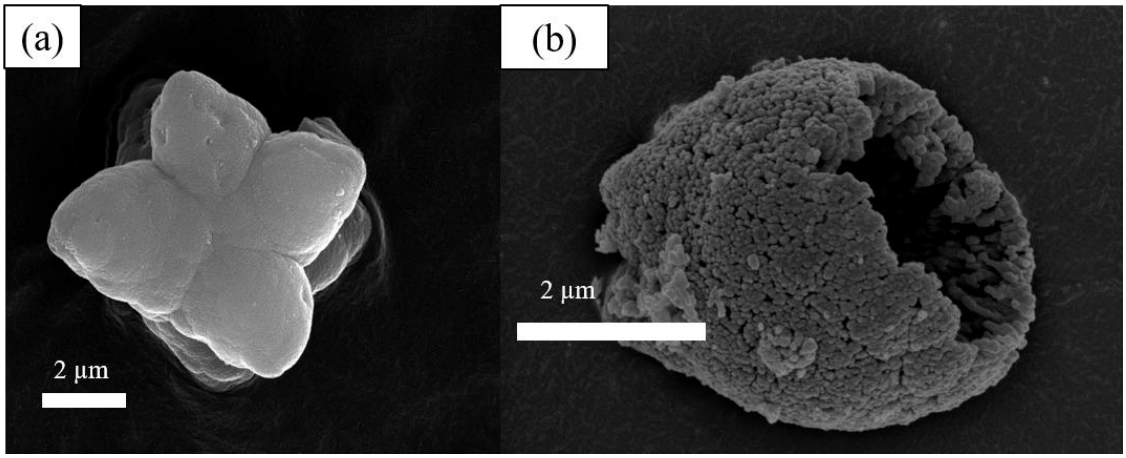



Figure 4. 4. SEM micrographs of: (a) "Flower" shaped vaterite particle formed from the fusion of the individual vaterite ellipsoids; (b) Broken hollow vaterite ellipsoid.

Morphological examination of the broken vaterite ellipsoids by scanning electron microscopy (Figure 4.4 (b)) showed that the PCC vaterite ellipsoids had a hollow structure. This was mostly likely because during crystal growth, vaterite nucleated from amorphous calcium carbonate (ACC) whose free energy was higher than that of vaterite, which would have led to its instability and subsequent dissolution, hence the hollow core[40], [6]. This dissolution-reprecipitation mechanism is explained later in the discussion by *ex situ* measurements.

A variation of the polar aprotic and polar protic binary solvent system ratio was used to manipulate the polymorphic distribution of the precipitated calcium carbonate (PCC), shown in Figure 4.5. Figure 4.5 (a)-(d) are the PXRD patterns showing the polymorph distributions (peaks denoted "C" in the calcite patterns and indexed according to the crystallographic data published by Markgraf *et al*[34]. (**ICSD 040107**)), to vaterite (denoted "V" in peak patterns and indexed according to the crystallographic data published by Kamhi[35] (**ICSD 015879**)) as a function of increasing alcohol solvent ratio.

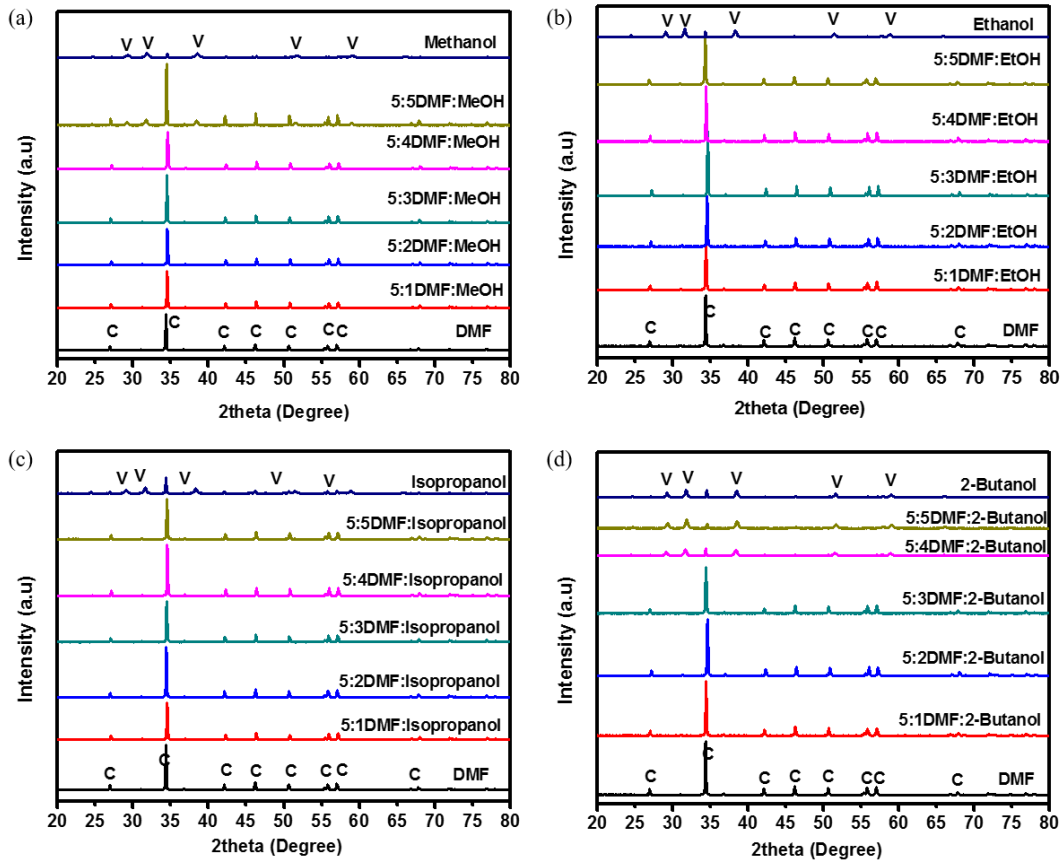



Figure 4. 5. PXRD patterns showing the polymorphism of the PCC as a function of the binary solvent ratio. (a) Ratios of DMF to methanol, (b) Ratios of DMF to ethanol, (c) Ratios of DMF to isopropanol, and (d) Ratios of DMF to 2-butanol.

It was observed from the PXRD patterns that as the ratio of the polar protic solvent relative to the polar aprotic solvent within the bulk crystallizing solvent medium increased, the polymorphism of the PCC predominantly (the most intense (104) peak of calcite was still observed in all of the PXRD patterns) favored the of the formation of vaterite. This was due to the kinetic inhibition effect of the presence of the polar protic solvent on the nucleating calcite polymorph, by inhibiting the dissolution of vaterite and crystallisation of aragonite and calcite[41], [42].

The interesting thing to note in the PXRD data was that the polymorphic composition across the different solvent ratios varied with the molecular weight of the polar protic solvent present in the binary solvent system. For instance, 2-butanol gave a higher selectivity towards the formation of vaterite (Figure 4.5 (d)). Unlike other solvent ratio combinations, vaterite

diffraction peaks were observed from 5:3 DMF to 2-butanol solvent ratio combination up until 5:5 DMF to 2-butanol ratio. A similar trend was also observed for DMSO to 2-butanol solvent ratios (see Figure 4.6 below).

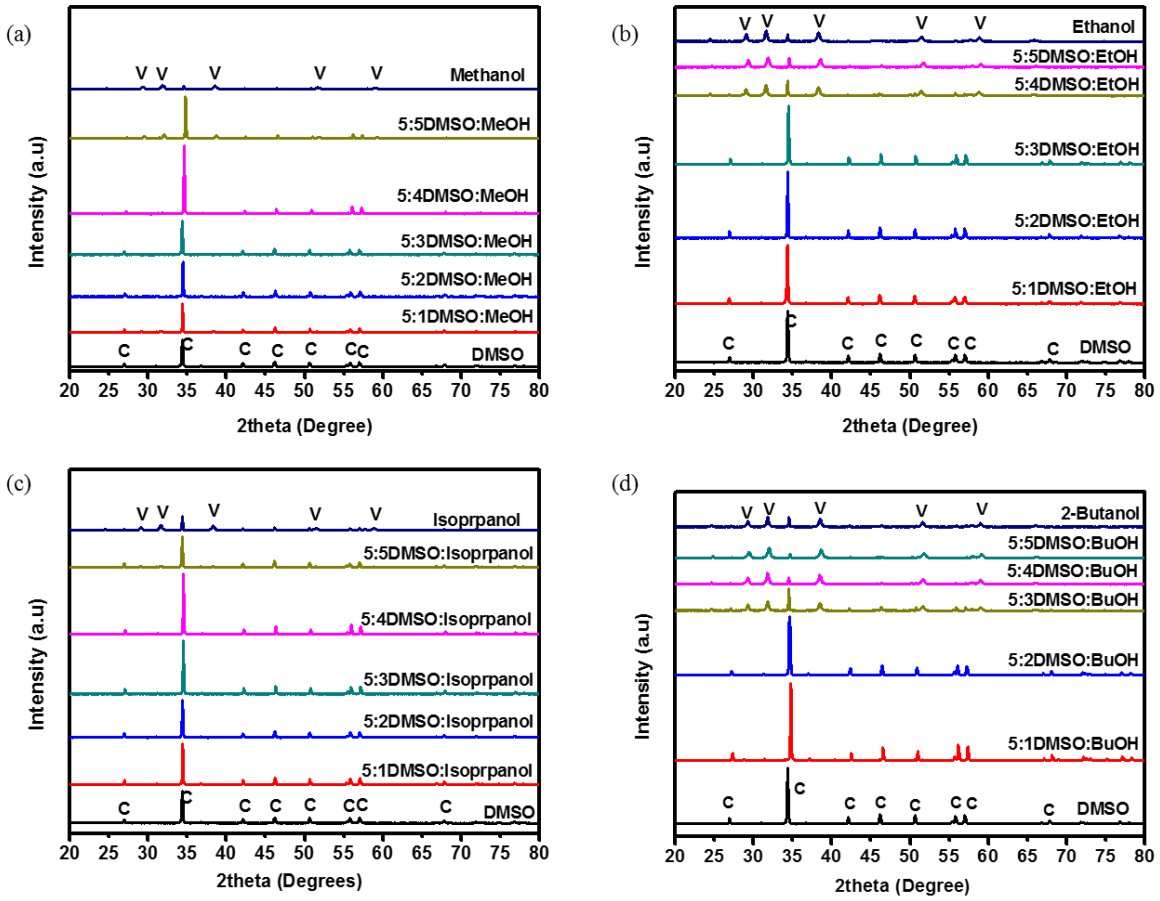



Figure 4. 6. PXRD patterns showing the polymorphism of the PCC as a function of the binary solvent ratio. (a) Ratios of DMSO to methanol, (b) Ratios of DMSO to ethanol, (c) Ratios of DMSO to isopropanol, and (d) Ratios of DMSO to 2-butanol.

To get a clear sense of the polymorphic distributions, a PXRD standard calibration (Figure 4.7) curve was constructed using known mixtures of the pure polymorphs (vaterite and calcite) in terms of mass percentage. Ratios of the peak areas of the most intense peaks ((104) of calcite, and (101) of vaterite) were used to construct the calibration curve, from which the estimated percentages of the polymorphic distribution in each sample were obtained.

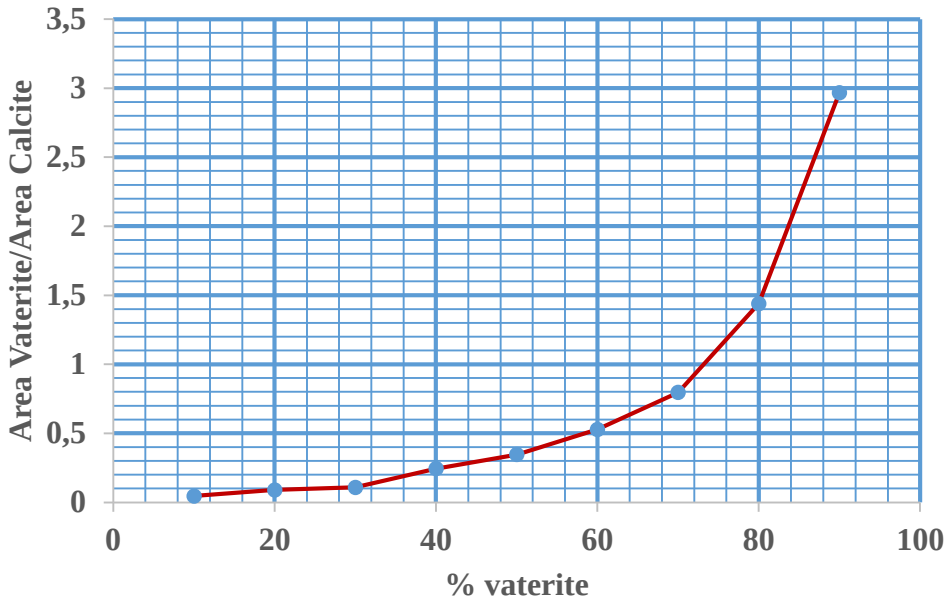



Figure 4. 7. Standard calibration curve of the ratio of vaterite to calcite peak areas versus (mass) percentage of vaterite.

The results of the phase quantification are summarized in Table 4.1. For each case (for DMF and DMSO ratio combinations), the amount of vaterite within the PCC was found to be higher at high polar protic solvent ratios within the crystallising bulk solvent. However, calcite was still dominant in most of the PCC, and present in all the PCC samples that were examined by PXRD. This was not a surprising observation because calcite is indeed the most thermodynamically stable polymorph of $CaCO_3$, and therefore the presence of a polar protic solvent did not totally kinetically inhibit its nucleation (explained by kinetic time-resolved studies later in the discussion). In fact calcite was predominantly favoured by polar aprotic solvents (DMF and DMSO). However the results presented demonstrate a unique way to manipulate the polymorphic distribution during the crystallisation of calcium carbonate - a phenomenon that is well perfected in the biomineralisation of shells in biological species[21].

Table 4. 1. Polymorph distributions in the PCC, as a function of solvent ratio.

| 1ST RATIOS | | | 2ND RATIOS | | |
|---|---|---|---|---|---|
| **Sample ratios** | **% Vaterite** | **% Calcite** | **Sample ratios** | **% Vaterite** | **% Calcite** |
| DMF:methanol | | | DMSO:methanol | | |
| 0:5 | >90 | <10 | 0:5 | >90 | <10 |
| 5:5 | 36 | 64 | 5:5 | 38 | 62 |
| 5:4 | *- | 100 | 5:4 | 10 | 90 |
| 5:3 | - | 100 | 5:3 | - | 100 |
| 5:2 | - | 100 | 5:2 | - | 100 |
| 5:1 | - | 100 | 5:1 | - | 100 |
| 5:0 | - | 100 | 5:0 | - | 100 |
| DMF:ethanol | | | DMSO:ethanol | | |
| 0:5 | >90 | <10 | 0:5 | >90 | <10 |
| 5:5 | 41 | 59 | 5:5 | >90 | <10 |
| 5:4 | - | 100 | 5:4 | 85 | 15 |
| 5:3 | - | 100 | 5:3 | - | 100 |
| 5:2 | - | 100 | 5:2 | - | 100 |
| 5:1 | - | 100 | 5:1 | - | 100 |
| DMF:isopropanol | | | DMSO:isopropanol | | |
| 0:5 | 72 | 28 | 0:5 | 72 | 28 |
| 5:5 | - | 100 | 5:5 | 17 | 83 |
| 5:4 | - | 100 | 5:4 | - | 100 |
| 5:3 | - | 100 | 5:3 | - | 100 |
| 5:2 | - | 100 | 5:2 | - | 100 |
| 5:1 | - | 100 | 5:1 | - | 100 |
| DMF:2-butanol | | | DMSO:2-butanol | | |
| 0:5 | 85 | 15 | 0:5 | 85 | 15 |
| 5:5 | >90 | <10 | 5:5 | >90 | <10 |
| 5:4 | 86 | 14 | 5:4 | >90 | <10 |
| 5:3 | - | 100 | 5:3 | 74 | 26 |
| 5:2 | - | 100 | 5:2 | - | 100 |
| 5:1 | - | 100 | 5:1 | - | 100 |

*undetectable

Time-resolved studies were then performed in order to gain deeper insights into the kinetics, mechanism of nucleation and phase transformation over time under polar protic and polar aprotic pure solvents. The time-resolved powder diffraction data collected *ex situ* is presented in Figure 4.8. When DMSO was used as a crystallising solvent (Figure 4.8 (a), corresponding to the SEM micrographs labelled (g)-(j) in Figure 4.9), the initial PCC collected after 5 min of crystallisation time comprised mostly of amorphous $CaCO_3$ (ACC), and also exhibited poorly crystalline calcite reflections, the most pronounced being the (104) peak around 34˚ 2θ. The crystals showed poorly defined rhombohedral morphology of calcite (Figure 4.9 (f)). The vaterite diffraction peaks on the other hand could hardly be identified, the same was observed on Figure 4.9 (f) by SEM. This suggested that the nucleation and transformation of ACC into crystalline phases was very fast and probably occurred upon mixing the precursor solutions[42]. Poorly crystalline vaterite diffraction peaks became pronounced 10 min after mixing the precursor solutions due to the dissolution of ACC and re-precipitation into vaterite. The PCC crystals exhibited regular rhombohedral morphology which resembled calcite, and the spherical-type crystals resembled vaterite (Figure 4.9 (g)). Both phases were seen to be properly crystalline after 30 min (Figure 4.9 (h)), with the vaterite diffraction peaks being at their maximum intensity relative to the calcite diffraction peaks.

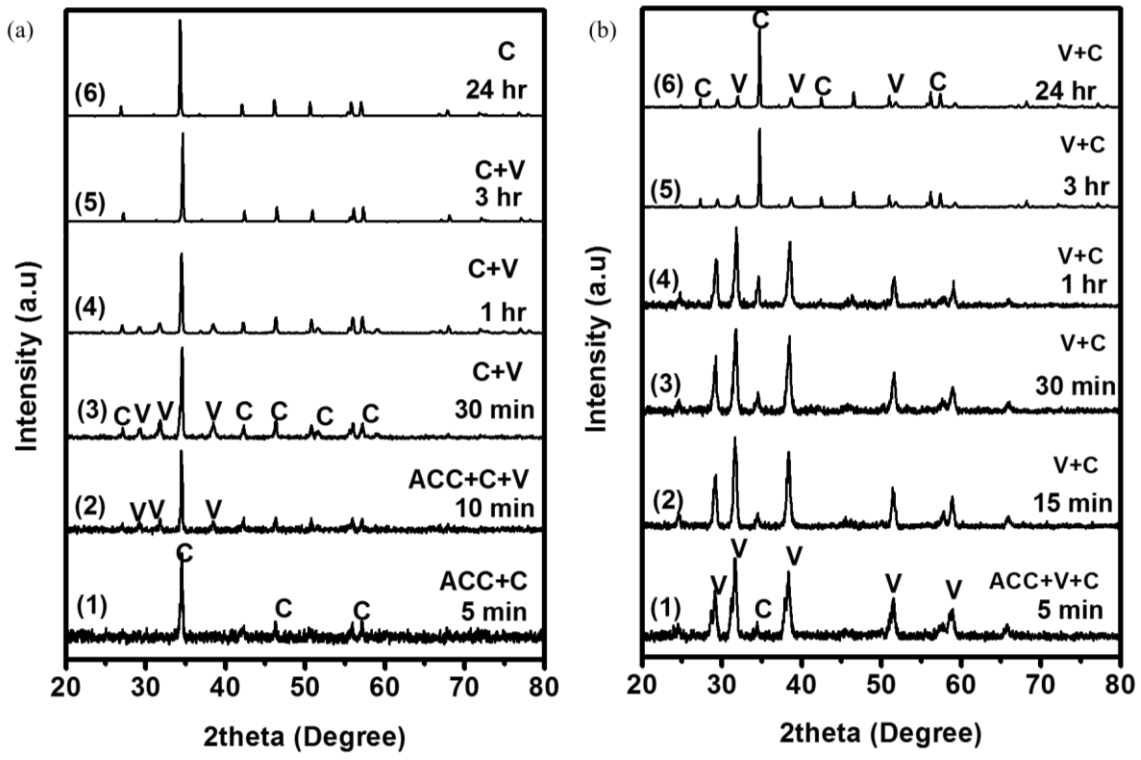



Figure 4. 8. Time-resolved ex-situ PXRD patterns showing the kinetics, mechanism of nucleation and phase transformation of the PCC under polar aprotic solvent and polar protic solvent: (a) DMSO, (b) Isopropanol.

A decrease in the relative intensity of the vaterite diffraction peaks in the PCC collected after an hour was observed, this was due to the dissolution of vaterite and its transformation into calcite via re-precipitation, alluding to the fact that DMSO could not kinetically inhibit the nucleation and growth of calcite by stabilising vaterite. This dissolution was reflected in Figure 4.9 (j) by the decrease in the relative number of vaterite crystals. Calcite became the preferred polymorph, with good crystallinity, in the PCC until 24 hrs. This time-resolved *ex situ* PXRD study showed that phase transformation under a polar aprotic solvent occurs within 3 hrs of mixing the precursor solutions.

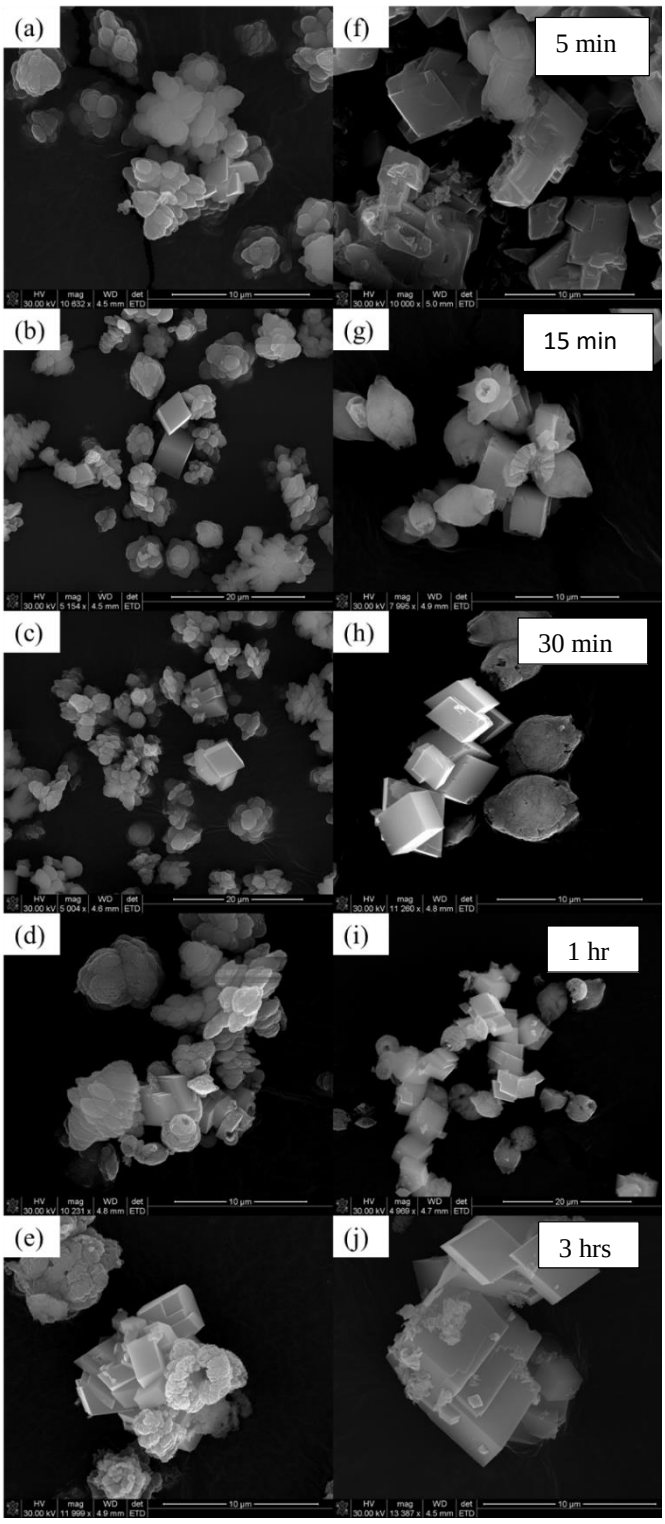



Figure 4. 9. Time-resolved SEM micrographs showing the kinetics, mechanism of nucleation and phase transformation of the PCC under a polar aprotic solvent and a polar protic solvent: (a)-(e) Isopropanol; at 5, 15, 30 min, 1, and 3 hrs, respectively. (f)-(j) DMSO; at 5, 15, 30 min, 1, and 3 hrs, respectively.

When the crystallising solvent was changed to a polar protic solvent (Figure 4.8 (b)), i.e. isopropanol, the initial PCC collected after 5 min showed that the PCC was amorphous, with poorly crystalline vaterite diffraction peaks as the main polymorph, and a small (104) peak of calcite around 34˚ 2θ. This suggested that the nucleation and transformation of ACC into vaterite was also very fast, however unlike DMSO, isopropanol could kinetically inhibit the dissolution of vaterite and its transformation into calcite 5 min after mixing the precursor solutions. The morphology of the PCC was "flower-like" crystals which were attributed to vaterite, and some cuboids resembling the rhombohedral morphology of calcite (Figure 4.9 (a)). The vaterite crystallinity increased with crystallisation time (from 15 min to 1 hr), as seen in Figures 4.9 (b)-(d). There was also an increase in the relative intensity of the (104) diffraction peak of calcite with increase in crystallisation time (Figure 4.8 (b)).

The PCC collected after 3 hrs showed a significant decrease in the relative intensities of the vaterite diffraction peaks due to the slow dissolution of vaterite and its transformation into calcite, but the vaterite crystals were still observed regardless ((Figure 4.9 (d)). Isopropanol proved to be fairly able to kinetically stabilize vaterite better than DMSO by inhibiting its dissolution and transformation into calcite, resulting in a mixture of phases at the end of 24 hrs of crystallisation time (Figure 4.8 (b), (6)), unlike the pure calcite phase in the case of DMSO (Figure 4.8 (a), (6)). Both these *ex situ* studies showed a nucleation and growth mechanism of $CaCO_3$ via the Ostwald-Lussac law of phases,[40], [41] which were kinetically controlled in different ways by using either a polar aprotic or polar protic solvent.

Changing the crystallising solvent ratio (DMF to methanol or DMSO to methanol) of polar aprotic solvent to polar protic solvent resulted in a morphological change in the crystallites of calcite initially, followed by the formation of spherical vaterite crystals with increase in the polar protic solvent content within the crystallising solvent mixture (as seen in Figure 4.10). It was observed that polar aprotic solvent(s), in this case DMF, favoured the precipitation of calcite rhombohedral cubes (Figure 4.10 (a)). As the ratio of methanol (one of the selected polar protic solvent) was increased from 5:0 to 5:4 (Figure 4.10 (b)-(e)) topographical defects in the morphology of the calcite "blocks" were observed.

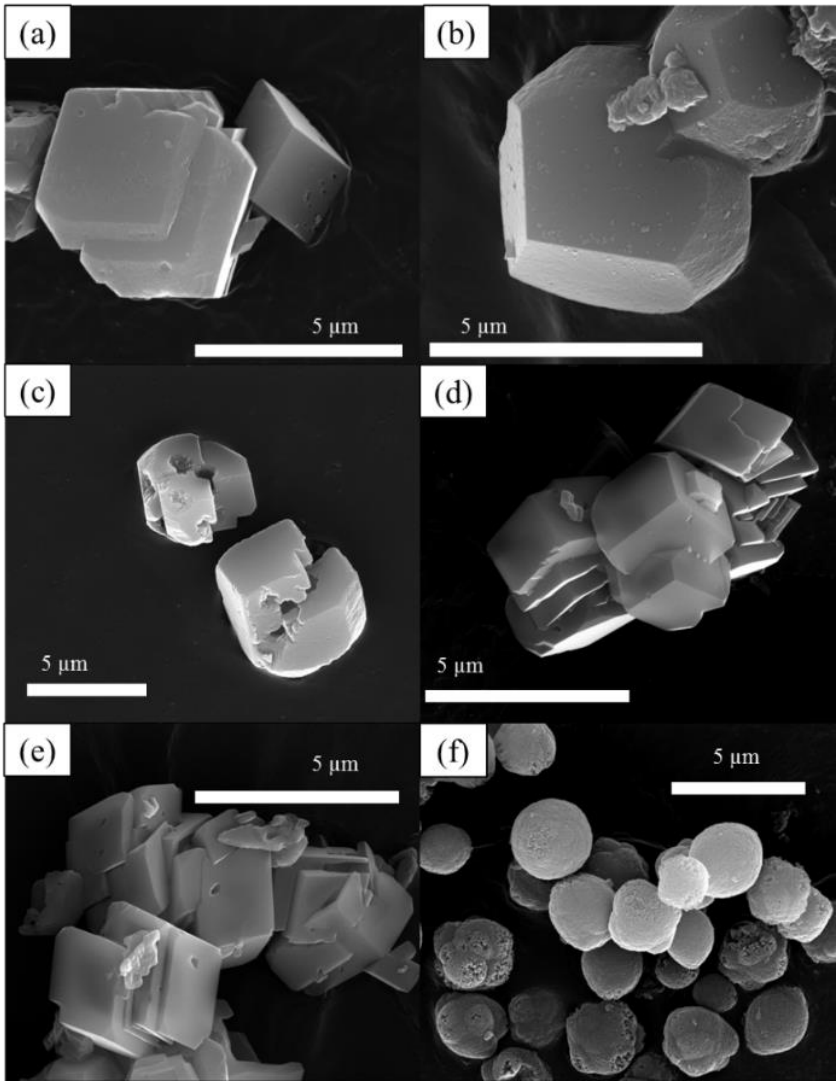



Figure 4. 10. SEM micrographs showing the effect of the solvent ratio of DMF and methanol on the morphology of the PCC. (a) Pure DMF, (b) 5:1 of DMF to methanol, (c) 5:2 of DMF to methanol, (d) 5:3 of DMF to methanol, (e) 5:4 of DMF to methanol, and (f) 5:5 of DMF to methanol. Crystallites of calcite were present in (a)-(e), while vaterite and calcite (PXRD proved calcite was also present) were present in (f).

These were attributed to the interactions of the added PEG crystal modifier and the solvent molecules with the calcite step edges or crystal facets at different degrees of solute-solvent binding, and this could either inhibit or kinetically promote crystal growth on specific crystal habit planes of the calcite crystals[33], [43]. However, a 5:5 ratio of DMF to methanol (Figure 4.10 (f)) resulted in the crystallisation of vaterite spheres due to the kinetic effects of methanol

in the binary solvent. Similar trends were observed with DMSO to methanol solvent (Figure 4.11).

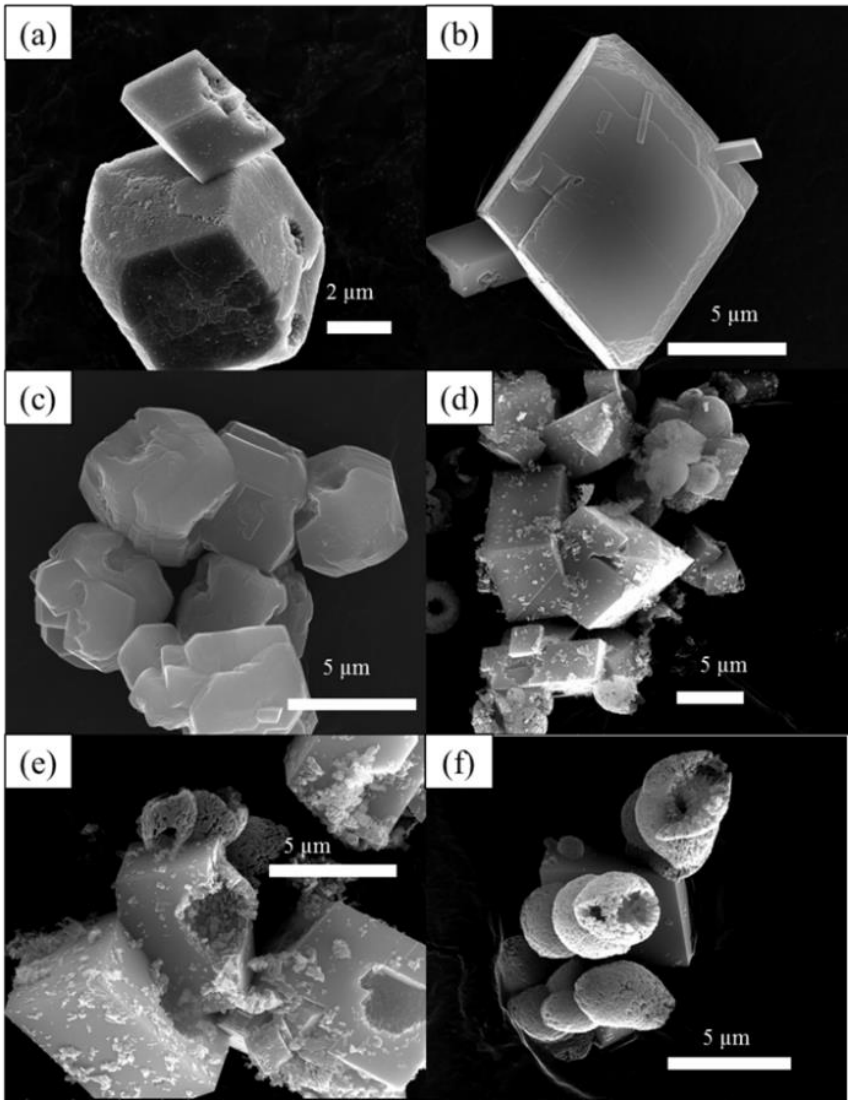



Figure 4. 11. SEM micrographs showing the effect of the solvent ratio of DMSO and methanol on the morphology of the PCC. (a) Pure DMSO, (b) 5:1 of DMSO to methanol, (c) 5:2 of DMSO to methanol, (d) 5:3 of DMSO to methanol, (e) 5:4 of DMSO to methanol, and (f) 5:5 of DMSO to methanol. Crystallites of calcite were present in (a)-(c), while mixtures of vaterite and calcite were present in (e)-(f).

DMF and ethanol mixture ratios gave a much similar trend to that of DMF and methanol (Figure 4.12 (a)-(f)). Figure 4.12 (a) shows the normal rhombohedral morphology of calcite bulk crystals precipitated in pure DMF, and the same was observed for crystals grown in a 5:1 ratio of DMF to ethanol (Figure 4.12 (b)). However there were some morphological defects in

calcite bulk crystals with increasing ethanol content (Figure 4.12 (c)-(d)). There seemed to be a fusion of the calcite crystals during growth, resulting in a stepped block-like morphology. In the case of DMSO to ethanol solvent mixture ratios (Figure 4.13), it is interesting to note that vaterite crystals were observed at a lower ratio (5:4) of ethanol in the solvent mixture. However, the morphological and polymorphic manipulation trend was still similar.

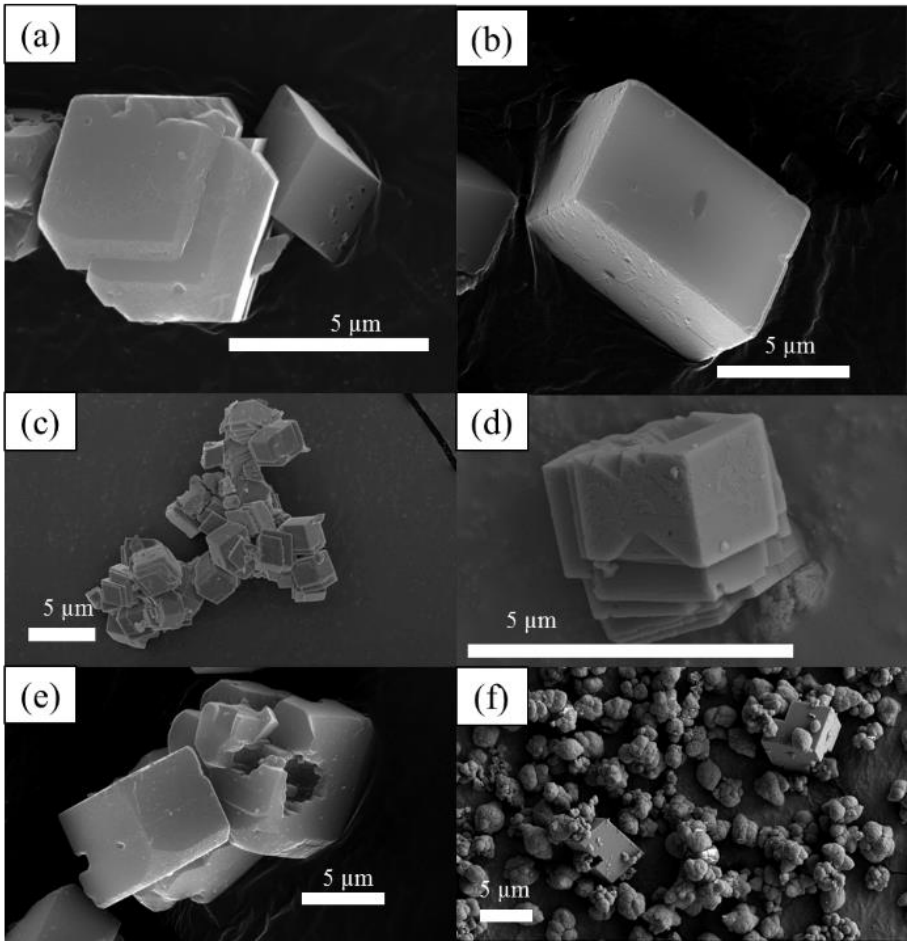



Figure 4. 12. SEM micrographs showing the effect of the solvent ratio of DMF and ethanol on the morphology of the PCC. (a) Pure DMF, (b) 5:1 of DMF to ethanol, (c) 5:2 of DMF to ethanol, (d) 5:3 of DMF to ethanol, (e) 5:4 of DMF to ethanol, and (f) 5:5 of DMF to ethanol. Crystallites of calcite are present in (a)-(e), while crystallites of vaterite were present in (f).

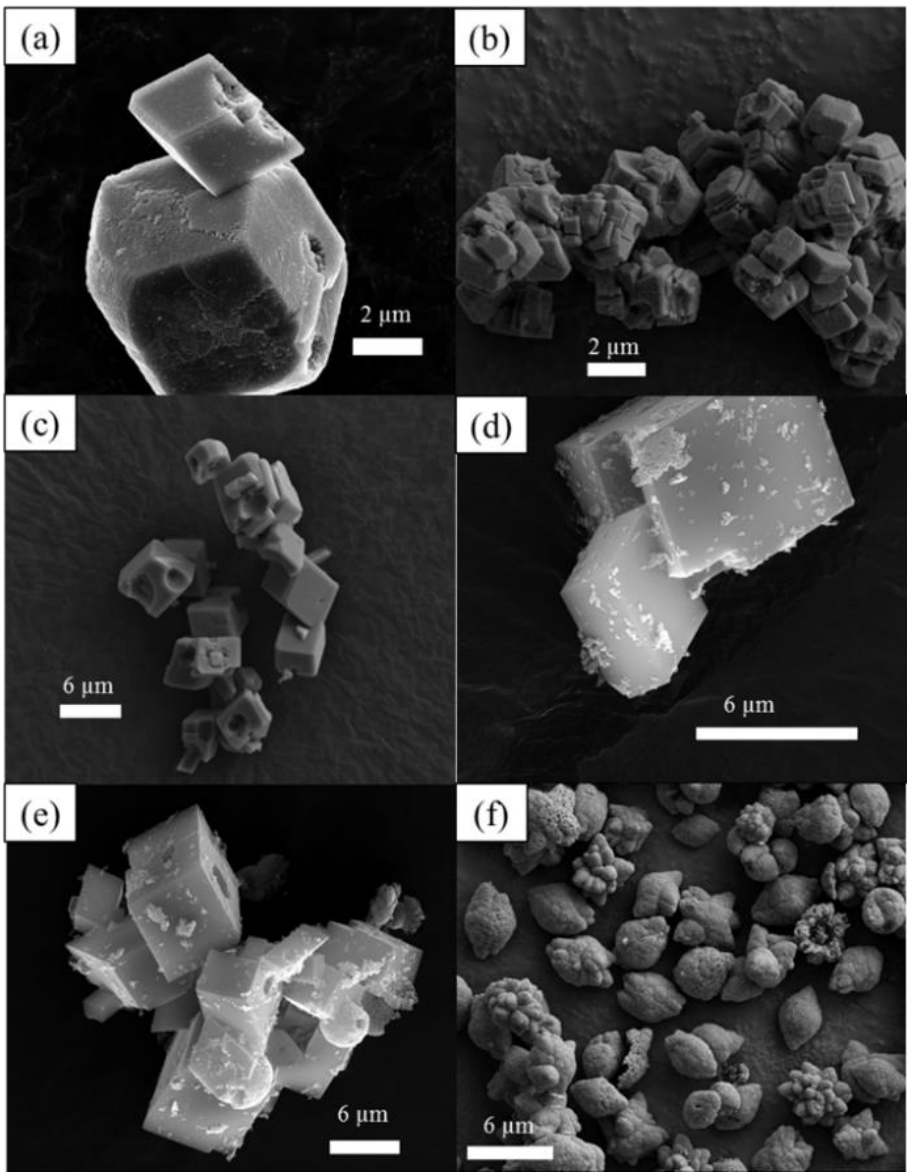



Figure 4. 13. SEM micrographs showing the effect of the solvent ratio between DMSO and ethanol on the morphology of the PCC. (a) Pure DMSO, (b) 5:1 of DMSO to ethanol, (c) 5:2 of DMSO to ethanol, (d) 5:3 of DMSO to ethanol, (e) 5:4 of DMSO to ethanol, and (f) 5:5 of DMSO to ethanol. Crystallites of calcite were present in (a)-(c), while crystallites of vaterite were present in (e)-(f).

The solvent mixtures of ratios of DMF to isopropanol (Figure 4.14), and DMF to 2-butanol (Figure 4.16), showed a very interesting trend which was different from methanol and ethanol. A slight selectivity towards the crystallisation of vaterite in the lower alcohol ratios was observed. In Figure 4.14, vaterite crystals can be seen in the ratio from 5:4 of DMF to isopropanol (Figure 4.14 (e)), and in Figure 4.16, vaterite crystals were observed in the ratio

from 5:2 of DMF to 2-butanol (Figure 4.16 (c)). It was also observed that the increase in the alcohol ratio (Figure 4.14 and 4.16) caused morphological defects in the calcite crystals, from the original calcite cubes that were precipitated in pure DMF (Figure 4.14 (a)) to elongated rectangular-type cubes (Figures 4.14 (f) and 4.16 (c)-(e)). Similar trends were observed in all the solvent mixtures with DMSO used as the polar aprotic solvent (as shown in Figures 4.15 and 4.17).

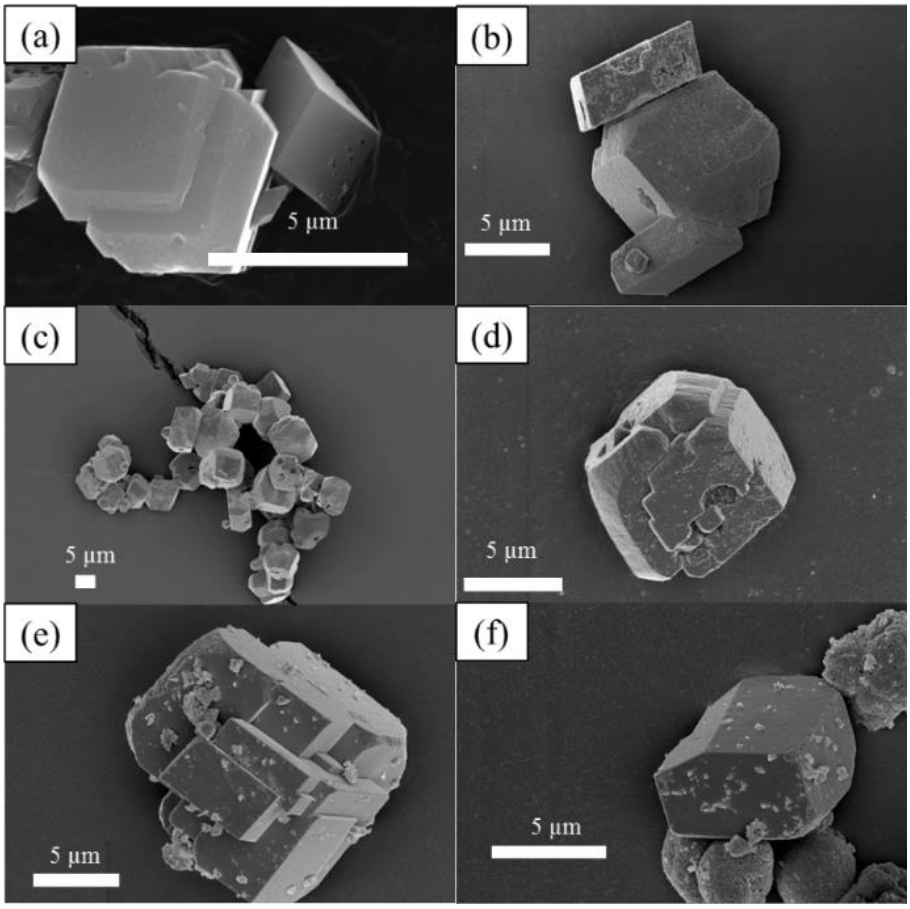



Figure 4. 14. SEM micrographs showing the effect of the solvent ratio of DMF and isopropanol on the morphology of the PCC. (a) Pure DMF, (b) 5:1 of DMF to isopropanol, (c) 5:2 of DMF to isopropanol, (d) 5:3 of DMF to isopropanol, (e) 5:4 of DMF to isopropanol, and (f) 5:5 of DMF to isopropanol. Crystallites of calcite were present in (a)-(d), and mixtures of calcite and vaterite were present in (e)-(f).

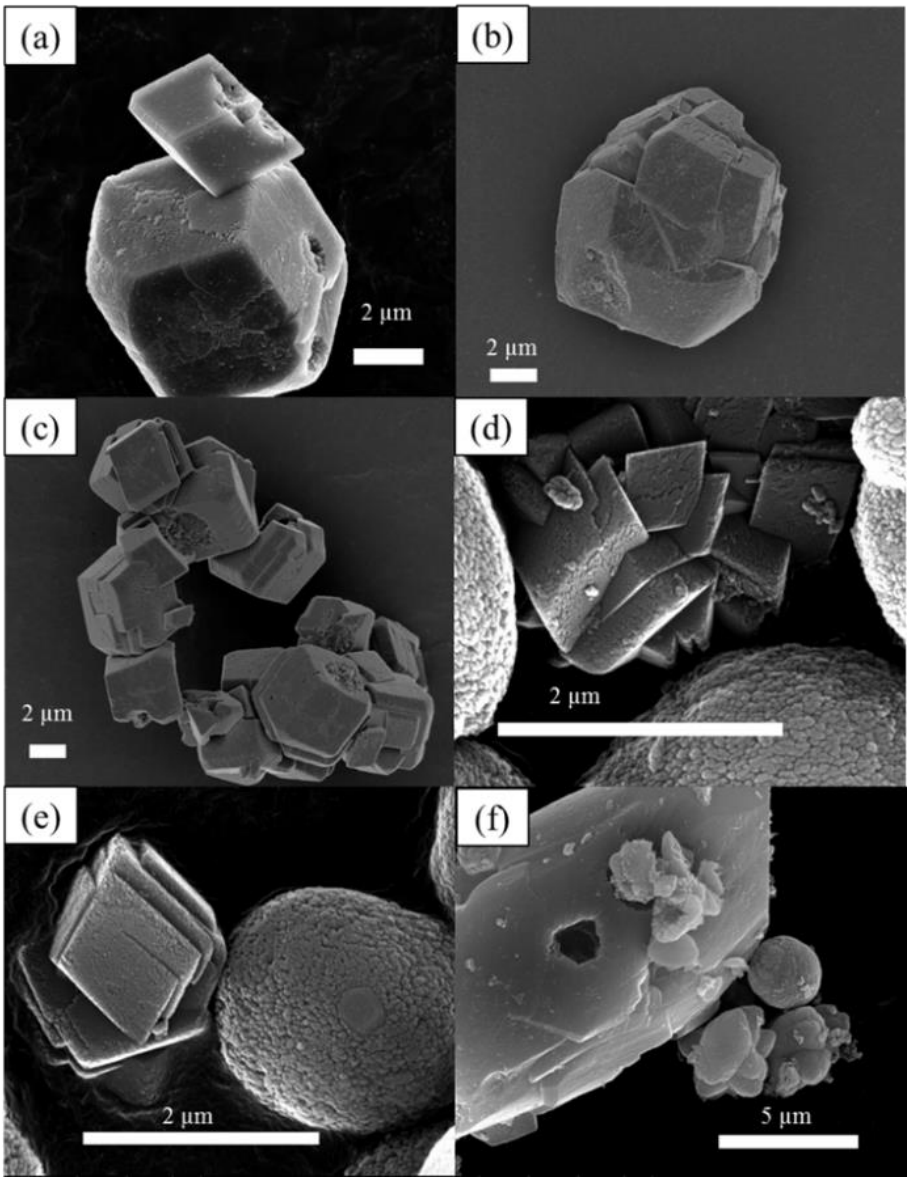



Figure 4. 15. SEM micrographs showing the effect of the solvent ratio of DMSO and isopropanol on the morphology of the PCC. (a) Pure DMSO, (b) 5:1 of DMSO to isopropanol, (c) 5:2 of DMSO to isopropanol, (d) 5:3 of DMSO to isopropanol, (e) 5:4 of DMSO to isopropanol, and (f) 5:5 of DMSO to isopropanol. Crystallites of calcite were present in (a)-(c), and mixtures of calcite and vaterite were present in (d)-(f).

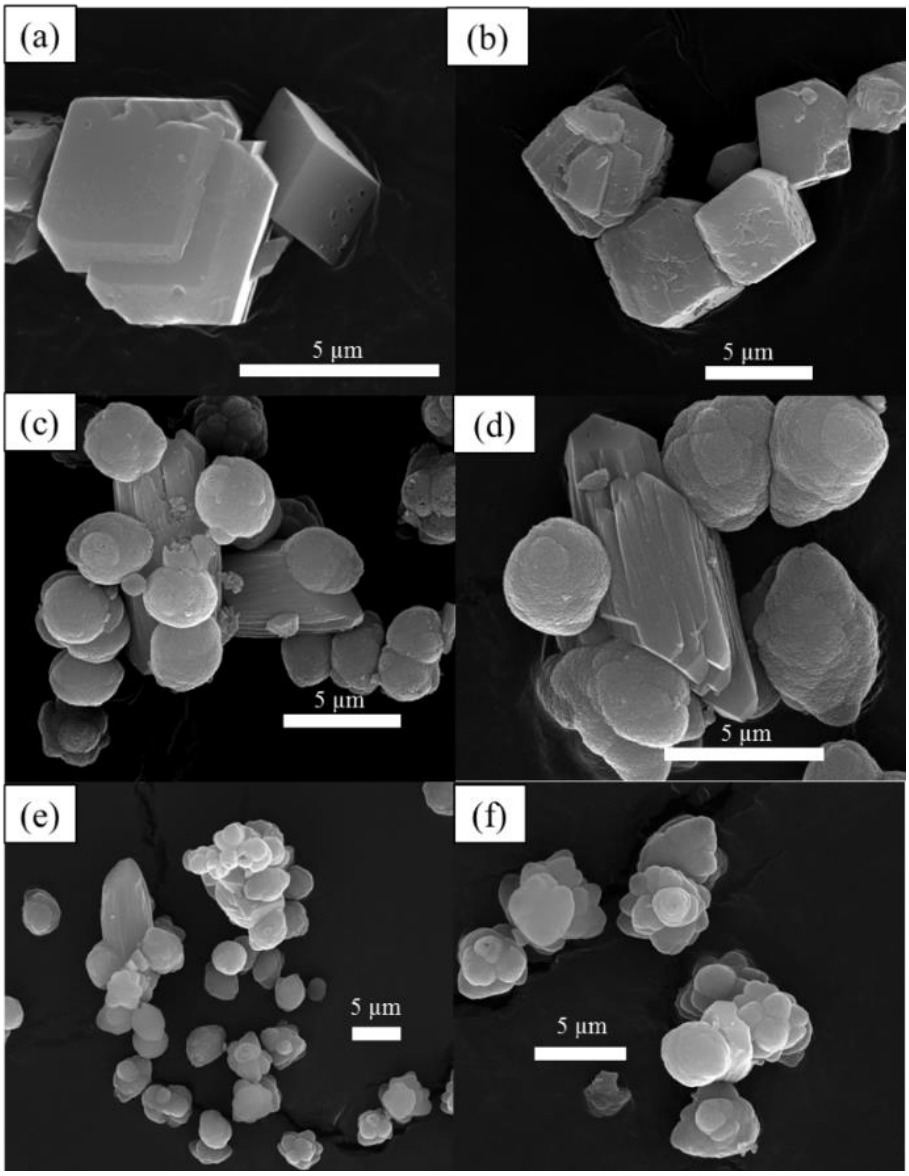



Figure 4. 16. SEM micrographs showing the effects of solvent ratio of DMF and 2-butanol on the morphology of the PCC. (a) Pure DMF, (b) 5:1 of DMF to 2-butanol, (c) 5:2 of DMF to 2-butanol, (d) 5:3 of DMF to 2-butanol, (e) 5:4 of DMF to 2-butanol, and (f) 5:5 of DMF to 2-butanol. Crystallites of calcite were present in (a)-(b), while mixtures of vaterite and calcite were present in (c)-(f).

This deviation from the thermodynamically predicted crystal habit was as a result of kinetically controlled crystal growth by the face-specific crystal surface binding effect of the alcohol and the PEG crystal modifier in the crystallising media[44]–[46]. The extent of interfacial binding energy strength between the specific nucleating crystal plane and specific solvent molecule, with matching crystallochemical properties, reduced the free energy and thus favoured

nucleation on that crystal plane[40], which led to elongation of the crystal shape as observed in the above calcite morphologies. With this being said, when looking at the main difference in the chemical natures (structures) of the polar and aprotic solvents, the presence of the –OH group, the polar protic solvents played an important role in increasing the surface binding of the growing vaterite crystals. This effect slowed down the rate of growth and hence kinetically stabilised the vaterite polymorph. This effect was observed in the *ex situ* PXRD studies.

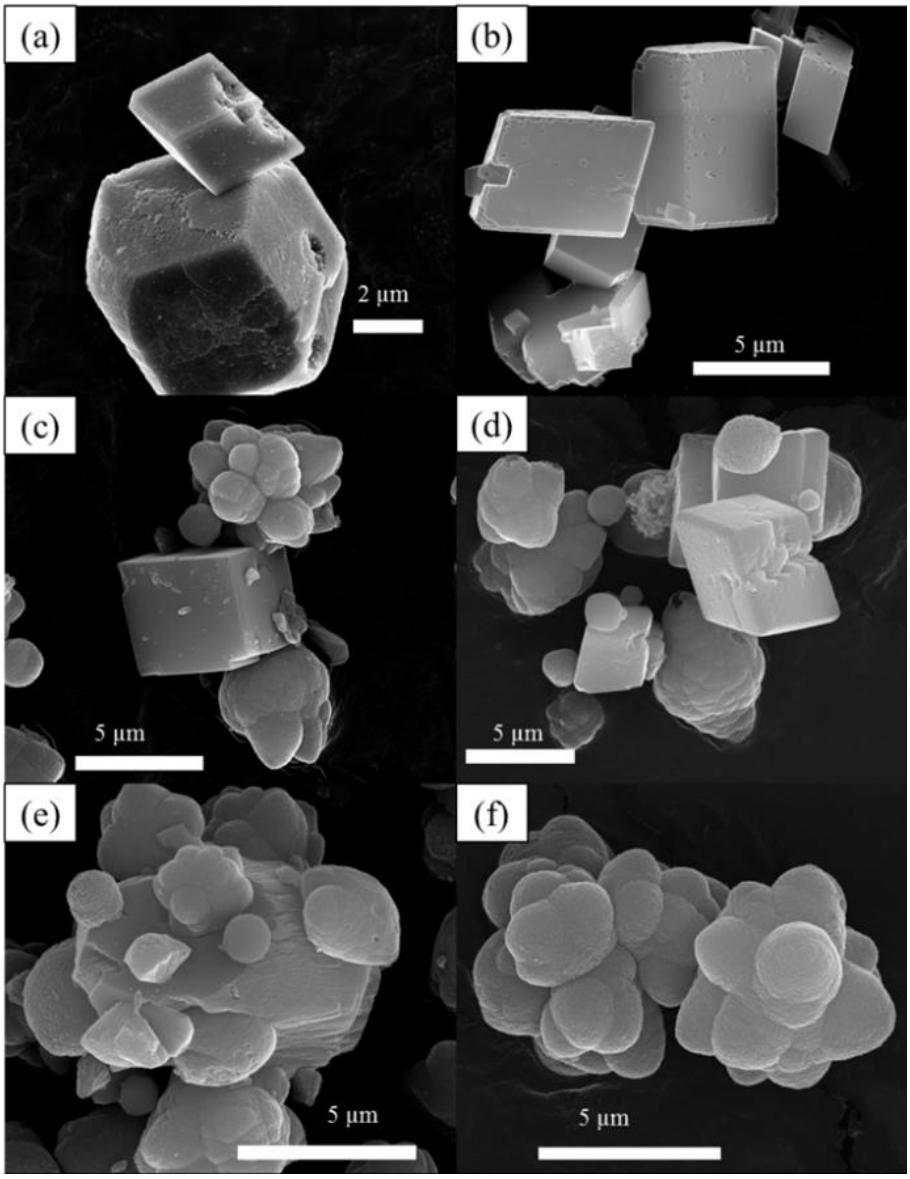



Figure 4. 17. SEM micrographs showing the effect of the solvent ratio of DMSO and 2-butanol on the morphology of the PCC. (a) Pure DMSO, (b) 5:1 of DMSO to 2-butanol, (c) 5:2 of DMSO to 2-butanol, (d) 5:3 of DMSO to 2-butanol, (e) 5:4 of DMSO to 2-butanol, and (f) 5:5 of DMSO to 2-butanol. Crystallites of calcite were present in (a)-(b), while mixtures of vaterite and calcite were present in (c)-(f).

## 4.4 Conclusions

This work demonstrated that the morphology and polymorphic composition of PCC could be manipulated by the use of a binary solvent system consisting of different ratios of polar protic and polar aprotic solvents with PEG. An increase in the ratio of the polar protic solvent (methanol, ethanol, isopropanol, and 2-butanol) relative to the polar aprotic solvent (DMF and DMSO) within the binary solvent mixture favoured the formation of hollow spherical vaterite particles. An increase in the ratio of polar aprotic solvent (DMF and DMSO) within the binary solvent mixture favoured the precipitation of rhombohedral calcite crystals. Time-resolved *ex situ* PXRD and SEM measurements revealed that the nucleation and phase transformation of the PCC under polar protic and aprotic solvents followed the dissolution-reprecipitation mechanism. Here the major phase transformation occurred within 3 hrs of mixing the precursor solutions. Isopropanol, a polar protic solvent favoured the nucleation of vaterite at initial stages (5 min after mixing the precursor solutions), and DMSO a polar aprotic solvent favoured the nucleation of calcite. This work contributes scientific understanding of the controlled polymorphism, crystal growth, and design of inorganic crystals within the field of biomineralisation. This knowledge may be used to tailor novel organic-inorganic composites and novel shapes with potential applications in materials science.

## 4.5 References


[1] H. Tong, W. Ma, L. Wang, P. Wan, J. Hu, and L. Cao, "Control over the crystal phase, shape, size and aggregation of calcium carbonate via a L-aspartic acid inducing process," *Biomaterials*, vol. 25, no. 17, pp. 3923–9, 2004.

[2] M. Lei, P. G. Li, Z. B. Sun, and W. H. Tang, "Effects of organic additives on the morphology of calcium carbonate particles in the presence of CTAB," *Mater. Lett.*, vol. 60, no. 9–10, pp. 1261–1264, 2006.

[3] R. Q. Song, H. Cölfen, A. W. Xu, J. Hartmann, and M. Antonietti, "Polyelectrolyte-directed nanoparticle aggregation: Systematic morphogenesis of calcium carbonate by nonclassical Crystallisation," *ACS Nano*, vol. 3, no. 7, pp. 1966–1978, 2009.

[4] P. J. M. Smeets, K. R. Cho, R. G. E. Kempen, N. a. J. M. Sommerdijk, and J. J. De Yoreo, “Calcium carbonate nucleation driven by ion binding in a biomimetic matrix revealed by in situ electron microscopy,” *Nat. Mater.*, vol. 14, no. 4, pp. 394–399, 2015.

[5] S. Mann, B. R. Heywood, S. Rajam, and J. D. Birchall, “Controlled Crystallisation of $CaCO_3$ under stearic acid monolayers,” *Nature*, vol. 334, no. 6184, pp. 692–695, 1988.

[6] M. H. Nielsen, S. Aloni, and J. J. De Yoreo, “*In situ* TEM imaging of $CaCO_3$ nucleation reveals coexistence of direct and indirect pathways,” *Science*, vol. 218, no. 2004, pp. 213–218, 2013.

[7] D. Walsh, B. Lebeau, and S. Mann, “Morphosynthesis of calcium carbonate (vaterite) microsponges,” *Adv. Mater.*, vol. 11, no. 4, pp. 324–328, 1999.

[8] Y. Xu, G. Ma, and M. Wang, “Fabrication and Growth Mechanism of Pumpkin-Shaped Vaterite Hierarchical Structures,” *Cryst. Growth Des.*, vol. 14, no. 12, pp. 6166–6171, 2014.

[9] H. Cölfen, “Precipitation of carbonates: recent progress in controlled production of complex shapes,” *Curr. Opin. Colloid Interface Sci.*, vol. 8, no. 1, pp. 23–31, 2003.

[10] Y. J. Han, L. M. Wysocki, M. S. Thanawala, T. Siegrist, and J. Aizenberg, “Template-Dependent Morphogenesis of Oriented Calcite Crystals in the Presence of Magnesium Ions,” *Angew. Chemie*, vol. 117, no. 16, pp. 2438–2442, 2005.

[11] S. S. Wang, A. Picker, H. Cölfen, and A. W. Xu, “Heterostructured calcium carbonate microspheres with calcite equatorial loops and vaterite spherical cores,” *Angew. Chemie - Int. Ed.*, vol. 52, no. 24, pp. 6317–6321, 2013.

[12] K. Lee, W. Wagermaier, A. Masic, K. P. Kommareddy, M. Bennet, I. Manjubala, S.-W. Lee, S. B. Park, H. Cölfen, and P. Fratzl, “Self-assembly of amorphous calcium carbonate microlens arrays,” *Nat. Commun.*, vol. 3, p. 725, 2012.

[13] H. Cölfen and L. Qi, “A systematic examination of the morphogenesis of calcium carbonate in the presence of a double-hydrophilic block copolymer,” *Chemistry*, vol. 7, no. 1, pp. 106–116, 2001.

[14] S. Mann, “Molecular recognition in biomineralisation,” *Nature*, vol. 332, no. 6160, pp.

119–124, 1988.

[15] Y. G. Bushuev, A. R. Finney, and P. M. Rodger, “Stability and Structure of Hydrated Amorphous Calcium Carbonate,” *Cryst. Growth Des.*, vol 15, no 11, pp. 5269–5279, 2015.

[16] J. Yu, J. C. Yu, L. Zhang, X. Wang, and L. Wu, “Facile fabrication and characterisation of hierarchically porous calcium carbonate microspheres,” *Chem. Commun.*, vol. 1, no. 21, pp. 2414, 2004.

[17] D. Walsh and S. Mann, “Fabrication of hollow porous shells of calcium carbonate from self-organizing media,” *Nature*, vol. 377, no. 6547, pp. 320–323, 1995.

[18] S. Mann, “Biomineralisation and biomimetic materials chemistry,” *J. Mater. Chem.*, vol. 5, no. 7, p. 935, 1995.

[19] S. Blank, M. Arnoldi, S. Khoshnavaz, L. Treccani, M. Kuntz, K. Mann, G. Grathwohl, and M. Fritz, “The nacre protein perlucin nucleates growth of calcium carbonate crystals,” *J. Microsc.*, vol. 212, no. 3, pp. 280–291, 2003.

[20] L. Treccani, K. Mann, F. Heinemann, and M. Fritz, “Perlwapin, an abalone nacre protein with three four-disulfide core (whey acidic protein) domains, inhibits the growth of calcium carbonate crystals.,” *Biophys. J.*, vol. 91, no. 7, pp. 2601–8, 2006.

[21] J. Young, S. Davis, P. Bown, and S. Mann, “Coccolith ultrastructure and biomineralisation,” *J. Struct. Biol.*, vol. 126, no. 3, pp. 195–215, 1999.

[22] M. Marsh, “Regulation of $CaCO_3$ formation in coccolithophores,” *Comp. Biochem. Physiol. Part B Biochem. Mol. Biol.*, vol. 136, no. 4, pp. 743–754, 2003.

[23] H. Balard and E. Papirer, “Characterisation and modification of fillers for paints and coatings,” *Prog. Org. Coatings*, vol. 22, no. 1–4, pp. 1–17, 1993.

[24] J. Y. Gal, J. C. Bollinger, H. Tolosa, and N. Gache, “Calcium carbonate solubility: a reappraisal of scale formation and inhibition,” *Talanta*, vol. 43, no. 9, pp. 1497–509, 1996.

[25] S. R. Dickinson and K. M. McGrath, “Switching between kinetic and thermodynamic control: calcium carbonate growth in the presence of a simple alcohol,” *J. Mater. Chem.*, vol. 13, no. 4, pp. 928–933, 2003.

[26] X. Wang, H. Bai, Y. Jia, L. Zhi, L. Qu, Y. Xu, C. Li, and G. Shi, “Synthesis of $CaCO_3$/graphene composite crystals for ultra-strong structural materials,” *RSC Adv.*, vol. 2, no. 5, p. 2154, 2012.

[27] C. H. See and A. T. Harris, “$CaCO_3$ supported Co-Fe catalysts for carbon nanotube synthesis in fluidized bed reactors,” *AIChE J.*, vol. 54, no. 3, pp. 657–664, 2008.

[28] K. Fujihara, M. Kotaki, and S. Ramakrishna, “Guided bone regeneration membrane made of polycaprolactone/calcium carbonate composite nano-fibers.,” *Biomaterials*, vol. 26, no. 19, pp. 4139–47, 2005.

[29] Q. Shen, H. Wei, L. Wang, Y. Zhou, Y. Zhao, Z. Zhang, D. Wang, G. Xu, and D. Xu, “Crystallisation and Aggregation Behaviors of Calcium Carbonate in the Presence of Poly(vinylpyrrolidone) and Sodium Dodecyl Sulfate,” *J. Phys. Chem. B*, vol. 109, no. 39, pp. 18342–18347, 2005.

[30] Y. Kitano, “A Study of the Polymorphic Formation of Calcium Carbonate in Thermal Springs with an Emphasis on the Effect of Temperature,” *Bull. Chem. Soc. Jpn.*, vol. 35, no. 12, pp. 1980–1985, 1962.

[31] J. Chen and L. Xiang, “Controllable synthesis of calcium carbonate polymorphs at different temperatures,” *Powder Technol.*, vol. 189, no. 1, pp. 64–69, Jan. 2009.

[32] K. S. Seo, C. Han, J.-H. Wee, J.-K. Park, and J.-W. Ahn, “Synthesis of calcium carbonate in a pure ethanol and aqueous ethanol solution as the solvent,” *J. Cryst. Growth*, vol. 276, no. 3–4, pp. 680–687, 2005.

[33] X. H. Guo, S. H. Yu, and G.-B. Cai, “Crystallisation in a Mixture of Solvents by Using a Crystal Modifier: Morphology Control in the Synthesis of Highly Monodisperse $CaCO_3$ Microspheres,” *Angew. Chemie*, vol. 118, no. 24, pp. 4081–4085, 2006.

[34] S. A. Markgraf and R. J. Reeder, “High-temperature structure refinements of calcite and magnesite,” *Am. Mineral.*, vol. 70, no. 5–6, pp. 590–600, 1985.

[35] S. R. Kamhi, “On the structure of vaterite $CaCO_3$,” *Acta Crystallogr.*, vol. 16, no. 8, pp. 770–772, 1963.

[36] U. Wehrmeister, L. Soldati, D. E. Jacob, T. Häger, and W. Hofmeister, “Raman spectroscopy of synthetic, geological and biological vaterite: A Raman spectroscopic study,” *J. Raman Spectrosc.*, vol. 41, no. 2, pp. 193–201, 2010.

[37] M. L. Frezzotti, F. Tecce, and A. Casagli, “Raman spectroscopy for fluid inclusion analysis,” *J. Geochemical Explor.*, vol. 112, pp. 1–20, 2012.

[38] P. Brüesch, *Phonons: Theory and Experiments II*, 65th ed. Berlin: Springer-verlag, 1986.

[39] L. Kabalah-Amitai, B. Mayzel, Y. Kauffmann, A. N. Fitch, L. Bloch, P. U. P. a Gilbert, and B. Pokroy, “Vaterite crystals contain two interspersed crystal structures.,” *Science*, vol. 340, no. 6131, pp. 454–7, 2013.

[40] J. J. DeYoreo and P. G. Vekilov, “Principles of Crystal Nucleation and Growth,” *Rev. Mineral. Geochemistry*, vol. 54, no. 1, pp. 57–93, 2003.

[41] A. Navrotsky, “Energetic clues to pathways to biomineralisation: precursors, clusters, and nanoparticles,” *Proc. Natl. Acad. Sci. U. S. A.*, vol. 101, no. 33, pp. 12096–12101, 2004.

[42] J. D. Rodriguez-Blanco, S. Shaw, and L. G. Benning, “The kinetics and mechanisms of amorphous calcium carbonate (ACC) Crystallisation to calcite, viavaterite,” *Nanoscale*, vol. 3, no. 1, pp. 265–271, 2011.

[43] X. Geng, L. Liu, J. Jiang, and S. H. Yu, “Crystallisation of $CaCO_3$ mesocrystals and complex aggregates in a mixed solvent media using polystyrene sulfonate as a crystal growth modifier,” *Cryst. Growth Des.*, vol. 10, no. 8, pp. 3448–3453, 2010.

[44] B. Pokroy, A. N. Fitch, F. Marin, M. Kapon, N. Adir, and E. Zolotoyabko, “Anisotropic lattice distortions in biogenic calcite induced by intra-crystalline organic molecules,” *J. Struct. Biol.*, vol. 155, no. 1, pp. 96–103, 2006.

[45] B. Pokroy, A. N. Fitch, and E. Zolotoyabko, “The microstructure of biogenic calcite: A view by high-resolution synchrotron powder diffraction,” *Adv. Mater.*, vol. 18, no. 18, pp. 2363–2368, 2006.

[46] B. Pokroy, A. N. Fitch, P. L. Lee, J. P. Quintana, E. N. Caspi, and E. Zolotoyabko, “Anisotropic lattice distortions in the mollusk-made aragonite: a widespread phenomenon,” *J. Struct. Biol.*, vol. 153, no. 2, pp. 145–50, 2006.

# Chapter 5: Crystal Tectonics - Temperature induced self-assembly of PSSA-stabilized vaterite nanocrystals into hierarchical spheres

## 5.1 Introduction

Crystal tectonics is the directed or spontaneous self-assembly of preformed nanocrystals into higher-order structures of complex form and superior properties[1]–[3]. Underpinned by the briskly evolving field of nanoscience and nanotechnology, *in vitro* directed-assembly of nanoparticles into hierarchal superstructures (that retain the size-dependent properties of the nanoscale building blocks), has been suggested to be one of the most effective bottom-up synthetic methods towards advanced functional materials[4]–[7]. Such materials have received immense application in various scientific fields such as: "smart" drugs (pharmaceuticals),[8]–[10] bone regeneration,[11] thin films[12], and catalysis[13], [14].

Manipulating the crystal growth through polyelectrolyte-directed particle attachment towards desired intricate morphologies and size is often a challenging task[15], [16]. Such sophisticated tectonic ability and complexity is reflected quite well in biominerals of natural organisms[17]–[19]. This has driven most of the research output into the biomimetic self-assembly of inorganic crystals (mostly for calcium carbonate), leading to the discovery of mesocrystals by Cölfen [20]. These mesocrystals are grown by polymer-directed assembly of preformed nanocrystals into highly ordered structures, through face-specific interactions of the organic polymer moieties and the growing crystal facets, analogous to those that grow during the biomineralisation process. Here crystal proliferation doesn't proceed by classical ion-by-ion attachment but by assembly of nucleated nanocrystals, resulting in bulk crystals which are highly ordered with occluded organic macromolecules within their structure, and morphologies which do not resemble the symmetry of the unit cell[21]–[23].

Crystallisation by orientated particle attachment (CPA) reactions are often carried out at isothermal conditions close to room temperature, over lengthy periods of time[24], [25]. Here self-assembly and crystal proliferation is very sensitive to the local environment, such that: temperature, stirring rate, polymer concentration, polymer molecular weight, saturation and

time all affect the kinetics and thermodynamics of the process, leading to selective morphogenesis and polymorphism[25], [26].

In this chapter, crystal tectonics based upon the temperature induced poly (4-styrenesulfonic acid) (PSSA)-directed assembly of PSSA-stabilized vaterite crystals into hierarchically structured spheres, is described. The ability to stabilize the metastable polymorph of $CaCO_3$ under atmospheric pressure and at a wide range of crystallisation temperatures: 30, 40, 75, and 100 ˚C using PSSA was investigated. The influence of crystallisation time on the particle attachment pathway was investigated.

## 5.2 Experimental

### 5.2.1 Materials

All chemicals were of analytical grade. Calcium chloride, ammonium carbonate, poly (4-styrenesulfonic acid) $M_w$ ~75,000, 18 wt. % in $H_2O$, were purchased from Sigma-Aldrich. Sodium hydroxide pellets were purchased from Merck (Pty) Ltd South Africa. The 25% (weight %) ammonia solution, hydrochloric acid (HCl) 32 % (weight %) were obtained from Associated Chemical Enterprises (Pty) Ltd. All chemicals were used without any further purification.

### 5.2.2 Self-assembly crystallisation reactions

Each crystallisation reaction was carried out in a 250 mL round bottom flask in an oil bath that was maintained at one of four different reaction temperatures: 30 °C, 40 °C, 75 °C, and 100 °C. Typically, 3% of poly (4-styrenesulfonic acid) aqueous solution (100 ml) was prepared with distilled water, and the pH of the resulting mixture was adjusted to pH 10 with aqueous sodium hydroxide solution (2 M). To this mixture, 50 mL (i.e. 5 mmol) of a 0.100 M $CaCl_2$ aqueous solution, prepared with distilled water (adjusted to pH 9 using an aqueous $NH_3$ solution), was added drop-wise under gentle stirring at each of the four desired temperatures. The reaction mixtures were left to stir for an hour and then 50 mL of (i.e. 5 mmol) of a 0.100 M $(NH_4)_2CO_3$ aqueous solution (prepared with distilled water), was added drop-wise to each mixture under gentle stirring. These reaction mixtures were kept at each of the four desired temperatures under gentle stirring for four different reaction durations: 3, 6, 12, and 24 hrs. The precipitated products were centrifuged, washed with distilled water several times and then left to dry overnight at room temperature.

### 5.2.3 Characterisation

Characterisation of all samples was performed as described in Chapter 3 (section 3.4), except for those analysed by focused ion beam - scanning electron microscopy (FIB-SEM). FIB-SEM micrographs were obtained using a FEI Nova Nanolab 600 FIB-SEM microscope at an applied voltage of 30 kV, using a secondary electron (SE) detector. The FIB beam settings were 2.8 n at 30 kV (beam at 90 ˚ incident angle), and cuts were performed using consecutive rectangle patterning until the sample was cut through as desired. For the SEM imaging, samples were mounted on a double sided carbon tape (SPI Supplies, West Chester, PA, USA) which was mounted on 35 mm aluminium stubs (SPI Supplies, West Chester, PA, USA). The mounted samples were then sputter coated with a 5 nm carbon layer deposited by an Emitech 950x Carbon Vacuum Evaporator (Quorum Technologies; Ashford, Kent, UK), and a 5 nm gold-palladium layer deposited by an Emitech 550x Sputter Coater (Quorum Technologies; Ashford, Kent, UK) using a gold-palladium target from Electron Microscopy Sciences (EMS; Hatfield, PA, USA) prior to imaging.

## 5.3 Results and Discussion

The polymorphs of the precipitated calcium carbonate powders at different reaction times (3, 6, 12, and 24 hrs) and temperatures (30, 40, 75, and 100 ˚C) were determined by PXRD (shown in Figure 5.1 (a)-(d)). In all cases the precipitated calcium carbonate powders were found to be pure vaterite (ICSD 015879), which is quite interesting because one would have expected the formation of calcite at lower temperatures (< 30 ˚C), a mixture of all three polymorphs at intermediate temperatures (35-55 ˚C), and a formation of aragonite at higher temperatures (> 60 ˚C), as previously reported[27].

However, here the presence of PSSA affected the interplay between the kinetics and thermodynamics during proliferation and self-assembly of the vaterite crystals. This was believed to have taken place by modification of the free energy landscape through surface interaction between the PSSA and the crystal facets - a kinetic inhibition phenomenon[5]. This PSSA kinetic control was observed most clearly from the *ex situ* PXRD data for the crystallisation time studies (Figure 5.1 (a)-(d)). Consequently only the pure vaterite polymorph was observed at temperatures where other polymorphs would otherwise have been expected[27].

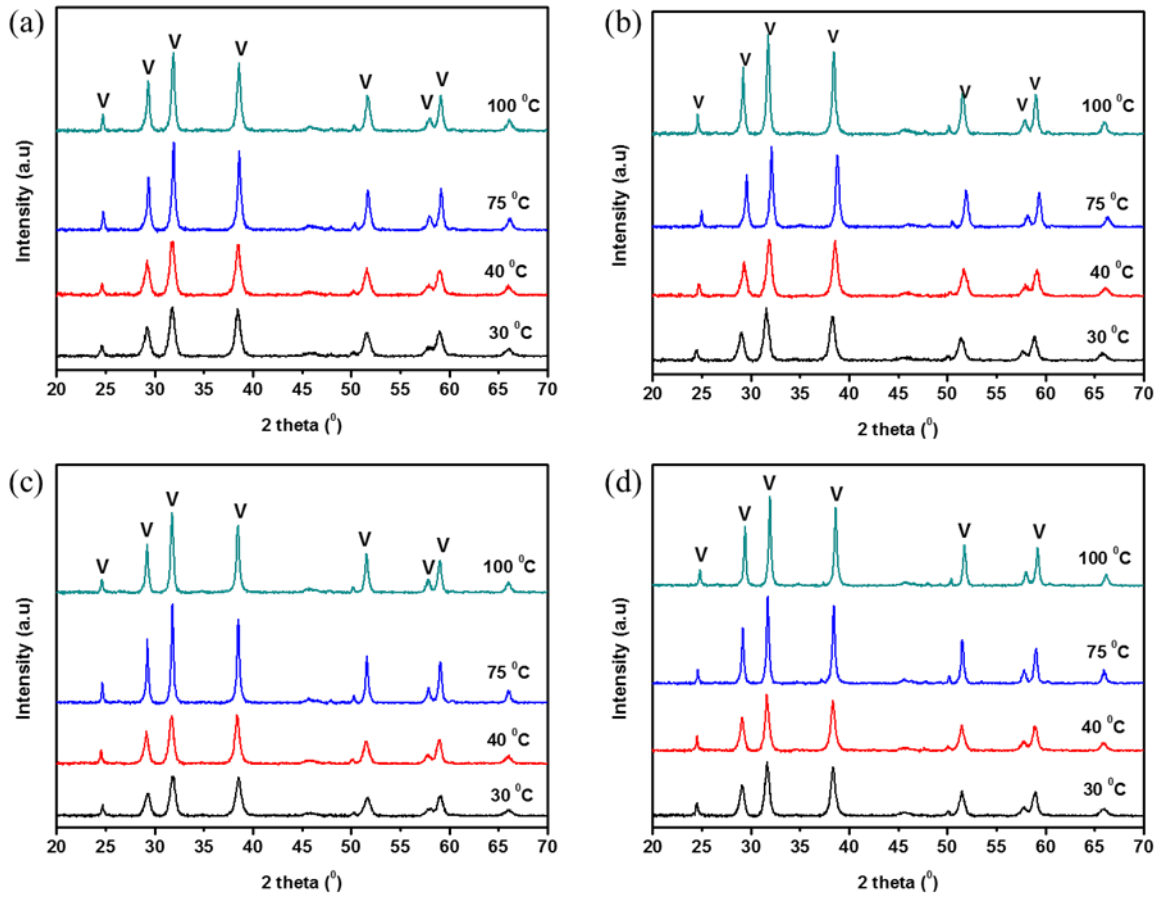



Figure 5. 1. PXRD diffractograms showing the ability of PSSA to stabilize the vaterite polymorph across different reaction temperatures and times, i.e. at: (a) 3 hrs, (b) 6 hrs, (c) 12 hrs, and (d) 24 hrs. Indexed according to ICSD 015879.

Similarly no change in the polymorph of the precipitated calcium carbonate throughout the different reaction times i.e. from 3 hrs to 24 hrs (Figure 5.1 (a)-(d)) was observed, not even the reflection of the most intense (104) calcite peak. Conversely, in the absence of any additives Rodriguez-Blanco *et al*. have shown that the transformation of vaterite to calcite was time dependent, with the first reflection of the calcite (104) peak appearing in just over 5 hrs of crystallisation, through the dissolution and reprecipitation mechanism[28]. In their study it was also shown that the rate of this transformation (i.e. vaterite to calcite) was controlled by the surface area of calcite. The observations of this present study support the argument that PSSA had a kinetic inhibition effect on the activation-energy barrier of the phase transformation from vaterite to calcite.

A schematic of the influence of temperature in the self-assembly of pre-formed vaterite crystals is shown in Figure 5.2.

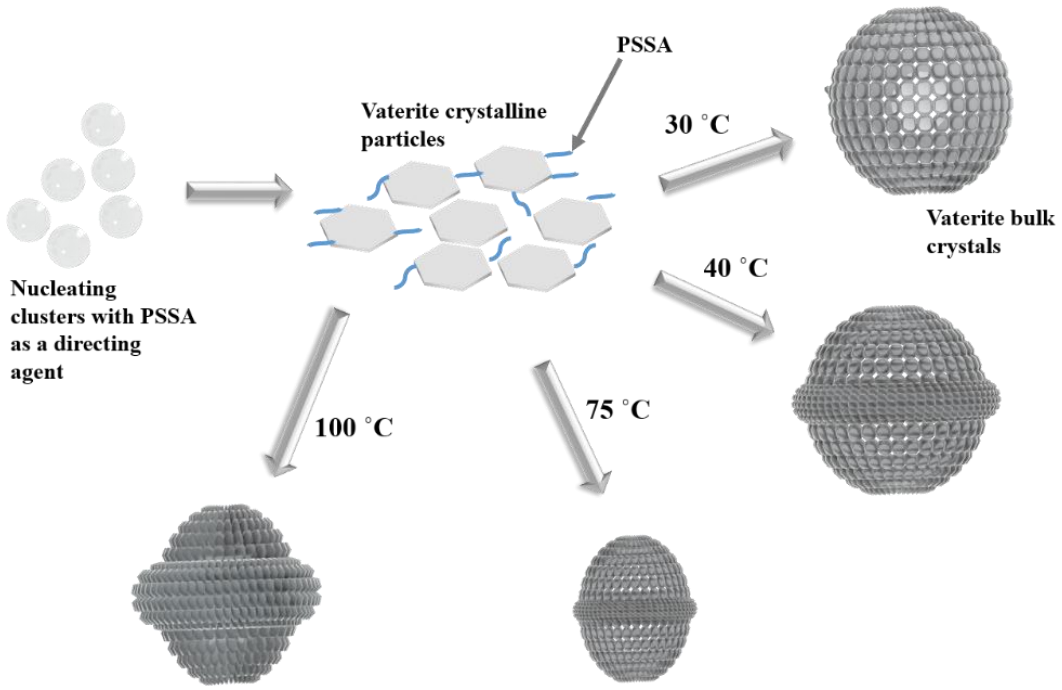



Figure 5. 2. Schematic of the effect of temperature on the self-assembly of vaterite crystals: systematic morphogenesis.

In addition to its kinetic inhibition effect, resulting in the stabilisation of the vaterite polymorph, organic macromolecules such as PSSA have been reported to induce assembly of nanocrystalline particles into highly ordered bulk crystals of intricate morphologies[24]. The size and shape of these bulk crystals and the particles from which they were formed were dependent of the conditions under which growth took place[7].

The effect of the various reaction temperatures, on the morphology of the bulk self-assembled vaterite crystals, was investigated by SEM at 3 hrs into the crystallisation process (Figure 5.3).

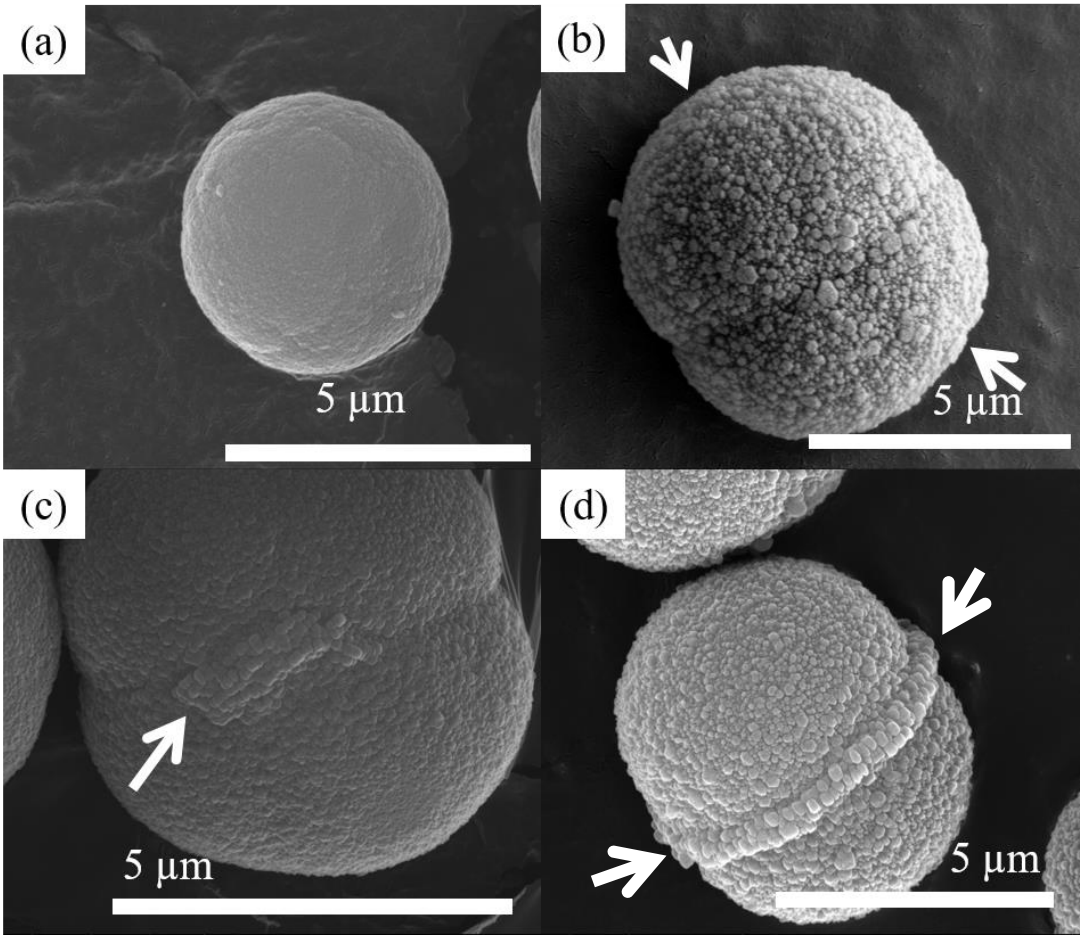



Figure 5. 3. SEM micrographs showing the effect of reaction temperature on the morphology of the bulk self-assembled vaterite crystals precipitated at 3 hrs into the crystallisation process at: (a) 30 ˚C, (b) 40 ˚C, (c) 75 ˚C, (d) 100 ˚C.

Here it was observed that at a crystallisation temperature of 30 ˚C (Figure 5.3 (a)) the attachment of the vaterite particles favoured a spherical bulk crystal morphology which had a relatively smooth topography. However, as the crystallisation temperature was increased to 40, 75, and 100 ˚C, attachment of the particles led to what appeared to be two fused vaterite spheres (Figure 5.3 (b)-(d) – see double arrow), whose surface textures were much rougher than their 30 ˚C counterparts. However, here an interesting change in the assembly of the vaterite particles was observed, where an orientated attachment of particles began to form along the equatorial region (along the line which the two spheres had appeared to have fused (i.e. single arrow in Figure 3 (c)) of the bulk crystal. This orientated attachment of tangentially aligned particles around the equatorial region of the bulk sphere was more pronounced at 100 ˚C (Figure 5.3 (d) – see arrows). It was also interesting to note that both the different final bulk

vaterite crystal morphologies and the tangentially aligned particles around their equatorial regions were the same polymorph, irrespective of crystallisation temperature (as confirmed by PXRD in Figure 1 (a)), owing to the kinetic effects of PSSA.

Figure 5.4 (a)-(c) is a magnification series of static TEM (Figure 5.4 (a)) and SEM (Figure 5.4 (b-c)) micrographs showing the assemblies of aligned vaterite particles. Real-time observations of liquid-based crystal growth via particle attachment are rare, complex and limited to few *in situ* techniques such as transmission electron microscopy (TEM)[29], [30]. However, static high-resolution TEM or SEM micrographs showing assemblies of nanocrystals into a bulk crystals have been accepted as adequate evidence of self-assembly[22].

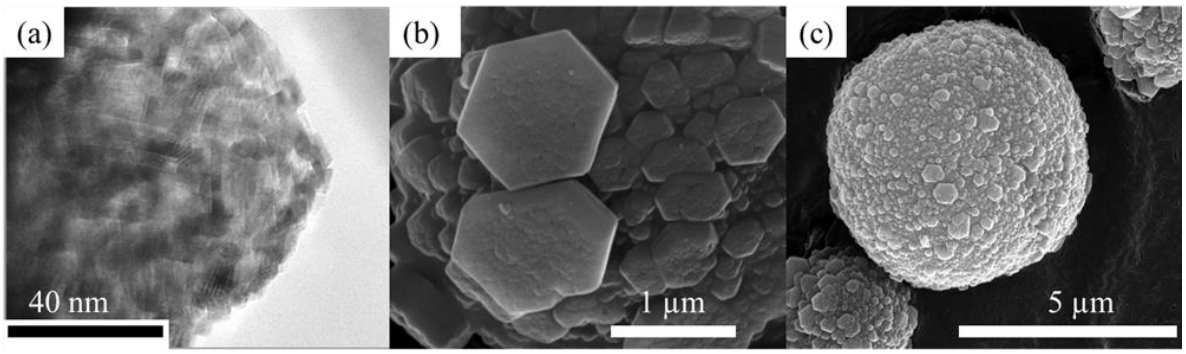



Figure 5. 4. Magnification series of the self-assembly of vaterite nanocrystals showing: (a) The oriented attachment of nanocrystalline particles from a thin section at the edge a bulk sphere (TEM micrograph), (b) The directed self-assembly of hexagonal vaterite particles into a vaterite sphere (SEM micrograph), and (c) A vaterite sphere formed from self-assembled hexagonal vaterite particles (SEM micrograph).

In this magnification series, the surface architecture of the bulk crystal formed by assembled hexagonal vaterite particles is shown in Figure 5.4 (b). The interplay between kinetics and thermodynamics (as a result of synergistic effects of PSSA and temperature) during assembly controlled the size of the hexagonal particle growth up to the thermodynamically stable size in an attempt to increase the surface energy, while it minimised the bulk crystal free energy at different stages of the particle attachment process[31]. All these factors directed the formation and assembly of vaterite particles, leading to systematic morphogenesis of vaterite bulk crystals which did not resemble the symmetry of the (hexagonal) vaterite unit cell (Figure 5.4 (c)). This observation has been accepted as evidence of self-assembly[21], [24], [32], [33].

The effect of crystallisation temperature on the directed assembly of vaterite particles was investigated when the crystallisation time was increased to 6 hrs, and the resultant products were analysed as shown in Figure 5.5 (a)-(d). It has been reported that crystallisation time can influence the morphology and polymorphism of $CaCO_3$[25]. The final bulk crystal morphology of the assembled vaterite crystals at 30 ˚C was found to be spherical and these had relatively smooth surfaces as at 3 hrs with solid cores– see arrows (Figure 5.5 (a)). To confirm this, representative self-assembled bulk vaterite crystals were cut in half using a focused-ion beam (FIB) (Figure 5.6).

Despite the fact that the FIB had destroyed the cross-sectional topographical details, it could still be deduced from the broken bulk vaterite crystal (Figure 5.5 (a)) formed at 30 ˚C, that the crystal nucleation and growth by self-assembly had followed what appeared to be a radially aligned particle attachment pathway (i.e. from the centre of the sphere to the periphery of the bulk crystal), which had given rise to this solid core. It was interesting to note that, irrespective of the CPA pathway which lead to varying bulk crystal morphologies, only one polymorph had formed throughout i.e. pure vaterite (as was previously confirmed by PXRD earlier in the discussion).

The bulk crystal morphologies of the products that had assembled at: 40 ˚C (Figure 5.5 (b)), 75 ˚C (Figure 5.5 (c)) and 100 ˚C (Figure 5.5 (d)) were also examined at 6 hrs into the crystallisation process. It became apparent from the SEM micrographs that the crystallisation time had not substantially changed the assembly pathway towards the bulk crystal morphology at the different temperatures, when the products formed at 3 hrs (Figure 5.3 (a)-(d)) and 6 hrs (Figure 5.5 (a)-(d)) were compared with one another. However, it was noted that the tangentially aligned particles around the equatorial region of the bulk spheres at 75 ˚C and 6 hrs (Figure 5.5 (c) – see arrows) were more pronounced than at 75 ˚C and 3 hrs (Figure 5.3 (c) – see arrow).

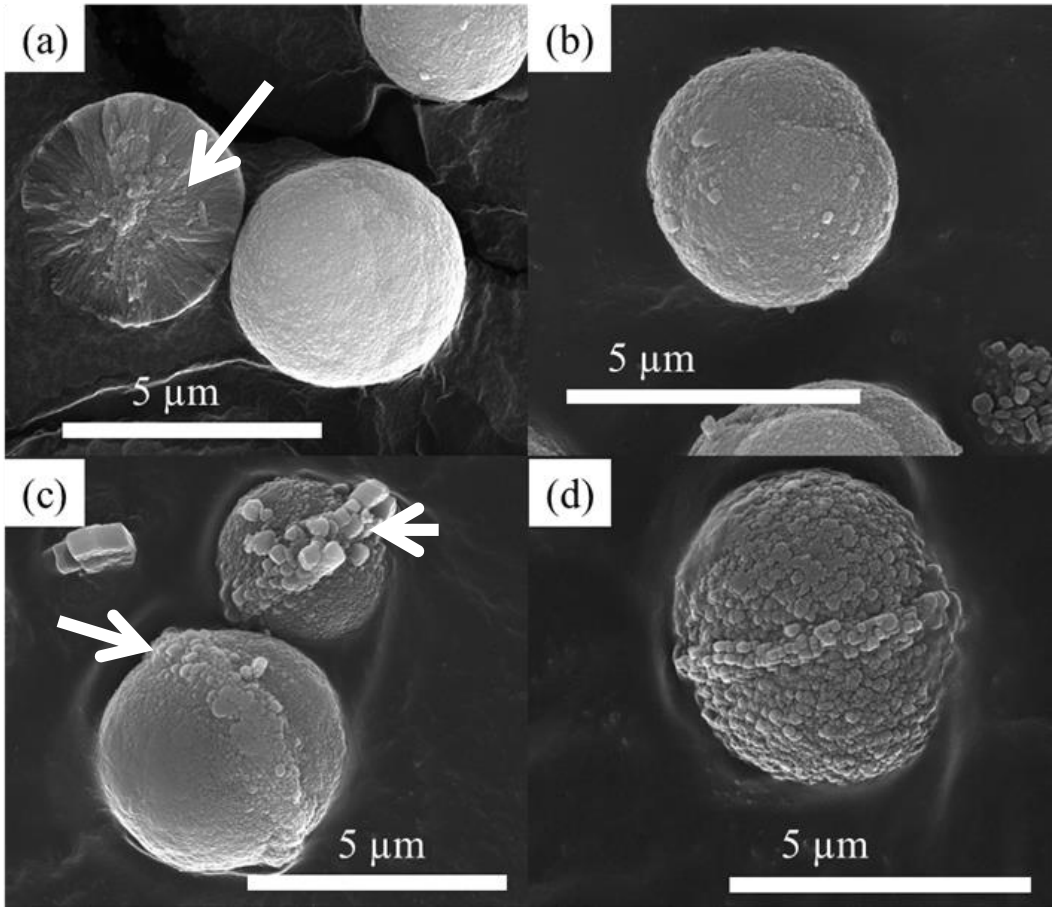



Figure 5. 5. SEM micrographs showing the effect of temperature on the morphology of the bulk self-assembled vaterite crystals precipitated at 6 hrs into the crystallisation process at: (a) 30 ˚C, (b) 40 ˚C, (c) 75 ˚C, (d) 100 ˚C.

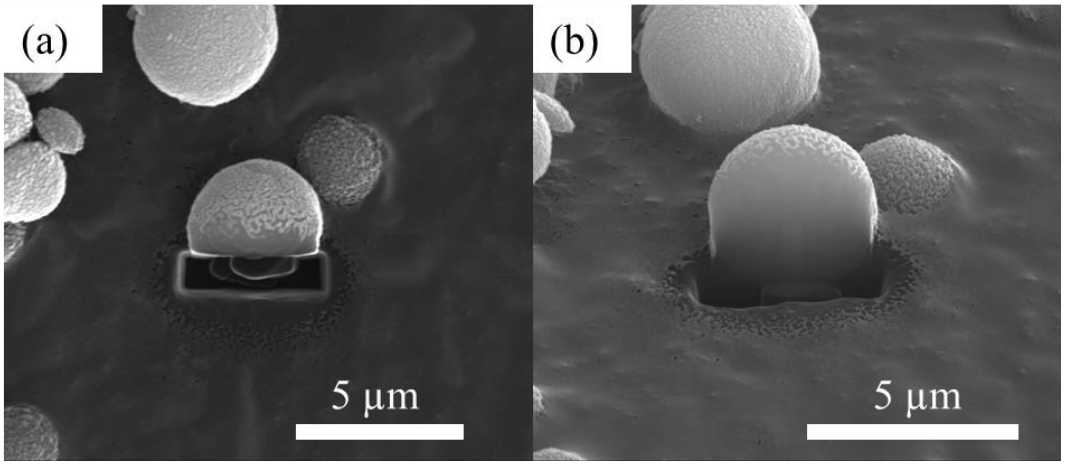



Figure 5. 6. SEM-FIB micrographs of the dissected solid core vaterite bulk crystals. (a) 90 ˚ incident angle, (b) 51 ˚ incident angle.

The change in the particle attachment pathway (from regular smooth spheres to spheres with tangentially aligned particles) with increase in crystallisation temperature during assembly resulted in the increase in surface roughness of the bulk spherical crystals observed in the SEM micrographs of the vaterite spheres crystallised at 75 and 100 ˚C at 6 hrs.

The bulk self-assembled vaterite crystals that were formed at the various temperatures (30-100 ˚C) at fixed times (3-24 hrs) were then subjected to analysis by laser Raman spectroscopy. Literature has indicated that a typical laser Raman spectrum of a vaterite polymorph of calcium carbonate would consist of sharp, intense symmetrical carbonate stretching modes with split peaks at 1075 and 1090 $cm^{-1}$, as well as broad lattice modes with split peaks found below 400 $cm^{-1}$[34]. Furthermore, it indicated that symmetrical stretching of the sulfonate groups (at 1120 $cm^{-1}$) and the aromatic groups (at 1600 $cm^{-1}$) would also have been expected if PSSA had been used as a directing agent and had become occluded within the bulk vaterite crystals[35].

All of these peaks were observed when the various bulk self-assembled vaterite crystals previously mentioned were analysed by laser Raman spectroscopy (Figure 5.7). However, in these results it was noted that the relative intensities of the Raman peaks generally decreased with increased crystallisation temperature, as shown in Figure 5.7 (a)-(d). This was due to the fact that there was less scattering of the laser light on a smooth crystal surface crystallised at 30 ˚C, and hence more laser light was collected by the detector as opposed to a much rougher crystal surface crystallised at higher temperatures (40, 75, and100 ˚C), which led to more scattering of the laser light and less collection of light by the detector, resulting in relatively lower intensities[36]. These laser Raman results were in good agreement with the SEM data on the effect of crystallisation temperature on the surface roughness of the bulk vaterite spherical crystals at different times (i.e. 3-24 hrs).

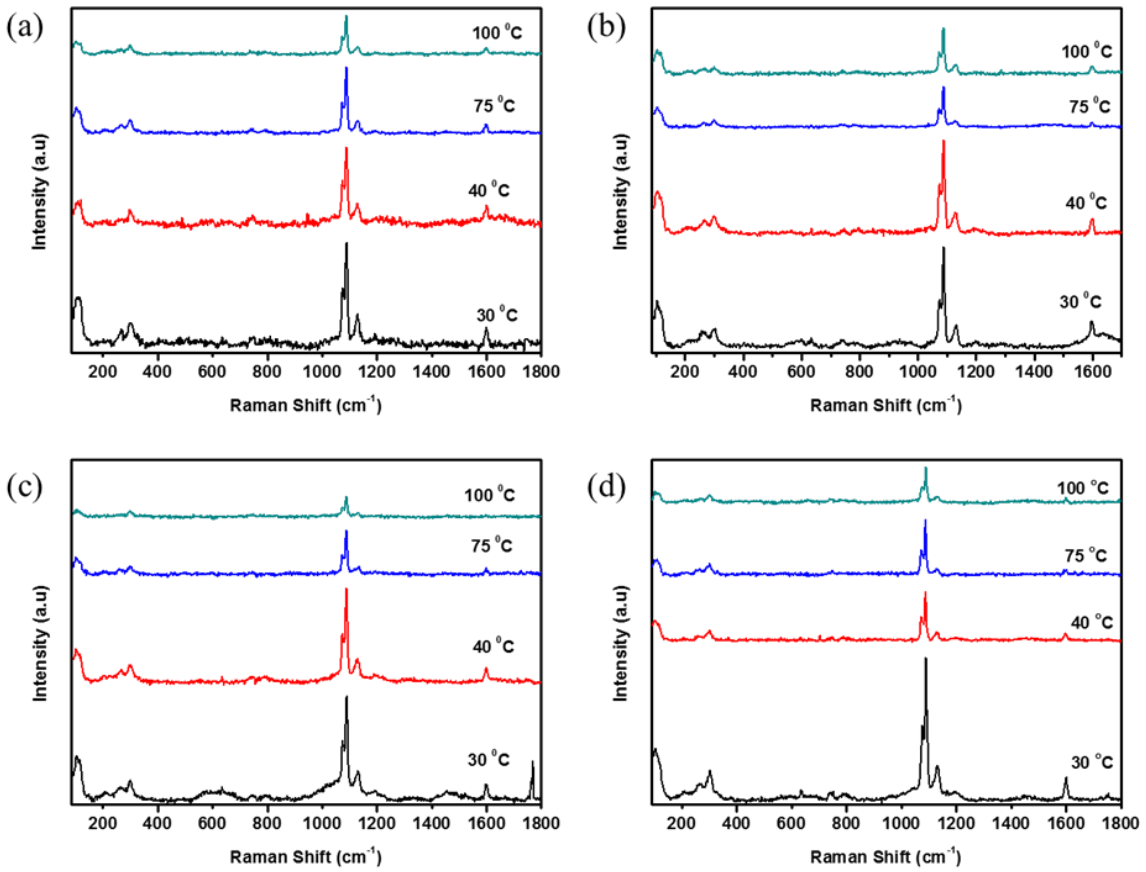



Figure 5. 7. Laser Raman spectra showing the pure vaterite polymorph and the effect of reaction temperature on the surface roughness of the vaterite spheres at different reaction times, i.e. at: (a) 3 hrs, (b) 6 hrs, (c) 12 hrs, and (d) 24 hrs.

The bulk self-assembled vaterite crystals that were formed at the various temperatures (30-100 ˚C) at fixed times (3-24 hrs) were then subjected to thermogravimetric analysis in order to investigate their thermal stability. Here the presence of occluded PSSA within the bulk vaterite crystals was confirmed, in each case, by the decomposition of PSSA at 450 ˚C (as seen in Figure 5.8 (a)-(d))[25]. The presence of occluded organic molecules within bulk crystals formed by particle attachment has been accepted as evidence of self-assembly or the so-called crystallisation by particle attachment (CPA)[22].

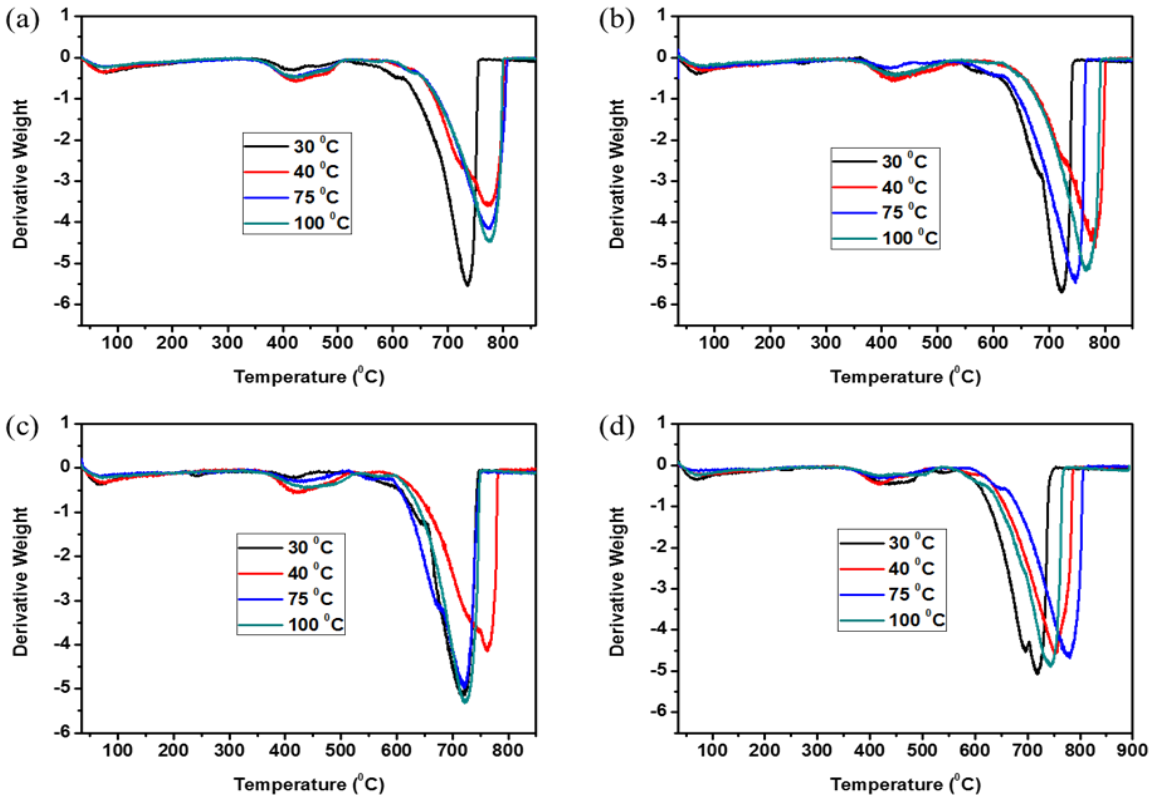



Figure 5. 8. The first derivatives of the TGA thermograms for the bulk self-assembled vaterite crystals formed at: (a) 3 hrs, (b) 6 hrs, (c) 12 hrs and (d) 24 hrs.

Figure 5.8 (a)-(d) shows the first derivatives of the TGA thermograms of the bulk vaterite crystals at different crystallisation temperatures (30-100 ˚C) for the various crystallisation times (3, 6, 12, and 24 hrs), respectively. All of these thermograms exhibited a similar decomposition pattern i.e. the first decomposition peak at around 90-100 ˚C was attributed to the loss of adsorbed water, the second decomposition peak at around 450 ˚C was attributed to the loss of occluded PSSA (as previously mentioned)[25], and the last decomposition peak (between 700 ˚C and 800 ˚C) was attributed to the loss of carbon dioxide ($CO_2(g)$) by the decomposition of calcium carbonate ($CaCO_3(s)$) to give calcium oxide ($CaO(s)$). It was also observed that the increase in the amount of occluded PSSA (estimated by the visual observation of the 450 ˚C the peaks and quantified in Figure S.3, Appendix 1) within the bulk vaterite crystals resulted in the increase in the decomposition temperature of $CaCO_3(s)$ to give $CO_2(g)$ and $CaO(s)$.

The effect of temperature dependency on the systematic morphogenesis of bulk vaterite crystals through different CPA pathways after 12 hrs of crystallisation is shown in Figure 5.9 (a)-(d).

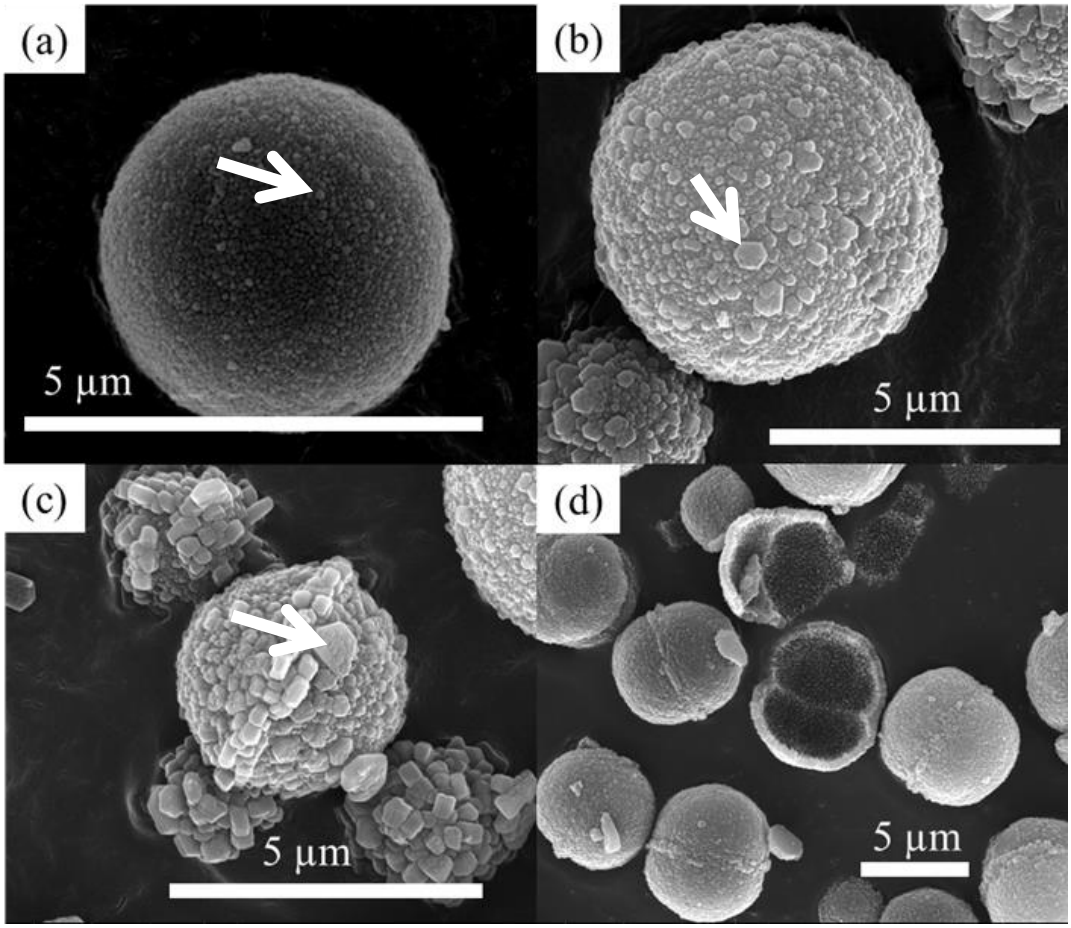



Figure 5. 9. SEM micrographs showing the effect of temperature on the morphology of bulk self-assembled vaterite crystals precipitated 12 hrs into the crystallisation process at: (a) 30 ˚C, (b) 40 ˚C, (c) 75 ˚C and (d) 100 ˚C.

Here, after 12 hrs into the crystallisation process, a trend consistent with the CPA pathway that was noted at lower times and for the various temperatures (30-100 ˚C), was also observed. Once again the morphological transformation into calcite (as would be expected in the absence of PSSA) was not observed.

A visual inspection of the bulk self-assembled vaterite crystals formed at a lower crystallisation temperature (i.e. 30 ˚C) revealed that their surface topography was much smoother than the bulk crystals at higher crystallisation temperature (i.e. 40, and 75 ˚C). This was due to the fact that the preformed particles which underwent attachment were of different sizes, as shown by

the arrows in Figures 5.9 (a-c). This was due to the changes in surface energy at the different reaction temperatures during nucleation and proliferation of the vaterite polymorph in the presence of PSSA, which resulted in kinetic barriers and bias towards particular crystalline particle sizes which were more thermodynamically stable[31]. Hence higher temperatures resulted in bigger preformed particles which assembled in a thermodynamically stable morphology.

Further examination by SEM of the bulk self-assembled vaterite crystals revealed interesting features which provided some important insight into their crystal formation and proliferation under different temperatures. For instance, not only did it appear that bulk crystals were composed of two spheres which had fused and formed equatorially aligned crystals at higher reaction temperatures (i.e. 100 ˚C) as was previously observed, but from the limited presence of broken spheres, the cores of these appeared to be hollow as seen in Figure 5.9 (d) (see Appendix 1, Figure S.2). This observation suggested that the crystal formation and proliferation mechanism of dissolution-reprecipitation via the Ostwald-Lussac law of phases may have occurred, where it has been suggested that in the first instance amorphous calcium carbonate (ACC) would have nucleated, followed by its dissolution during the precipitation of vaterite around it, hence the hollow spherical morphology[16]. Indeed De Yoreo's group, using *in situ* TEM, observed that in some cases internal dissolution of bulk self-assembled crystals had occurred, which had led to the formation of vaterite particles which had hollow cores[29].

The effects of crystallisation temperature on the morphology of the bulk vaterite crystals after 24 hrs of self-assembly are shown in Figure 5.10. As before a similar CPA trend was observed, however here the oriented attachment of particles on the equatorial region of the bulk vaterite spheres were observed at 40 ˚C, as opposed to at 75 ˚C for the 3, 6, and 12 hrs. This was attributed to the longer crystallisation time, which allowed the nucleation and attachment of particles on the equatorial region of the bulk crystal in order to assume a thermodynamically stable bulk crystal morphology and size.

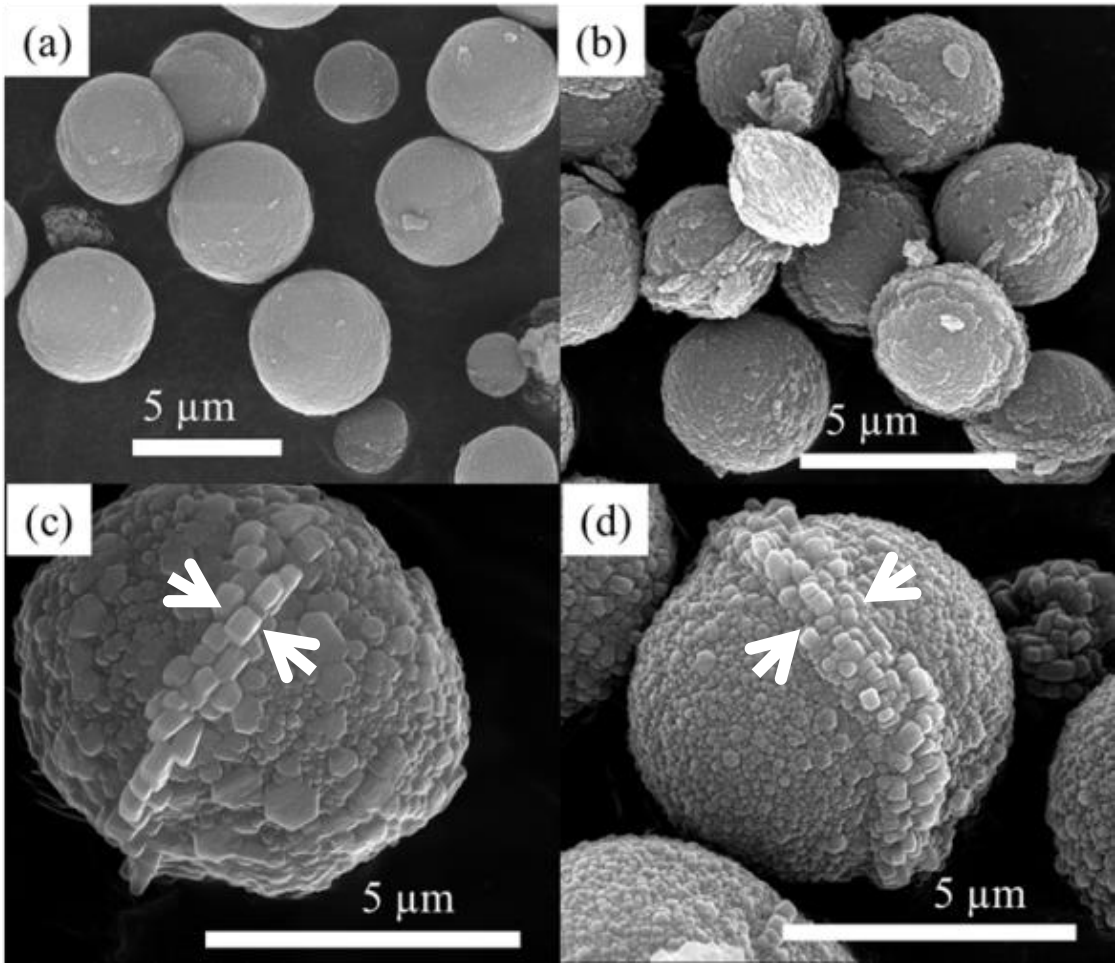



Figure 5. 10. SEM micrographs showing the effect of temperature on the morphology of self-assembled vaterite crystals precipitated after 24 hrs at: (a) 30 ˚C, (b) 40 ˚C, (c) 75 ˚C and (d) 100 ˚C.

The width of the equatorially aligned crystals on the bulk crystal was observed to have increased with the increase in the reaction temperature (see double arrows in Figure 5.10 (c) and (d)). This was due to the interplay between the kinetics and energetics that were governed by: PSSA, crystallisation time, and crystallisation temperature.

## 5.4 Conclusions

Various hierarchically structured morphologies of pure vaterite bulk crystals were successfully synthesized by PSSA-directed particle attachment through the influence of temperature. Here it was observed that varying the crystallisation/reaction temperature led to different CPA pathways, which in turn resulted in bulk crystal morphologies that varied. For instance, a crystallisation temperature of 30 ˚C gave relatively smooth bulk crystals which were spherical. At 40 ˚C it appeared that two bulk spherical crystals had fused and give rise to ellipsoidal-shaped bulk crystals. On the other hand, at crystallisation temperatures of 75 and 100 ˚C, oriented attachment of particles around the equatorial region of the bulk spherical crystals were noted.

Changes in the crystallisation temperature were found not to have changed the polymorphism of the precipitated $CaCO_3$ due to the kinetic stabilisation effects of PSSA, as opposed to previous reports[27]. Similarly, crystallisation time predominantly did not affect the polymorphism of the precipitated $CaCO_3$ and the CPA pathway at different temperatures. However, after 24 hrs of crystallisation the oriented attachment of equatorially aligned crystals were observed to form at a lower temperature (i.e. 40 ˚C) than previously observed (i.e. 75 ˚C) for lower crystallisation times. Significantly, at higher reaction temperatures (i.e. 75 and 100 ˚C) hollow bulk crystals were formed, while at lower temperatures solid core bulk vaterite crystals were formed.

## 5.5 References


[1] S. Mann, “Biomineralization and biomimetic materials chemistry,” *J. Mater. Chem.*, vol. 5, no. 7, p. 935, 1995.

[2] S. Mann, *Biomineralization, Principles and Concepts in Bioinorganic Materials Chemistry*. New York: oxford university press, 2001.

[3] S. Mann, S. A. Davis, S. R. Hall, M. Li, K. H. Rhodes, W. Shenton, S. Vaucher, and B. Zhang, “Crystal tectonics: Chemical construction and self-organization,” *J. Chem. Soc. Dalt. Trans.*, no. 21, pp. 3753–3763, 2000.

[4] M. Grzelczak, J. Vermant, E. M. Furst, and L. M. Liz-Marzán, “Directed Self-Assembly of Nanoparticles,” *ACS Nano*, vol. 4, no. 7, pp. 3591–3605, 2010.

[5] H. Cölfen and S. Mann, “Higher-order organization by mesoscale self-assembly and transformation of hybrid nanostructures,” *Angew. Chemie - Int. Ed.*, vol. 42, no. 21, pp. 2350–2365, 2003.

[6] A. J. Patil, M. Li, and S. Mann, “Integrative self-assembly of functional hybrid nanoconstructs by inorganic wrapping of single biomolecules, biomolecule arrays and organic supramolecular assemblies,” *Nanoscale*, vol. 5, no. 16, pp. 7161–74, 2013.

[7] S. Mann, “Self-assembly and transformation of hybrid nano-objects and nanostructures under equilibrium and non-equilibrium conditions,” *Nat. Mater.*, vol. 8, no. 10, pp. 781–792, 2009.

[8] Z. Xiao, C. Ji, J. Shi, E. M. Pridgen, J. Frieder, J. Wu, and O. C. Farokhzad, “DNA self-assembly of targeted near-infrared-responsive gold nanoparticles for cancer thermo-chemotherapy,” *Angew. Chemie - Int. Ed.*, vol. 51, no. 47, pp. 11853–11857, 2012.

[9] M. Daniel and D. Astruc, “Gold Nanoparticles : Assembly , Supramolecular Chemistry , Quantum-Size-Related Properties , and Applications toward Biology , Catalysis , and Nanotechnology,” *Chem. Rev.*, vol. 104, no. 1, pp. 293–346, 2004.

[10] J. S. Kim, W. J. Rieter, K. M. L. Taylor, H. An, W. Lin, and W. Lin, “Self-Assembled Hybrid Nanoparticles for Cancer-Specific Multimodal Imaging,” *J. Am. Chem. Soc.*, vol. 129, no. 29, pp. 8962–8963, 2007.

[11] K. Fujihara, M. Kotaki, and S. Ramakrishna, “Guided bone regeneration membrane made of polycaprolactone/calcium carbonate composite nano-fibers,” *Biomaterials*, vol. 26, no. 19, pp. 4139–4147, 2005.

[12] J. Paczesny, M. Wójcik, K. Sozański, K. Nikiforov, C. Tschierske, A. Lehmann, E. Górecka, J. Mieczkowski, and R. Hołyst, “Self-assembly of gold nanoparticles into 2D arrays induced by bolaamphiphilic ligands,” *J. Phys. Chem. C*, vol. 117, no. 45, pp. 24056–24062, 2013.

[13] B. Jiang, C. Li, M. Imura, J. Tang, and Y. Yamauchi, “Multimetallic Mesoporous Spheres Through Surfactant-Directed Synthesis,” *Adv. Sci.*, vol. 2, no. 8, p. n/a–n/a,

2015.

[14] D. Gu and F. Schüth, “Synthesis of non-siliceous mesoporous oxides.,” *Chem. Soc. Rev.*, vol. 43, no. 1, pp. 313–44, 2014.

[15] S. Mann and G. A. Ozin, “Synthesis of inorganic materials with complex form,” *Nature*, vol. 382, no. 6589, pp. 313–318, 1996.

[16] J. J. DeYoreo and P. G. Vekilov, “Principles of Crystal Nucleation and Growth,” *Rev. Mineral. Geochemistry*, vol. 54, no. 1, pp. 57–93, 2003.

[17] J. Young, S. Davis, P. Bown, and S. Mann, “Coccolith ultrastructure and biomineralisation,” *J. Struct. Biol.*, vol. 126, no. 3, pp. 195–215, 1999.

[18] M. . Marsh, “Regulation of $CaCO_3$ formation in coccolithophores,” *Comp. Biochem. Physiol. Part B Biochem. Mol. Biol.*, vol. 136, no. 4, pp. 743–754, 2003.

[19] L. Treccani, K. Mann, F. Heinemann, and M. Fritz, “Perlwapin, an abalone nacre protein with three four-disulfide core (whey acidic protein) domains, inhibits the growth of calcium carbonate crystals,” *Biophys. J.*, vol. 91, no. 7, pp. 2601–8, 2006.

[20] H. Cölfen and M. Antonietti, “Mesocrystals: Inorganic Superstructures Made by Highly Parallel Crystallization and Controlled Alignment,” *Angew. Chemie Int. Ed.*, vol. 44, no. 35, pp. 5576–5591, 2005.

[21] M. Niederberger and H. Cölfen, “Oriented attachment and mesocrystals: Non-classical crystallization mechanisms based on nanoparticle assembly,” *Phys. Chem. Chem. Phys.*, vol. 8, no. 28, p. 3271, 2006.

[22] J. J. De Yoreo, P. U. P. A. Gilbert, N. A. J. M. Sommerdijk, R. L. Penn, S. Whitelam, D. Joester, H. Zhang, J. D. Rimer, A. Navrotsky, J. F. Banfield, A. F. Wallace, F. M. Michel, F. C. Meldrum, H. Colfen, and P. M. Dove, “Crystallization by particle attachment in synthetic, biogenic, and geologic environments,” *Science*, vol. 349, no. 6247, pp. aaa6760–aaa6760, 2015.

[23] A. P. Alivisatos, “BIOMINERALIZATION: Enhanced: Naturally Aligned Nanocrystals,” *Science*, vol. 289, no. 5480, pp. 736–737, 2000.

[24] R. Q. Song, H. Cölfen, A. W. Xu, J. Hartmann, and M. Antonietti, “Polyelectrolyte-directed nanoparticle aggregation: Systematic morphogenesis of calcium carbonate by

nonclassical crystallization," *ACS Nano*, vol. 3, no. 7, pp. 1966–1978, 2009.

[25] S. S. Wang, A. Picker, H. Cölfen, and A. W. W. Xu, "Heterostructured Calcium Carbonate Microspheres with Calcite Equatorial Loops and Vaterite Spherical Cores," *Angew. Chemie Int. Ed.*, vol. 52, no. 24, pp. 6317–6321, 2013.

[26] S. Thachepan, M. Li, S. a. Davis, and S. Mann, "Additive-mediated crystallization of complex calcium carbonate superstructures in reverse microemulsions," *Chem. Mater.*, vol. 18, no. 15, pp. 3557–3561, 2006.

[27] T. Ogino, T. Suzuki, and K. Sawada, "The formation and transformation mechanism of calcium carbonate in water," *Geochim. Cosmochim. Acta*, vol. 51, no. 10, pp. 2757–2767, 1987.

[28] J. D. Rodriguez-Blanco, S. Shaw, and L. G. Benning, "The kinetics and mechanisms of amorphous calcium carbonate (ACC) crystallization to calcite, viavaterite.," *Nanoscale*, vol. 3, no. 1, pp. 265–271, 2011.

[29] M. H. Nielsen, S. Aloni, and J. J. De Yoreo, "*In situ* TEM imaging of $CaCO_3$ nucleation reveals coexistence of direct and indirect pathways," *Science*, vol. 218, no. 2004, pp. 213–218, 2013.

[30] P. J. M. Smeets, K. R. Cho, R. G. E. Kempen, N. a. J. M. Sommerdijk, and J. J. De Yoreo, "Calcium carbonate nucleation driven by ion binding in a biomimetic matrix revealed by in situ electron microscopy," *Nat. Mater.*, vol. 14, no. 4, pp. 394–399, Jan. 2015.

[31] A. Navrotsky, "Energetic clues to pathways to biomineralization: precursors, clusters, and nanoparticles.," *Proc. Natl. Acad. Sci. U. S. A.*, vol. 101, no. 33, pp. 12096–12101, 2004.

[32] S. Babu Mukkamala and A. K. Powell, "Biomimetic assembly of calcite microtrumpets: crystal tectonics in action," *Chem. Commun. (Camb).*, no. 8, pp. 918–919, 2004.

[33] T. Wang, H. Cölfen, and M. Antonietti, "Nonclassical crystallization: Mesocrystals and morphology change of $CaCO_3$ crystals in the presence of a polyelectrolyte additive," *J. Am. Chem. Soc.*, vol. 127, no. 10, pp. 3246–3247, 2005.

[34] U. Wehrmeister, L. Soldati, D. E. Jacob, T. Häger, and W. Hofmeister, "Raman

spectroscopy of synthetic, geological and biological vaterite: A Raman spectroscopic study," *J. Raman Spectrosc.*, vol. 41, no. 2, pp. 193–201, 2010.

[35] H. G. M. Edwards, D. R. Brown, J. A. Dale, and S. Plant, "Raman spectroscopy of sulfonated polystyrene resins," *Vib. Spectrosc.*, vol. 24, no. 2, pp. 213–224, 2000.

[36] P. Brüesch, *Phonons: Theory and Experiments II*, 65th ed. Berlin: Springer-verlag, 1986.

# Chapter 6: Morphogenesis of vaterite spheres: A novel “softer” colloidal template for the fabrication of hollow carbon spheres

## 6.1 Introduction

Hollow carbon spheres (HCS) ranging in size from nanometers[1] to micrometers[2] have received increasing interest over the past years due to their promising physico-chemical properties such as: low density, chemical inertness, high surface area, high electron density and surface permeability[3]. They have found a broad range of scientific applications, including: lithium ion batteries[4], Fischer-Tropsch synthesis[5], gas storage[6], and supercapacitors[7]. Functional HCS with superior properties have been synthesised through the use of pre-tailored templates[8]. The use of a pre-tailored template offers a high degree of control of the shape as well as structural dimensions, including the: pore volume, size, and carbon shell thickness[9], [10].

Templated fabrication of HCS involves at least four aspects:

1) The selection (and synthesis) of an appropriate template material, with a desired spherical shape and size that can withstand the conditions under which the synthesis will be carried out,
2) The development of appropriate techniques to reliably coat the template with carbon,
3) Where necessary, the establishment of a dependable procedure for the subsequent removal of the template to obtain HCS[8].

Amongst the different classes of templates, silica colloidal particles have received immense attention in the fabrication of HCS[3]. These are synthesised by the Stöber method[11], where a tetraethyl orthosilicate is hydrolysed in an aqueous ethanol solution that is catalysed by an ammonia solution at room temperature[12]. Although the Stöber method has been successful in the synthesis of hollow carbon spheres, it employs harsh chemicals like hydrofluoric acid (HF) to dissolve away the silica template. Hence alternative, environmentally friendly, colloidal templates that can easily be removed are needed.

Calcium carbonate ($CaCO_3$) is one of the most abundant biominerals on earth[13], which precipitates under basic conditions and dissolves under mildly acidic environments and meets the above-mentioned criteria to be used as an alternative template. Synthetically, $CaCO_3$ can be shaped into a variety of morphologies using additives such as organic molecules or inorganic ions[14], [15]. In this chapter, poly (4-styrenesulfonic acid) was used as an organic additive in order to influence the morphology of the precipitated $CaCO_3$. The $CaCO_3$ products were then used in the fabrication of hollow carbon spheres by chemical vapour deposition, after removing the template with acetic acid.

## 6.2 Experimental

### 6.2.1 Materials

All chemicals were of analytical grade. Calcium chloride, ammonium carbonate and poly (4-styrenesulfonic acid) $M_w$ ~75,000, 18 wt. % in $H_2O$**,** were all purchased from Sigma-Aldrich. Sodium hydroxide pellets were purchased from Merck (Pty) Ltd South Africa. The ammonia solution of 25 wt. %, and the hydrochloric acid (HCl) of 32 wt. % were purchased from Associated Chemical Enterprises (Pty) Ltd. All chemicals were used without any further purification. Acetylene Technical (99.9%) and argon Baseline 5.0 (99.9%) gases used in the Chemical Vapour Deposition (CVD) were purchased from AFROX (African Oxygen) Ltd.

### 6.2.2 Synthesis of calcium carbonate

Crystallisation reactions were carried out in a 250 mL round bottom flask kept at 30 °C in an oil bath. In a typical reaction, 3% of an aqueous solution of poly (4-styrenesulfonic acid) was prepared with distilled water, and the pH of the resulting mixture was adjusted to pH 10 with an aqueous sodium hydroxide solution. To this mixture, 50 mL (i.e. 5 mmol) of a 0.100 M $CaCl_2$ aqueous solution prepared with distilled water (adjusted to pH 9 using an aqueous $NH_3$ solution) was added drop-wise under gentle stirring at 30 °C. The reaction mixture was left to stir for an hour and then 50 mL of (i.e. 5 mmol) of a 0.100 M $(NH_4)_2\,CO_3$ aqueous solution prepared with distilled water was added drop-wise under gentle stirring. This reaction solution was maintained at 30 °C for 24 hours under gentle stirring. The precipitated products were centrifuged, washed with deionised water several times and then left to dry overnight at room temperature.

### 6.2.3 Synthesis of hollow carbon spheres

The as-synthesised white-coloured $CaCO_3$ spheres were then placed in a quartz boat which was inserted into a quartz reactor tube (ø = 20 mm, L = 1 m) (as shown in Chapter 3, Figure 3.1). The quartz tube with boat were then placed into a CVD furnace and the temperature was ramped to 600 °C at the rate of 10 °C/min with a constant flow of argon gas at a flow-rate of 100 ml/min. When the temperature reached 600 °C, gaseous acetylene was introduced into the quartz reactor tube at a flow-rate of 100 ml/min and maintained under these conditions for 90 min. The black-coloured products of this reaction were then retrieved from the quartz boat and then treated with an aqueous solution of pure acetic acid for 24 hrs.

### 6.2.4 Characterisation

The as-synthesised $CaCO_3$ products, the CVD products, and those reacted with acetic acid were then characterised by PXRD, SEM, TEM, laser Raman spectroscopy, TGA, and BET as described in Section 3.4 of Chapter 3.

## 6.3 Results and Discussion

The white-coloured precipitated products were analysed by PXRD (Figure 6.1). The peaks in the PXRD pattern were indexed according to ICSD 015879 (major peaks are labelled in Figure 6.1, all other peaks belong to the vaterite polymorph as compared to ICSD 015879) and were found to be that of the pure vaterite polymorph of calcium carbonate, with no other impurities from side reactions[16]. This demonstrated that the synthesis technique was ideal for reproducibly synthesising a single polymorph of calcium carbonate, in which all the particles had the same crystal structure.

The stabilisation of the metastable polymorph of calcium carbonate was achieved through the use of the PSSA during biomineralisation to influence the energy landscape[17]. This occurred through a surface interaction of the ionic motifs ($–COO^-$) of the added PSSA and the growing kinks and edges of the crystals at different degrees of surface binding, this resulted in the increase in the surface energy of vaterite, meanwhile decreasing the bulk free energy of the bulk vaterite crystals, and hence increasing the stability of the vaterite polymorph[18].

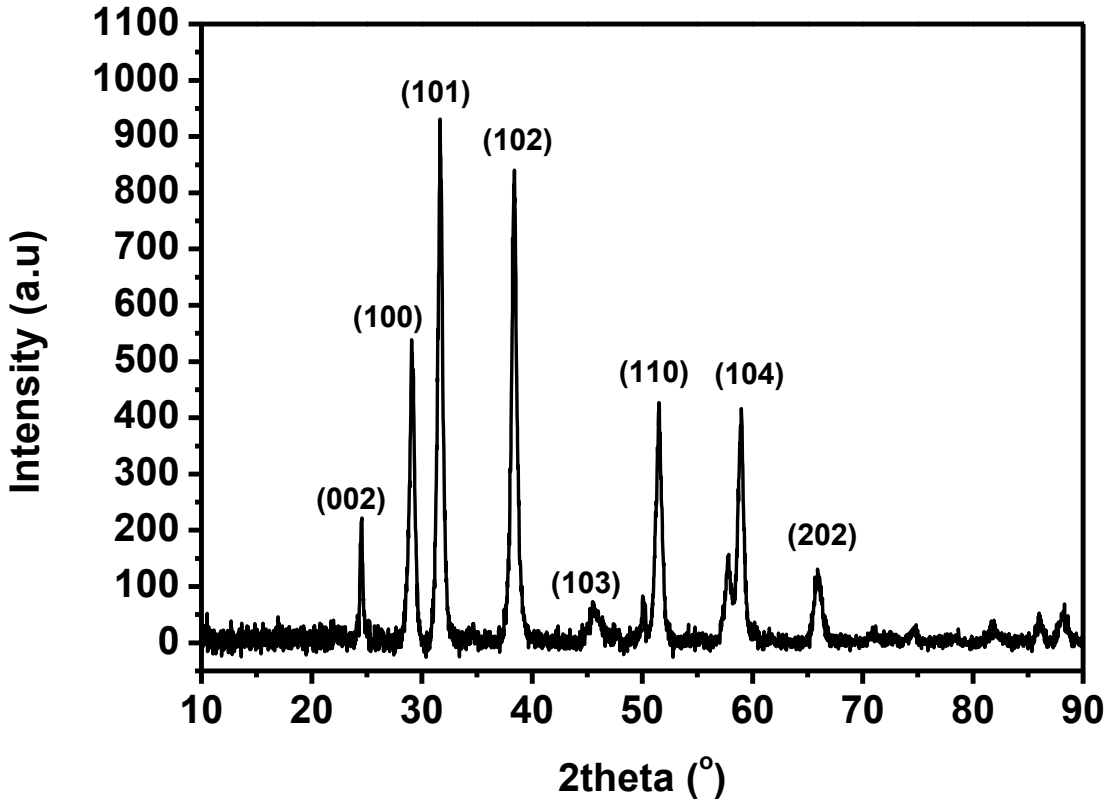



Figure 6. 1. A PXRD pattern of the white-coloured precipitate, which was found to be the vaterite polymorph of calcium carbonate.

Further analyses were performed to confirm the identity of the white-coloured precipitated products. Figure 6.2 shows the laser Raman spectrum taken of these products confirming the presence of the vaterite polymorph of calcium carbonate. Here the broad doublet peak below 400 $cm^{-1}$ displayed lattice mode vibrations due to movement of the entire vaterite unit cell. The weak in-plane bending modes of vaterite were also observed at 740 and 750 $cm^{-1}$, while the symmetrical carbonate stretching modes, which were the most intense peaks were observed at 1075 and 1090 $cm^{-1}$[19].

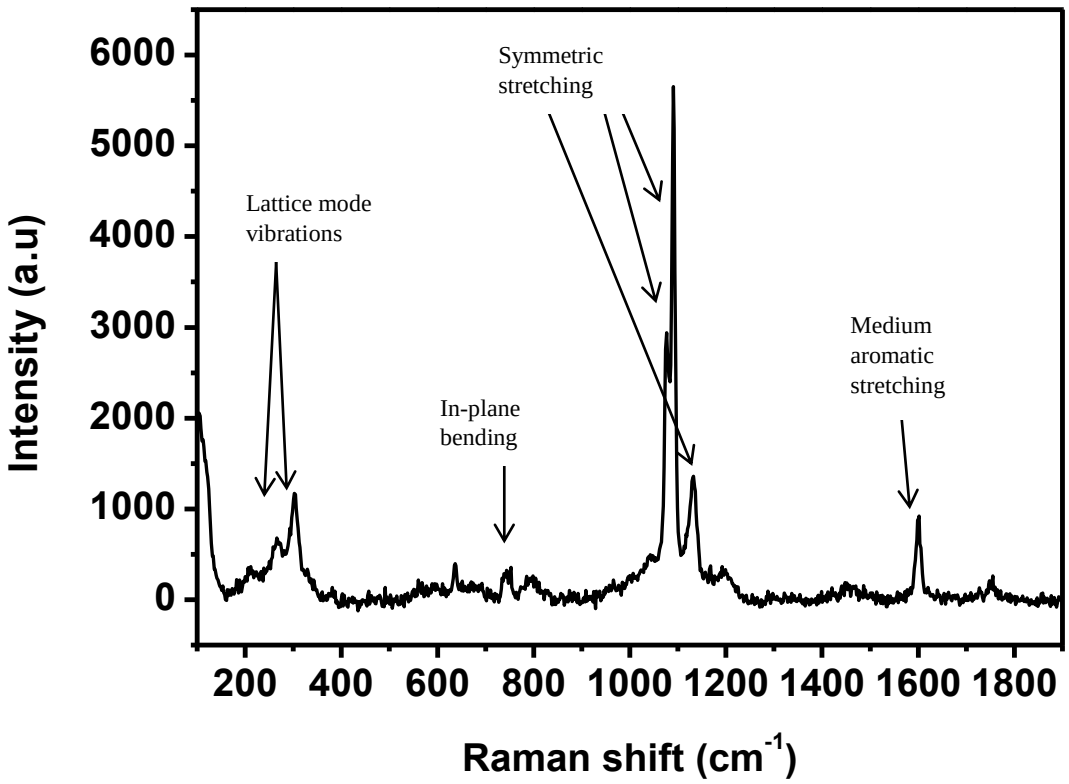



Figure 6. 2. A laser Raman spectrum of the white-coloured precipitate, which was found to be the vaterite polymorph of calcium carbonate.

The presence of the symmetrical stretching of the sulfonate groups around 1130 $cm^{-1}$, and the medium aromatic strecthing peak around 1600 $cm^{-1}$ were as a result of PSSA which was occluded within the vaterite crystals[20]. The presence of an organic matrix occluded within inorganic crystals like these has been widely accepted as evidence of biomineralisation[21]. This therefore confirmed that the organic polymer (PSSA) had acted as a directing agent (via kinetic effects) during nucleation and crystal proliferation in this study.

Having identified that the technique had reproducibly synthesised the vaterite polymorph of $CaCO_3$, the morphology of these particles was then examined by SEM (Figure 6.3 (a)-(b)). Micrographs of these particles showed that the crystal growth of $CaCO_3$ in the presence of PSSA had resulted in vaterite spheres with an average diameter of 4.2 µm (Figure 6.3 (c)).

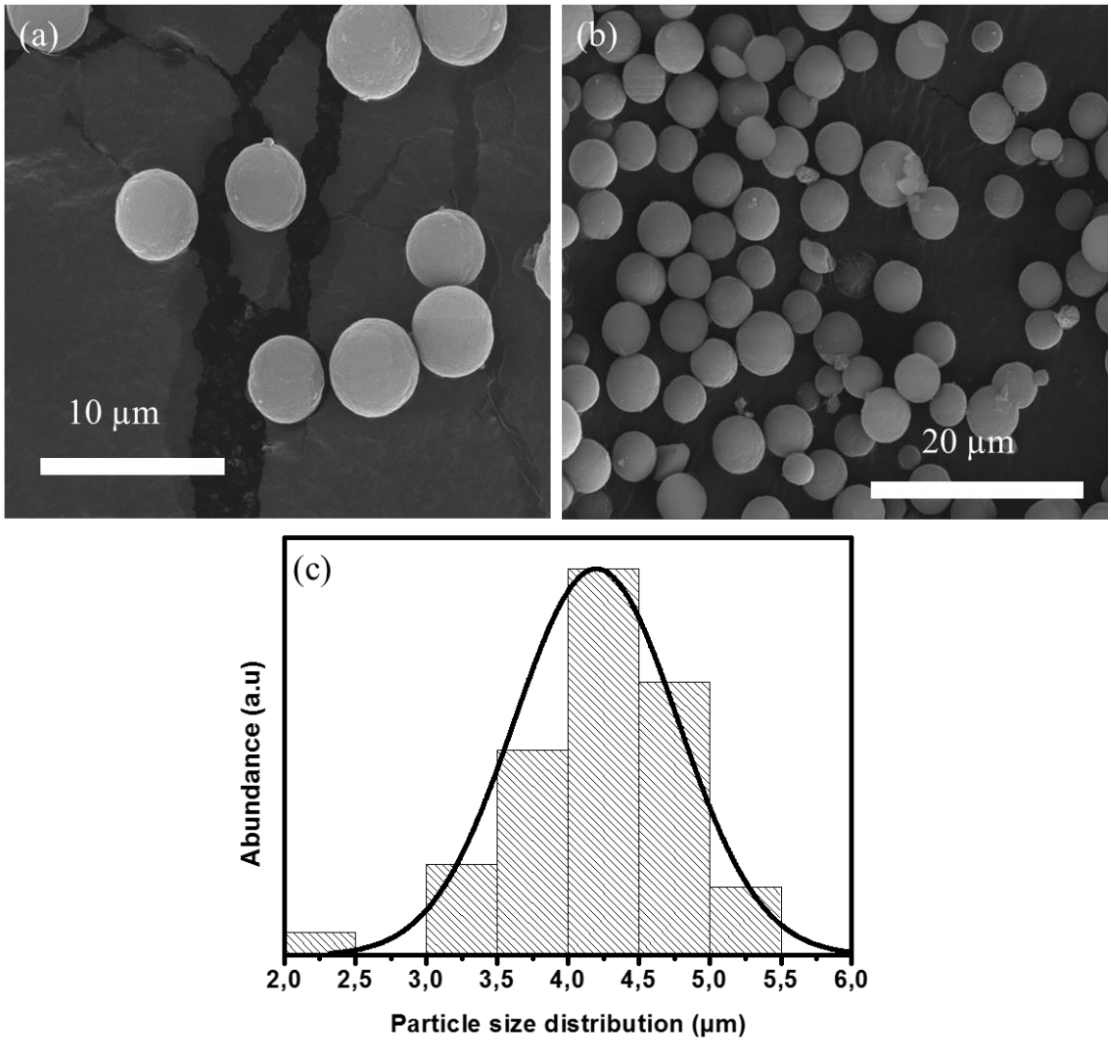



Figure 6. 3. SEM micrographs of the precipitated $CaCO_3$ spheres: (a)-(b) SEM magnification series showing the morphology of the spheres, (c) Particle size distribution of the $CaCO_3$ spheres.

The surface topography of these spheres was found to be relatively smooth and uniform. An interesting thing to note in this study was that the morphology of the vaterite spheres did not resemble the hexagonal symmetry of the vaterite unit cell. This implied that crystal proliferation to the bulk spheres had occurred through PSSA-directed attachment of vaterite nanoparticles. Crystals which grow through this route often have bulk morphologies which do not resemble the symmetry of the unit cell[22]. This too has been widely accepted as evidence of crystal growth by partcle attachment (CPA), and not the classical ion-by-ion attachment crystal growth[23]. This was also supported by the evidence of the presence of occluded PSSA within the vaterite spheres, as observed in the laser Raman spectrum (Figure 6.2). Hence the

SEM data revealed that PSSA-directed attachment of vaterite nanoparticles not only resulted in the synthesis of the vaterite polymorph of $CaCO_3$, but also (as in case of biomineralisation processes occurring in natural organisms such as the coccolith [24]), in the reproducible synthesis of a spherical morphology which was ideal for use as a template.

However, a further hurdle to the use of these spherical calcium carbonate particles as templates existed: $CaCO_3(s)$ is known to undergo thermal decomposition to give $CO_2(g)$ and $CaO(s)$ at temperatures between 750-800 °C[25], [26]. Thus if the calcium carbonate particles were to be used as a template under these conditions, this would result in a loss of almost half of the particle mass (i.e. 44 g/mol from the 100 g/mol) as gas. Now, the biggest question was: what would happen to the morphology and structural integrity of the $CaCO_3$ template when subjected to high reaction temperature conditions during the CVD carbonisation process? To answer this the products were collected, after having subjected them to gaseous acetylene at temperatures ranging from 600-800 °C, and then analysed by SEM, in order to examine their surface topography as shown in Figure 6.4 (a)-(f).

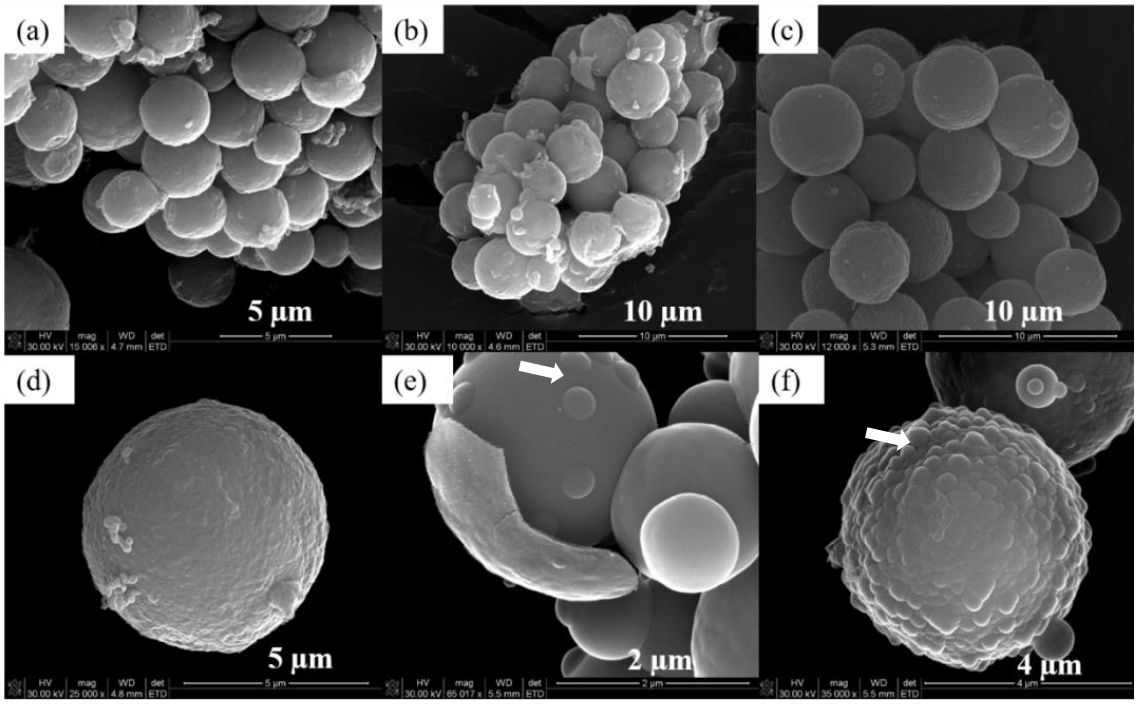



Figure 6. 4. SEM micrographs showing the effect of reaction temperature on the surface roughness of the spherical $CaCO_3$ particles after being exposed to acetylene at: 600 °C (a) & (d), 700 °C (b) & (e), and 800 °C (c) & (f). Arrows show the rough topography on the spheres.

Here, larger sample sizes of $CaCO_3$ spheres that were exposed to acetylene under reaction temperatures of: 600, 700, and 800 °C, were shown in Figure 6.4 (a) – (c) respectively. The surface topographies of the individual spheres at these temperatures (i.e. 600-800 °C) were also examined (Figure 6.4 (d) – (f)).

In each case the individual spheres appeared to be coated with a product, as the once white-coloured vaterite particles had turned black after exposure to acetylene. In order to establish the identity of the matetrial coating these particles, samples prepared at each temperature were then analysed by laser Raman spectroscopy (Figure 6.5).

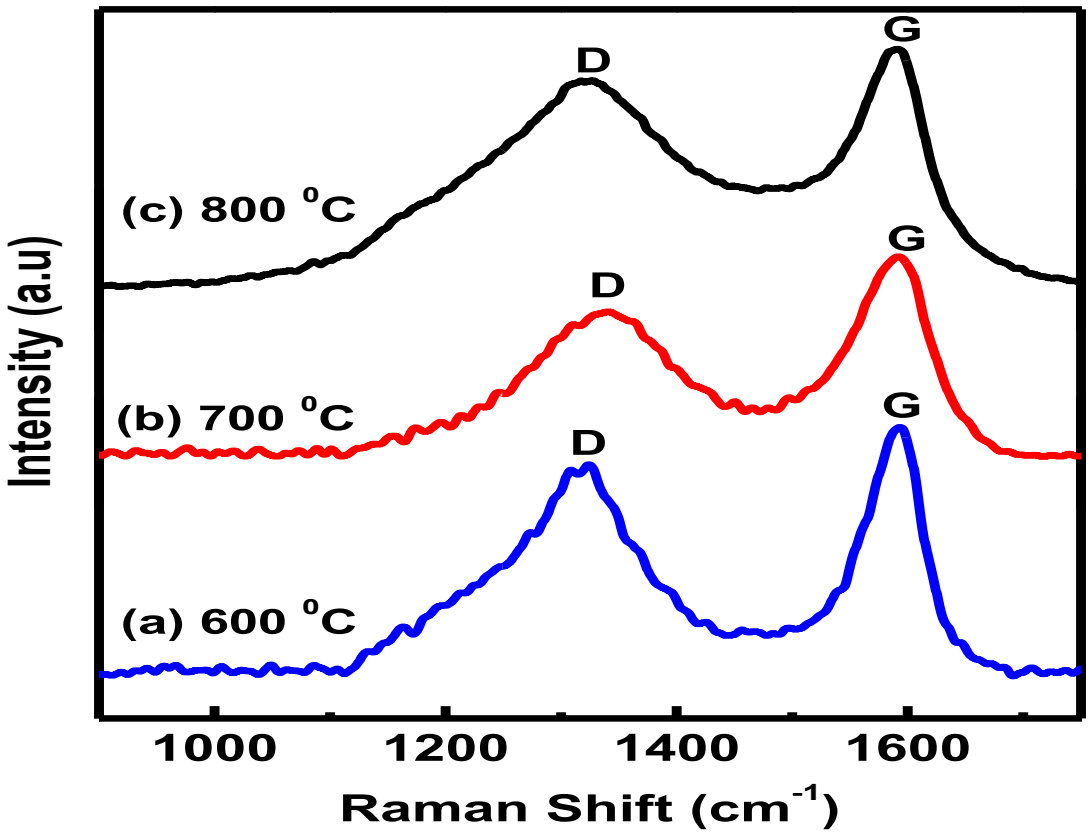



Figure 6. 5. Laser Raman spectra of spherical $CaCO_3$ particles which had been exposed to acetylene at reaction temperatures of: (a) 600 °C, (b) 700 °C, and (c) 800 °C.

Laser Raman spectra of the coated spherical $CaCO_3$ particles revealed the presence of G-peaks at 1580 $cm^{-1}$ (due to the bond stretching of pairs of $sp^2$ carbon atoms in both rings and chains), and the D-peaks at 1350 $cm^{-1}$ (due to the breathing modes of $sp^2$ carbon atoms in the rings)[27],

[28]. Thus the materials which had coated the spherical $CaCO_3$ particles, turning them black, was carbonaceous.

Returning to the SEM micrographs ((Figure 6.4 (d) – (f)), it was interesting to note that an examination of the topography of the carbon coated $CaCO_3$ spheres revealed that their surface roughness increased with increased reaction temperature. This brings us back to the question raised earlier in the discussion about the effect of the thermal decomposition of $CaCO_3$ at elevated temperatures. Here it was observed that the evolution of $CO_2(g)$ from $CaCO_3(s)$ during the reaction of acetylene on the surface of the $CaCO_3$ spheres, appeared to have resulted in the formation of a carbon coating that was roughened by the presence "bubble-like" structures (see arrows on Figure 6.4). This surface roughness appeared to be exacerbated from 700 °C to 800 °C, presumably because the partial pressure of $CO_2(g)$ or rather the rate of $CO_2(g)$ evolution increased with increased reaction temperature[29]–[32]. Significantly, while the topography of the carbon coated products had changed, the integrity of the spherical template appeared uncompromised with increased reaction temperature.

In an attempt to further establish the nature of the carbon coating and whether the template could indeed be removed, samples of each reaction temperature were then exposed to acetic acid for 24 hrs. The resultant products of this process were then analysed by TEM, as displayed in Figures 6.6 (a)–(c) for reaction temperatures from 600-800 °C.

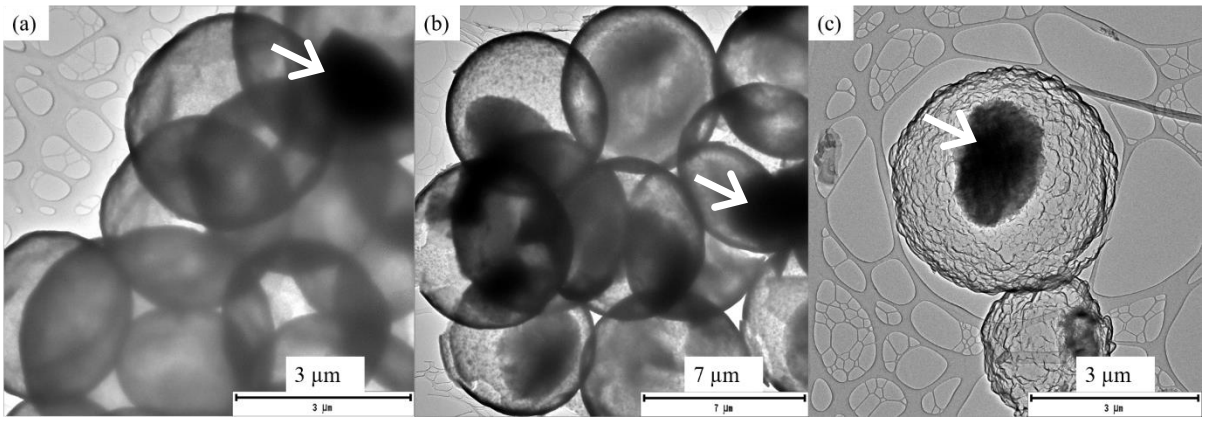



Figure 6. 6. TEM micrographs of the carbon coated vaterite spheres which had been synthesised at: (a) 600 °C, (b) 700 °C, and (c) 800 °C, after exposure to acetic acid for 24 hrs. Arrows show the presence of residue inside the spheres.

Numerous observations were made based upon the TEM micrographs that were obtained. Firstly, it was observed that the spherical $CaCO_3$ particles had indeed acted as templates. This was noted by the carbon spheres that had been formed upon the removal of the $CaCO_3$. Secondly, it was shown that acetic acid was able to etch away the majority of the spherical $CaCO_3$ template, leaving behind predominantly hollow carbon spheres (HCS) (see arrows in Figure 6.6 (a)–(c) where small portions of an unknown substance, assumed to be either CaO(*s*) or undecomposed $CaCO_3$(*s*) which had not been etched away by the acid, were observed). Thirdly, the surface topography of these HCS appeared to precisely match that of the $CaCO_3$ template as the reaction temperature was increased. In the case of this last observation, as mentioned earlier in the discussion, these topographical differences were believed to have been induced by the evolution of $CO_2$(*g*) from the $CaCO_3$(*s*) template which decomposed during the nucleation and growth of the carbon shell around the template (see the magnified images in Figure 6.7).

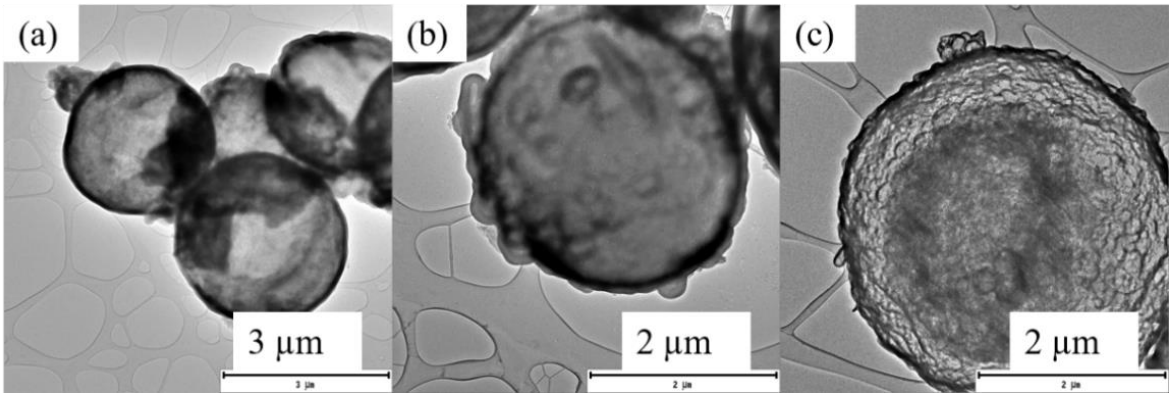



Figure 6. 7. Magnified TEM micrographs of the HCS synthesised at: (a) 600 °C, (b) 700 °C, and (c) 800 °C.

Recently Coville *et al.* have demonstrated that when HCS with roughened surfaces were used as catalyst supports the catalytic activity was enhanced[5]. This suggests one possible future application for the HCS produced in this study.

In order to understand the effects of the decomposition of $CaCO_3$ on the nature of the carbon deposited thereon, further analysis of the laser Raman spectra that were obtained (as shown in Figure 6.5) was made. As discussed previously, the ratio of the D and G-peak intensities (i.e. $I_D/I_G$) has been widely used to evaluate the level of disorder or defects within the $sp^2$ carbon lattice or the carbon framework[27]. These defects have often been observed in carbon

materials formed under carbonisation conditions in CVD reactors, and these have typically been ascribed: (a) structural ($sp^2$-like) defects, (b) topological ($sp^2$-like) defects, (c) doping or functionalisation ($sp^2$- and $sp^3$-like) defects, and (d) vacancies/edge type defects (non-$sp^2$-like)[33]. A summary of the $I_D/I_G$ ratio of the various HCS that were synthesised under different reaction temperatures is shown in Table 6.1.

Table 6. 1. The ratio of the D and G peak intensities ($I_D/I_G$) of HCS which were synthesised under different reaction temperatures.

| HCSs sample | $I_D/I_G$ |
|---|---|
| (a) 600 °C | 0,84 |
| (b) 700 °C | 0,71 |
| (c) 800 °C | 0,86 |

Typically the quantity of defects in carbon lattices decrease with an increase in the reaction temperature (i.e. the $I_D/I_G$ ratio should be lowered at higher reaction temperatures)[27], [28]. The $I_D/I_G$ ratio of the HCS, as presented in Table 6.1, seemed to decrease from 0.84 at 600 °C to 0.71 at 700 °C, which was consistent with an anticipated decrease. However, thereafter an increase in the $I_D/I_G$ ratio to 0.86 at 800 °C was observed. This suggested that the HCS synthesised at 800 °C had more defects in their carbon lattice that those at 700 °C or even 600 °C. In order to provide a deeper insight into the reasons behind the increase in the $I_D/I_G$ ratio at 800 °C, the surface of a typical HCS formed at 800 °C was analysed by TEM at a higher magnification (Figure 6.8 (a)-(b)).

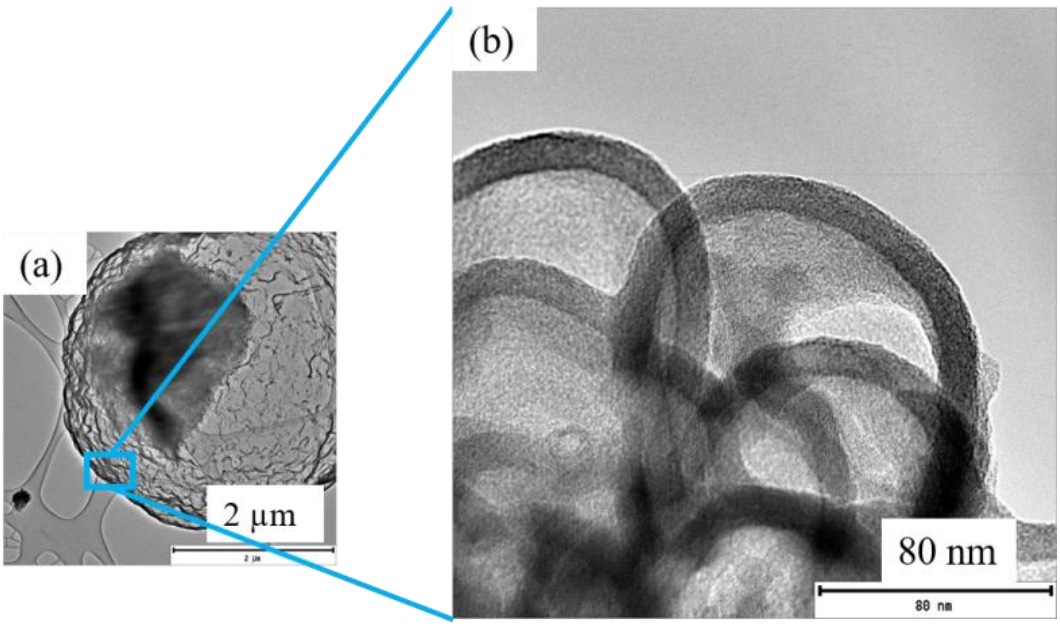



Figure 6. 8. TEM micrographs of HCSs synthesised at 800 °C. (a) Lower magnification displaying the larger portion of the HCS. (b) High magnification TEM micrograph of the surface of the same HCS synthesised at 800 °C.

Here it was observed that not only did the carbon coating have a roughened surface (Figure 6.8 (a)), but that upon closer inspection this consisted of various multiple-layered 'bubble-like' curvatures that were packed together to make up the shell of the HCS (Figure 6.8 (b)). Since the increase in the $I_D/I_G$ ratio occurred at a temperature between 700-800 °C, which is the same temperature range where $CaCO_3(s)$ is known to undergo thermal decomposition [25], [26], it was assumed that the two phenomena were directly related to each other. Furthermore it is speculated that the evolution of $CO_2(g)$ from the $CaCO_3(s)$ template, during the nucleation and growth of the carbon on the surface of the template, caused these 'bubble-like' curvatures to be formed. Indeed, the introduction of these 'bubble-like' curvatures (also observed on the carbon coated vaterite spheres by SEM Figure 6.4(f)), would have brought about structural/topological defects in the carbon lattice (including the formation of five, seven or eight membered carbon rings[33]). This could easily have explained the increase in the $I_D/I_G$ at 800 °C.

Previously an unknown material (suspected to be CaO or undecomposed $CaCO_3$) was observed inside the HCS after the carbon coated template had been exposed to acetic acid for 24 hrs (shown by the arrows on Figure 6.6). In an attempt to establish the identity of the unknown

material as well as the efficacy of the template removal process by acetic acid, the HCSs were subjected to thermogravimetric analysis (TGA). The percentage weight loss of the HCS synthesised at various temperatures and then treated in acid for 24 hrs were compared relative to an uncoated sample of spherical vaterite particles, as a function of temperature (Figure 6.9).

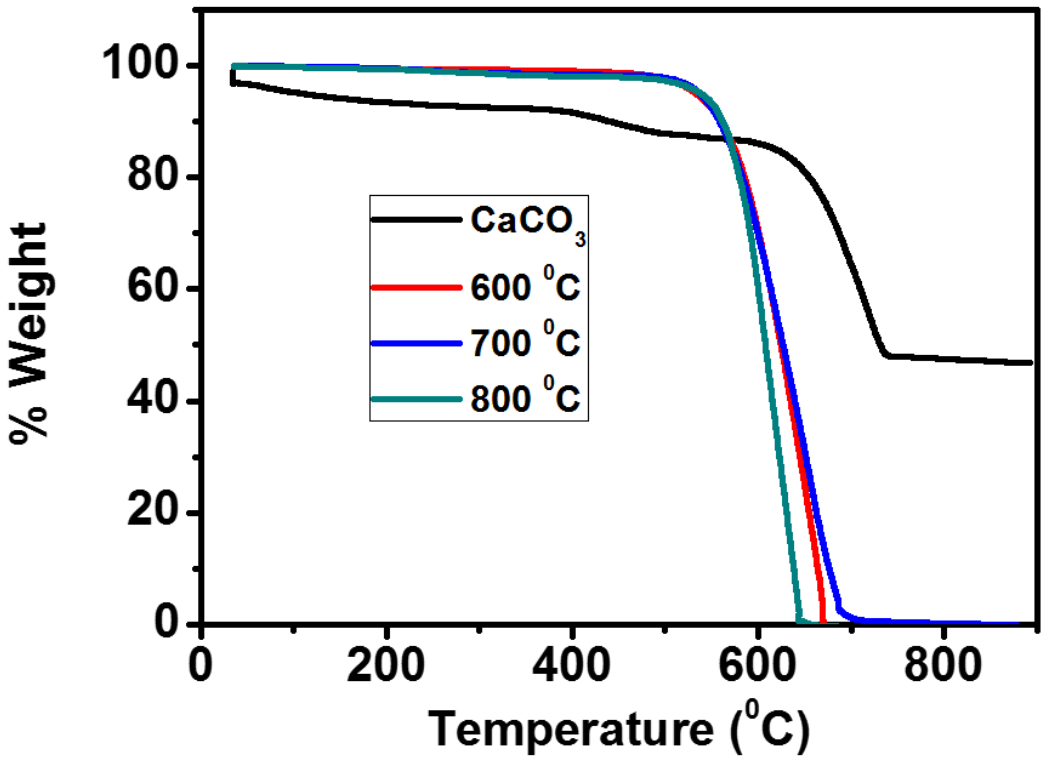



Figure 6. 9. TGA thermograms of the $CaCO_3$ template, and the HCSs synthesised at reaction temperatures between 600 °C and 800 °C.

The thermal decomposition of the $CaCO_3$ template is represented by the black coloured thermogram in Figure 6.9. Here the template exhibited a loss of adsorbed water at around 100 °C, followed by the decomposition of the PSSA polymer at around 480 °C[34]. Lastly the $CaCO_3$ template showed a loss of $CO_2(g)$ to give a $CaO(s)$ residue at a temperature between 660 °C to 730 °C. The broad decomposition temperature range (i.e. about 70 °C) of $CaCO_3$ into $CO_2(g)$ and $CaO(s)$ suggested that its purity was low[31].

The thermograms of the HCS synthesised at 600 °C (red), 700 °C (blue), and 800 °C (green) gave similar decomposition temperatures (i.e. 560 °C) which were attributed to the oxidation of carbon from the HCS to give $CO_2(g)$ under TGA conditions. It was interesting to note that in each case no solid residue remained after the complete oxidation of the HCS. At least two

explanations can be put forward. Firstly, that the unknown material (indicated by the arrows in Figure 6.6) was neither CaO(*s*) nor undecomposed $CaCO_3$, as either of these would have resulted in a solid residue that would have been observed in the thermogram. Rather, the data from the thermogram suggests that the unknown substance may have been combustible. For instance, it is possible that the carbon-rich poly (4-styrenesulfonic acid) (PSSA), which was occluded within the template (as confirmed by laser Raman spectroscopy – Figure 6.2), had been converted to a carbonaceous soot under the high reaction temperatures. This would explain the complete oxidation of the HCS with no residue under TGA conditions. A second possible explanation is that the residue was indeed CaO(*s*) or undecomposed $CaCO_3$, but the quantity present was so small (as seen by the minute amounts in the HCS – Figure 6.6 (a)-(c)) that the weight of the residue was outside the detection limits of the TGA. However, in order to establish which of these explanations are true, further elemental/qualitative analysis (such as SEM-FIB with EDX of the core of the HCS) will be required. What is however obvious from these results is that the acetic acid was capable of removing the vast majority (>99%) of the template, indicating that the template etching process had been very effective.

The uncoated $CaCO_3$ template and the HCS synthesised at different reaction temperatures were then subjected to Brunauer, Emmett and Teller (BET) surface area (SA) and pore volume measurements. The data obtained are summarised in Table 6.2.

Table 6. 2. BET surface area, pore volumes and average size (diameter) of the $CaCO_3$ template and the HCS synthesised at different reaction temperatures and etched with acetic acid for 24 hrs.

| HCSs sample | BET SA ($m^2/g$) | Pore Volume ($cm^3/g$) | Average particle size (µm) |
|---|---|---|---|
| (a) $CaCO_3$ | 56 | 0.115 | 4.2 |
| (b) 600 °C | 193 | 0.736 | 4.0 |
| (c) 700 °C | 55 | 0.417 | 3.6 |
| (d) 800 °C | 51 | 0.366 | 3.4 |

Based upon this data it was noticed that the HCS synthesised at 600 °C had the highest surface area of all the HCS that were synthesised and had a surface area approximately three and a half times that of the $CaCO_3$ template. It is speculated that this may have been due to the fact that the $CaCO_3$ hadn't decomposed to $CaO(s)$ at 600 °C, and hence could be easily etched out. Likewise, if the residue within the HCS was from PSSA which had been converted into carbon, there would have been less of it at this temperature and more of it at higher temperatures. This may have given rise to the reduction in the surface area at higher temperatures. It was also observed that the pore volume decreased with increased reaction temperature, and increased as with the surface area of the materials, which is quite a typical trend in carbon materials[2].

There was an observed decrease in the average particle size of the HCS with an increase in CVD reaction temperature due to the thermal contraction of the template at higher temperatures. Although the surface areas of the HCS from $CaCO_3$ as a template were lower as compared to other hollow carbon spheres that have been synthesised by other templating methods (for example Xia and Mokaya reported on the synthesis of HCS with a BET specific surface area of 1022 $m^2/g$ using silica microspheres as a template [2]), the concept of using $CaCO_3$ as a template for carbon material synthesis was successfully proven and might open up a new avenue for synthesising novel shaped carbon materials.

## 6.4 Conclusions

In this chapter, it was shown that $CaCO_3$ could be successfully shaped into spherical particles using PSSA. Despite the thermal decomposition of $CaCO_3(s)$ into $CO_2(g)$ and $CaO(s)$[31], the possibility to synthesise HCS using $CaCO_3$ as a template under CVD conditions has been demonstrated for the first time. The evolution of $CO_2(g)$ from the template during CVD appears to have resulted in the formation of a rough surface topography on the carbon shells of these HCS. The surface roughness of these HCS increased with increased reaction temperature, which appeared to correlated to the increased rate of decomposition of $CaCO_3(s)$ at the higher temperatures[32]. The spherical structural integrity of the template was unaffected by the decomposition of the $CaCO_3$ template and the evolution of $CO_2(g)$ during carbonisation, under all the reaction temperatures. The BET surface area of the HCS synthesised at 700 and 800 °C appear to have been negatively affected by the presence of an as-yet unidentified residue inside the HCS. Further elemental/qualitative analysis such as SEM-FIB with EDX of the core of the

HCS will be required to gain more insight into the nature of this, in order to improve the quality and hence surface areas of these HCS.

## 6.5 References


[1] G. Sun, K. Li, J. Wang, H. He, J. Wang, Y. Li, Y. Liu, and J. Gu, "A novel approach for fabrication of hollow carbon spheres with large size and high specific surface area," *Microporous Mesoporous Mater.*, vol. 139, no. 1–3, pp. 207–210, 2011.

[2] Y. Xia and R. Mokaya, "Synthesis of Ordered Mesoporous Carbon and Nitrogen-Doped Carbon Materials with Graphitic Pore Walls via a Simple Chemical Vapor Deposition Method," *Adv. Mater.*, vol. 16, no. 17, pp. 1553–1558, 2004.

[3] J. Liu, N. P. Wickramaratne, S. Z. Qiao, and M. Jaroniec, "Molecular-based design and emerging applications of nanoporous carbon spheres," *Nat. Mater.*, vol. 14, no. 8, pp. 763–774, 2015.

[4] S. Yang, X. Feng, L. Zhi, Q. Cao, J. Maier, and K. Müllen, "Nanographene-constructed hollow carbon spheres and their favorable electroactivity with respect to lithium storage," *Adv. Mater.*, vol. 22, no. 7, pp. 838–42, 2010.

[5] T. N. Phaahlamohlaka, D. O. Kumi, M. W. Dlamini, L. L. Jewell, and N. J. Coville, "Ruthenium nanoparticles encapsulated inside porous hollow carbon spheres: A novel catalyst for Fischer–Tropsch synthesis," *Catal. Today*, 2016.

[6] S. Feng, W. Li, Q. Shi, Y. Li, J. Chen, Y. Ling, A. M. Asiri, and D. Zhao, "Synthesis of nitrogen-doped hollow carbon nanospheres for $CO_2$ capture," *Chem. Commun. (Camb).*, vol. 50, no. 3, pp. 329–31, 2014.

[7] X. Chen, K. Kierzek, K. Wenelska, K. Cendrowski, J. Gong, X. Wen, T. Tang, P. K. Chu, and E. Mijowska, "Electrochemical characteristics of discrete, uniform, and monodispersed hollow mesoporous carbon spheres in double-layered supercapacitors," *Chem. Asian J.*, vol. 8, no. 11, pp. 2627–33, 2013.

[8] Y. Liu, J. Goebl, and Y. Yin, "Templated synthesis of nanostructured materials.," *Chem. Soc. Rev.*, vol. 42, no. 7, pp. 2610–53, 2013.

[9] X. Fang, S. Liu, J. Zang, C. Xu, M. Zheng, Q. Dong, D. Sun, and N. Zheng, “Precisely controlled resorcinol-formaldehyde resin coating for fabricating core-shell, hollow, and yolk-shell carbon nanostructures,” *Nanoscale*, vol. 5, no. 15, pp. 6908–16, 2013.

[10] J. Fu, Q. Xu, J. Chen, Z. Chen, X. Huang, and X. Tang, “Controlled fabrication of uniform hollow core porous shell carbon spheres by the pyrolysis of core/shell polystyrene/cross-linked polyphosphazene composites,” *Chem. Commun. (Camb).*, vol. 46, no. 35, pp. 6563–5, 2010.

[11] W. Stöber, A. Fink, and E. Bohn, “Controlled growth of monodisperse silica spheres in the micron size range,” *J. Colloid Interface Sci.*, vol. 26, no. 1, pp. 62–69, 1968.

[12] Y. Han, X. Dong, C. Zhang, and S. Liu, “Hierarchical porous carbon hollow-spheres as a high performance electrical double-layer capacitor material,” *J. Power Sources*, vol. 211, pp. 92–96, 2012.

[13] S. Mann, *Biomineralisation, Principles and Concepts in Bioinorganic Materials Chemistry*. New York: oxford university press, 2001.

[14] H. Cölfen and S. Mann, “Higher-order organisation by mesoscale self-assembly and transformation of hybrid nanostructures,” *Angew. Chemie - Int. Ed.*, vol. 42, no. 21, pp. 2350–2365, 2003.

[15] S. Ouhenia, D. Chateigner, M. A. Belkhir, E. Guilmeau, and C. Krauss, “Synthesis of calcium carbonate polymorphs in the presence of polyacrylic acid,” *J. Cryst. Growth*, vol. 310, no. 11, pp. 2832–2841, 2008.

[16] S. R. Kamhi, “On the structure of vaterite $CaCO_3$,” *Acta Crystallogr.*, vol. 16, no. 8, pp. 770–772, 1963.

[17] A. Navrotsky, “Energetic clues to pathways to biomineralisation: precursors, clusters, and nanoparticles.,” *Proc. Natl. Acad. Sci. U. S. A.*, vol. 101, no. 33, pp. 12096–12101, 2004.

[18] J. J. DeYoreo and P. G. Vekilov, “Principles of Crystal Nucleation and Growth,” *Rev. Mineral. Geochemistry*, vol. 54, no. 1, pp. 57–93, 2003.

[19] U. Wehrmeister, a. L. Soldati, D. E. Jacob, T. Häger, and W. Hofmeister, “Raman spectroscopy of synthetic, geological and biological vaterite: A Raman spectroscopic study,” *J. Raman Spectrosc.*, vol. 41, no. 2, pp. 193–201, 2010.

[20] H. G. M. Edwards, D. R. Brown, J. A. Dale, and S. Plant, “Raman spectroscopy of sulfonated polystyrene resins,” *Vib. Spectrosc.*, vol. 24, no. 2, pp. 213–224, 2000.

[21] A. P. Alivisatos, “BIOMINERALISATION: Enhanced: Naturally Aligned Nanocrystals,” *Science*, vol. 289, no. 5480, pp. 736–737, 2000.

[22] S. Babu Mukkamala and A. K. Powell, “Biomimetic assembly of calcite microtrumpets: crystal tectonics in action.,” *Chem. Commun. (Camb).*, no. 8, pp. 918–919, 2004.

[23] J. J. De Yoreo, P. U. P. Gilbert, N. J. M. Sommerdijk, R. L. Penn, S. Whitelam, D. Joester, H. Zhang, J. D. Rimer, A. Navrotsky, J. F. Banfield, A. F. Wallace, F. M. Michel, F. C. Meldrum, H. Colfen, and P. M. Dove, “Crystallisation by particle attachment in synthetic, biogenic, and geologic environments,” *Science*, vol. 349, no. 6247, pp. aaa6760–aaa6760, 2015.

[24] J. Young, S. Davis, P. Bown, and S. Mann, “Coccolith ultrastructure and biomineralisation,” *J. Struct. Biol.*, vol. 126, no. 3, pp. 195–215, 1999.

[25] M.-A. Popescu, R. Isopescu, C. Matei, G. Fagarasan, and V. Plesu, “Thermal decomposition of calcium carbonate polymorphs precipitated in the presence of ammonia and alkylamines,” *Adv. Powder Technol.*, vol. 25, no. 2, pp. 500–507, 2014.

[26] L. Yue, M. Shui, and Z. Xu, “The decomposition kinetics of nanocrystalline calcite,” *Thermochim. Acta*, vol. 335, no. 1–2, pp. 121–126, 1999.

[27] A. C. Ferrari and J. Robertson, “Resonant Raman spectroscopy of disordered, amorphous, and diamondlike carbon,” *Phys. Rev. B*, vol. 64, no. 7, p. 075414, 2001.

[28] A. C. Ferrari and J. Robertson, “Interpretation of Raman spectra of disordered and amorphous carbon,” *Phys. Rev. B*, vol. 61, no. 20, pp. 95–107, 2000.

[29] M. S. Murthy, B. R. Harish, K. S. Rajanandam, and K. Y. Ajoy Pavan Kumar, “Investigation on the kinetics of thermal decomposition of calcium carbonate,” *Chem. Eng. Sci.*, vol. 49, no. 13, pp. 2198–2204, 1994.

[30] A. W. D. Hills, “The mechanism of the thermal decomposition of calcium carbonate,” *Chem. Eng. Sci.*, vol. 23, no. 4, pp. 297–320, 1968.

[31] G. Narsimhan, “Thermal decomposition of calcium carbonate,” *Chem. Eng. Sci.*, vol.

16, no. 1–2, pp. 7–20, 1961.

[32] E. C. Lide, David R, G. Baysinger, L. I. Berger, R. N. Goldberg, H. V Kehiaian, K. Kuchitsu, G. Rosenblatt, D. L. Roth, and D. Zwillinger, *CRC Handbook of Chemistry and Physics*, 86th ed. CRC Press, 2005.

[33] H. Terrones, R. Lv, M. Terrones, and M. S. Dresselhaus, "The role of defects and doping in 2D graphene sheets and 1D nanoribbons.," *Rep. Prog. Phys.*, vol. 75, no. 6, p. 062501, 2012.

[34] S. S. Wang, A. Picker, H. Cölfen, and A. W. W. Xu, "Heterostructured Calcium Carbonate Microspheres with Calcite Equatorial Loops and Vaterite Spherical Cores," *Angew. Chemie Int. Ed.*, vol. 52, no. 24, pp. 6317–6321, 2013.

[35] F. Su, X. S. Zhao, Y. Wang, L. Wang, and J. Y. Lee, "Hollow carbon spheres with a controllable shell structure," *J. Mater. Chem.*, vol. 16, no. 45, p. 4413, 2006.

# Chapter 7: General conclusions and recommendations

## 7.1 Conclusions

The main objectives of this research project were to:

(1) Study the crystal growth of $CaCO_3$ under different solvents and organic additives,
(2) Manipulate the morphology and polymorphs of the precipitated $CaCO_3$ to the desired morphology, and
(3) Consequently select the desired morphology of the precipitated $CaCO_3$ and use it as a template in the templated-synthesis of HCS by CVD, and lastly
(4) Determine the conditions required to remove the template in order to obtain HCS with the dimensions of the template.

After subjecting all the products to: SEM, PXRD, TEM, TGA, laser Raman spectroscopy. The following conclusions were drawn:

SEM micrographs revealed hollow, porous spherical and ellipsoidal morphologies in the PCC crystals which had precipitated in the pure polar protic solvents. It was also noted that an increase in the molecular weight of the polar protic solvent (i.e. from methanol to 2-butanol) resulted in hierarchically structured "flower-like" products, that were believed to have formed from the fusion of the individual ellipsoids. From laser Raman spectra and PXRD patterns, it was concluded that all of these spheres were predominantly composed of the vaterite polymorph, irrespective of the type of polar protic solvent that was used. When mixtures of polar aprotic and polar protic solvents were used, these gave rise to a mixture of rhombohedral and spherically shaped crystals. The rhombohedral crystals of PCC were confirmed by laser Raman and PXRD to be composed of the calcite polymorph. It was concluded from quantitative PXRD data that an increase in the ratio of the polar protic solvent in the binary solvent mixture favoured the crystallisation of the vaterite polymorph, while an increase in the ratio of the polar aprotic solvent favoured the crystallisation of the calcite polymorph. It was further concluded from time-resolved *ex situ* PXRD and SEM measurements that the major phase transformation

occurred within 3 hrs of mixing the precursor solutions. From this, it was concluded that a dissolution-reprecipitation mechanism had most likely taken place.

The effect of poly (4-styrenesulfonic acid) (PSSA) as an additive in the crystallisation of $CaCO_3$ at different temperatures (i.e. 30, 40, 75, and 100 °C) and different crystallisation times (3, 6, 12, and 24 hrs) was investigated. It was concluded from laser Raman spectra and PXRD diffractograms that at all crystallisation temperatures and times, pure vaterite was formed. Morphological examination of the bulk vaterite crystals by SEM revealed a spherical morphology which appeared to have formed via crystal tectonics (crystallisation by particle attachment (CPA)). Laser Raman spectra and TGA showed the presence of the occluded PSSA within the vaterite spheres – supporting evidence of CPA. However, it was observed that varying the crystallisation/reaction temperature led to different CPA pathways, which in turn resulted in bulk crystal morphologies that varied. For instance, a crystallisation temperature of 30 ˚C gave relatively smooth bulk crystals which were spherical. At 40 ˚C it appeared that two bulk spherical crystals had fused and gave rise to bulk ellipsoidal-shaped crystals. On the other hand, at crystallisation temperatures of 75 and 100 ˚C, oriented attachment of particles around the equatorial region of the bulk spherical crystals were noted. It was also observed from SEM that crystallisation time did not predominantly affect the polymorphism of the precipitated $CaCO_3$ and the CPA pathway at different temperatures. However, after 24 hrs of crystallisation the oriented attachment of equatorially aligned crystals were observed to form at a lower temperature (i.e. 40 ˚C) than previously observed (i.e. 75 ˚C) for lower crystallisation times. From this observation it was concluded that longer reaction time (24 hrs) allows for the continued CPA into vaterite bulk crystals at a lower temperature (40 °C). Significantly, at higher reaction temperatures (i.e. 75 and 100 ˚C) hollow bulk crystals were formed, while at lower temperatures solid core bulk vaterite crystals were formed. It was then concluded that higher temperatures followed the dissolution-reprecipitation mechanism, which led to the dissolution of the cores of the vaterite bulk crystals.

The vaterite spheres crystallised at 30 °C for 24 hrs were used as templates in an attempt to synthesise hollow carbon spheres (HCS) by chemical vapour deposition (CVD), using acetylene as a carbon source at 600, 700 and 800 °C for 90 mins. SEM revealed that the structural integrity of the $CaCO_3$-templated carbon spheres remained intact after high reaction temperatures. However, an increase in the surface roughness of the coated $CaCO_3$ templates was observed which increased with the increase in the reaction temperature. The template was then removed by exposure to acetic acid for 24 hrs. The products were confirmed by TEM to

be hollow, with an unidentified residue inside. However, no solid residue was observed on the TGA thermograms of the products, suggesting that the unidentified material in the products was combustible. Laser Raman spectra confirmed these products to be carbonaceous, by the presence of the D and G peaks and hence were concluded to be hollow carbon spheres. The ratio of the D and G peak intensities ($I_D/I_G$) was used to estimate the level of order/disorder in the HCS structure. $I_D/I_G$ ratio decreased with increased reaction temperature (600 – 700 °C) from 0.84 to 0.71, but increased to 0.86 at 800 °C. This was the consequence of the $CO_2$(g) coming out of the thermally decomposing template during CVD. The HCS synthesised at 600, 700, and 800 °C gave specific BET surface areas of: 193, 55, and 51 $m^2$/g, respectively. This was suggested to the effect of the carbonaceous residue materials within the HCS or the blockage of the HCS' pores during the acid treatment.

## 7.2 Recommendations

Crystal growth of $CaCO_3$ is a very complex process, however it is recommended that better additive-based crystallisation methods (which would be able to produce nano-sized $CaCO_3$ spheres) need to be investigated and employed in order to produce HCS with surface areas comparable to current templating methods. This includes looking into possible organic additives that would influence the morphology of the $CaCO_3$ into hollow micro and nano-structures.

The BET surface areas of the HCS synthesised at 700 and 800 °C appeared to be compromised by the presence of solid residue material inside them. It is therefore recommended that elemental/qualitative analysis, such as FIB-SEM with EDX of the core of the HCS, be used to gain more insight into the nature of the residue observed inside the HCS, in order to improve their quality. It is also recommended that better and efficient etching methods be investigated; perhaps different organic acids apart from acetic acid should be considered. Solvothermal carbonisation techniques of HCS may also be looked into, in order to compare these products with the $CaCO_3$-templated HCS synthesised by CVD. Likewise, high pressure solvothermal syntheses of HCS could be undertaken, where a porogen (such as CTAB or Triton-X) could be used to improve the porosity of the resultant materials.

$CaCO_3$-templated synthesis of HCS is still in its infancy (this research is the first attempt), hence more studies need to be performed to gain greater insight into the processes occurring

during carbonisation and etching of the template. This will require efforts from both crystallographers and material scientists.

# APPENDIX 1

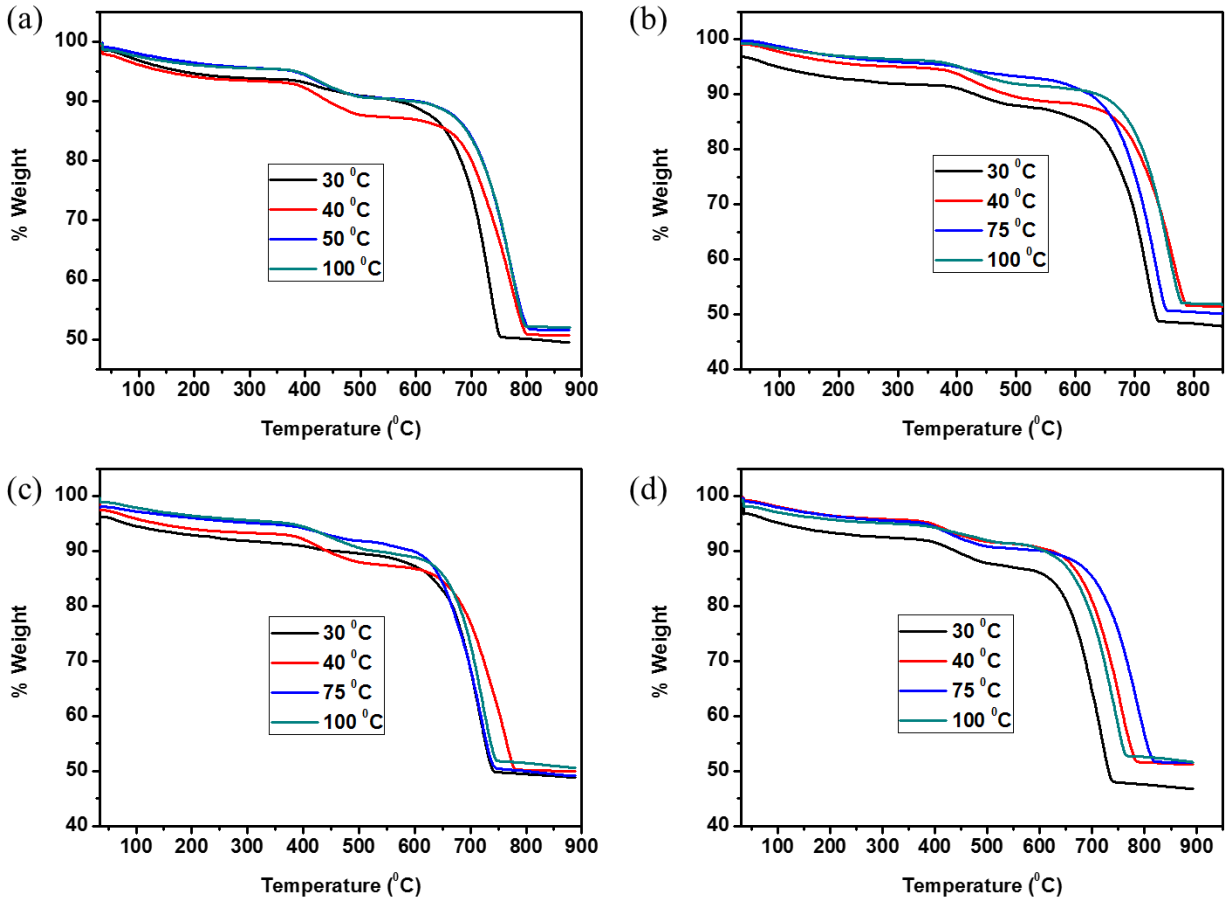



Figure S. 1. TGA patterns showing the presence of the PSSA within the vaterite spheres by the decomposition peak around 450 ˚C at, (a) 3 hrs, (b) 6 hrs, (c) 12 hrs, (d) 24 hrs reaction times.

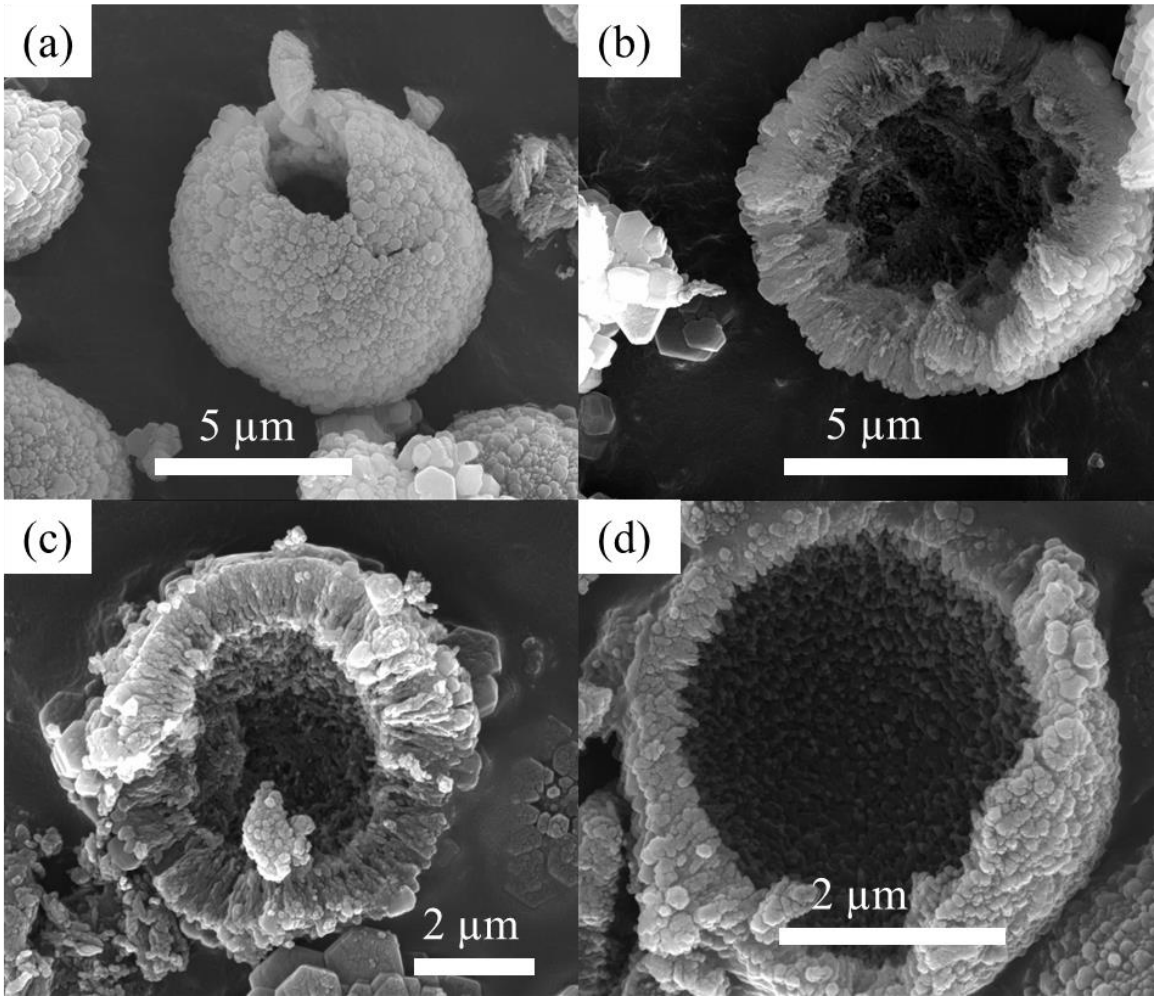



Figure S. 2. SEM micrographs showing the hollow nature of the bulk vaterite spheres crystallised at: (a) & (b) 75 °C, and (c) & (d) 100 °C.

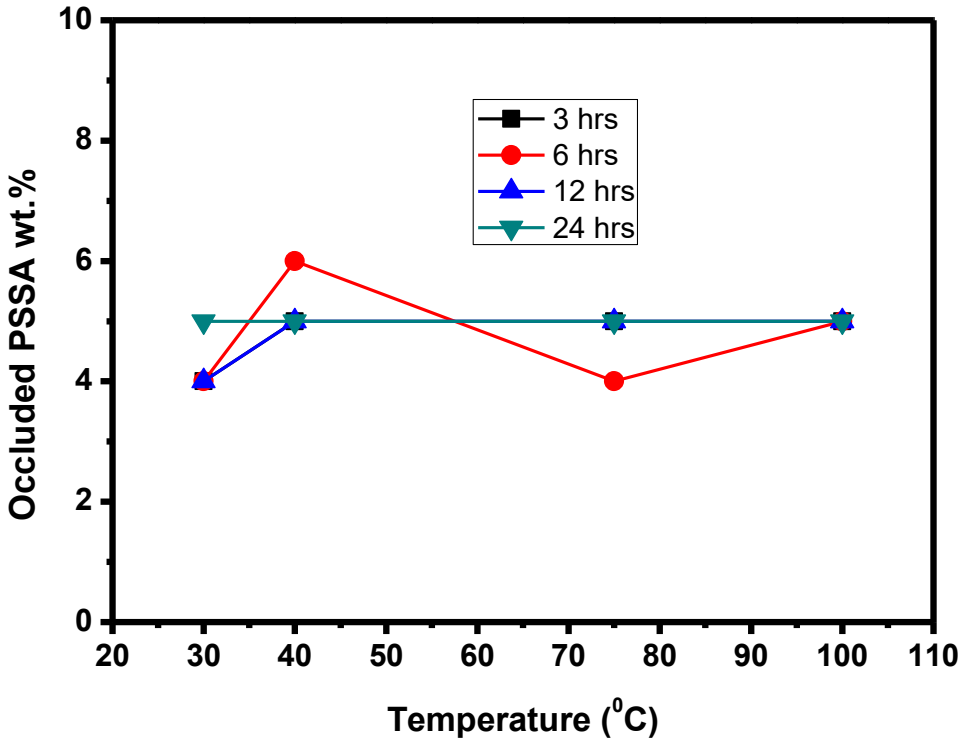



Figure S. 3. The amount (wt. %) of the occluded PSSA at different reaction temperatures for different reaction times.